Coherent delocalization in the light-matter interaction

by

Nadine Stritzelberger

A thesis
presented to the University of Waterloo
in fulfillment of the
thesis requirement for the degree of
Doctor of Philosophy
in
Applied Mathematics

Waterloo, Ontario, Canada, 2020

Examining Committee Membership

The following served on the Examining Committee for this thesis. The decision of the Examining Committee is by majority vote.

External Examiner:	Miles P. Blencowe Eleanor and A. Kelvin Smith Distinguished Professor Dept. of Physics and Astronomy, Dartmouth College
Supervisor:	Achim Kempf Professor Dept. of Applied Mathematics, University of Waterloo
Internal Member:	Florian Girelli Associate Professor Dept. of Applied Mathematics, University of Waterloo
Internal-External Member:	Robert Mann Professor Dept. of Physics and Astronomy, University of Waterloo
Other Member:	Eduardo Martín-Martínez Associate Professor Dept. of Applied Mathematics, University of Waterloo

Author's Declaration

This thesis consists of material all of which I authored or co-authored: see Statement of Contributions included in the thesis. This is a true copy of the thesis, including any required final revisions, as accepted by my examiners.

I understand that my thesis may be made electronically available to the public.

Statement of Contributions

Many of the ideas and results presented in Chapters 2 and 3 of this thesis can also be found in the publication "Coherent delocalization in the light-matter interaction" [1], which I co-authored together with Achim Kempf (University of Waterloo, Professor). While I performed all calculations, Achim Kempf and I developed in dialogue the conceptual ideas for this work, as well as the physical intuition behind the results.

The results presented in Chapter 4 of this thesis are adapted from the publication "Entanglement harvesting with coherently delocalized matter" [2], which I co-authored with Laura J. Henderson (University of Waterloo and RMIT University, PhD Student), Valentina Baccetti (RMIT University, Vice-Chancellor's Research Fellow), Nicolas C. Menicucci (RMIT University, Associate Professor) and Achim Kempf. This collaboration was based on ideas developed in discussions between Achim Kempf, Nicolas C. Menicucci and myself during our overlapping visits at the University of Queensland. The initial ideas were then further developed during weekly discussions with Laura J. Henderson, Valentina Baccetti, Nicolas C. Menicucci and Achim Kempf. While I performed most calculations and wrote the manuscript, all credit goes to Laura J. Henderson for creating the plots displayed in Chapter 4, for coming up with the idea of employing a compact sine switching, see Eq.(1.20), as well as for performing the calculations leading to Eq.(4.36)-(4.40).

The ideas and results of Chapter 5 of this thesis were obtained in collaboration with Vivishek Sudhir (Massachusetts Institute of Technology, Assistant Professor) and Achim Kempf. While I performed the calculations and created the plots presented, the ideas and physical intuition behind the results of Chapter 5 were obtained during numerous discussions between Vivishek Sudhir, Achim Kempf and myself.

Abstract

In this thesis, we study coherent delocalization in the light-matter interaction: we investigate how the coherent center of mass delocalization of a first quantized system affects its interaction with a second quantized field. We develop a suitably generalized Unruh-DeWitt model for the interaction between a delocalizing particle and a relativistic quantum field. We discuss the impact which the coherent spreading of the detector's center of mass wave function has on the simple processes of absorption, spontaneous emission and vacuum excitation. We find that the dynamical virtual delocalization process leads to interesting new phenomenology not only for the interaction of matter systems with the electromagnetic quantum field, but also with other fields such as a phonon field. For instance, we predict that in a medium, in the case of a supersonic coherent spreading of the center of mass wave function, a coherently delocalized detector may get excited and emit Cherenkov-like radiation. We further investigate how the coherent center of mass delocalization impacts the process of entanglement harvesting and the Unruh effect.

Acknowledgements

I acknowledge financial support through an Ontario Trillium scholarship (OTS) by the Ministry of Advanced Education and Skills Development of Ontario and the University of Waterloo. I further acknowledge financial support through a Mitacs Globalink Research Award, which allowed me to conduct research at the University of Queensland in collaboration with Tim Ralph and Achim Kempf.

I would like to thank Tim Ralph, for his kind hospitality at the University of Queensland, and Nick Menicucci, for his invitation to visit his group at RMIT and for being a welcoming host and fantastic collaborator. I also wish to thank Achim Kempf, Vivishek Sudhir, Laura Henderson, Valentina Baccetti, Flaminia Giacomini and Jason Pye, for being wonderful research collaborators. Special thanks goes to my examiners, Miles P. Blencowe, Eduardo Martín-Martínez, Robert Mann, Florian Girelli and Achim Kempf, for careful reading of my thesis, useful discussions and valuable comments.

Achim, thank you for your endless support and for always cheering me on, irrespective of the matters I pursued and the career paths I explored during my time in Waterloo. Your positive energy, your empathy and your joy for research and discovery are inspiring, and I could not have wished for a better advisor.

Aida, my sister from another mister, I cannot thank you enough for your most precious friendship and for inspiring me to think and dream big. I feel so blessed for the time we spent together, both in Waterloo and while traveling the world.

Mama, I am eternally grateful for the unconditional love and support you have shown me, not only while I pursued my PhD, but throughout my life. Thank you for countless instances in which you reassured me, gave me strength and helped me persevere.

Imagination is more important than knowledge. For knowledge is limited, whereas imagination embraces the entire world, stimulating progress, giving birth to evolution. It is, strictly speaking, a real factor in scientific research.

-Albert Einstein, 1931

Table of Contents

List of Figures

Introduction

A commonly employed model to explore light-matter interactions is the Unruh-DeWitt (UDW) detector model [3, 4]. The UDW detector model idealizes small matter systems (such as atoms, ions, molecules, or even electrons in a magnetic field) as qubit systems with classical center of mass degrees of freedom. It further idealizes the electromagnetic vector-valued quantum field, by replacing it by a simpler scalar-valued quantum field. Despite its simplicity, the UDW detector model qualitatively captures many aspects of the light-matter interaction [5, 6].

Historically, atoms, molecules or ions modeled in this way were called UDW *detectors*, since they were originally introduced to qualitatively describe the *detection* of field quanta, such as Hawking or Unruh radiation. Hawking discovered in 1974 that the gravitational fields of black holes formed by gravitational collapse can lead to particle production, referred to as Hawking radiation [7], while Fulling in 1973, Davies in 1975 and Unruh in 1976 discovered that in the Minkowski vacuum, that is, in the no-particle state of inertial observers, uniformly accelerated observers experience a thermal bath of particles, referred to as Unruh radiation [8, 9, 10, 11, 3, 4, 12, 13]. The UDW detector model turned out to be a powerful technical tool that could be used to explain particle production for quantum fields in a concrete and operational way, by allowing the extraction of local information from quantum fields [5, 14, 15, 16]. More recently, UDW detectors have proven to be very useful to explore a variety of topics in the research field of relativistic quantum information [17], such as for instance the process of entanglement harvesting [18, 19, 20, 21, 22, 23, 24] and quantum communication through quantum fields [25, 26, 27].

In this thesis, we ask whether, by employing the simplified UDW detector model to explore the light-matter interaction, we are missing out on interesting new phenomenology. In particular, we here focus on the fact that the UDW detector model is limited to the regime in which the detector's center of mass follows a classical trajectory. In the light-matter interaction, the motion of a matter system influences the particle's emission and absorption properties, e.g.,

through the Doppler effect or the Unruh effect. In situations where the motion can be described by a classical probability distribution, these effects can be calculated separately for each possible state of motion, to then be added up incoherently, and the conventional UDW detector model is an appropriate tool for doing so. However, the UDW detector model fails to account for phenomena that arise when the center of mass motion of a matter system is quantum uncertain, that is, when the center of mass motion is in a coherent superposition.

In chapter 2 of this thesis, we develop a generalized detector model (which we refer to as *coherently delocalized detector model*) that includes the quantum mechanical description of the center of mass degrees of freedom of the detector system [1]. We then investigate how the coherent spreading of the center of mass wave function of the detector system impacts its interaction with a quantum field. We do so by employing a technical tool, previously used, e.g., in [28, 29], that allows to couple quantum fields to first-quantized systems that possess quantum uncertain positions. Technically, we will work with quantum field operators that take position operators as their argument. Throughout this thesis, we will work in the non-relativistic regime, and we will neglect all competing effects, such as higher order quantum field theoretic corrections.

We show that simple processes, such as the processes of spontaneous emission, absorption and vacuum excitation, can depend on the center of mass delocalization of the detector system and on whether the delocalization is coherent or incoherent. For instance, we find that the more sharply the center of mass of a detector is initially localized, the faster it spontaneously emits. We further find that new phenomena can arise in media if parts of the center of mass wave function spread faster than the maximum wave propagation speed in the medium. We show that the coherent supersonic delocalization of the center of mass can trigger the excitation of the detector, along with the emission of Cherenkov-like radiation. We refer to this newly discovered effect as the *virtual Cherenkov-like effect*. We also discuss the time reversed process, which we refer to as the *inverse virtual Cherenkov-like effect*.

We can view the coherently delocalized detector model as an exploratory tool that allows us to uncover potential new phenomena that may arise with the coherent center of mass delocalization of a matter system. Whenever we come across a new effect within the coherently delocalized detector model, we might want to study in detail how the effect manifests itself for a specific physical system. For instance, in chapter 3, we present a framework that allows us to make quantitatively predictions for the effects discovered in chapter 2, for a *delocalized hydrogen atom* that interacts with the electromagnetic field. Namely, we consider a quantum delocalized electron and a quantum delocalized proton, which couple with each other via a

Coulomb potential and which respectively interact with the electromagnetic quantum field via minimal coupling. We then demonstrate how to calculate the spontaneous emission rate for this quantum delocalized hydrogen atom, and we find that the rate is indeed affected by the coherent spreading of the center of mass wave function.

In chapter 4, we qualitatively study the process of *entanglement harvesting* within our coherently delocalized detector model. It is a well-studied fact that the vacuum state of a quantum field is an entangled state [30, 31, 32, 33, 34]. The entanglement of the vacuum state has been studied extensively in the past, for instance in the context of holography [35, 36, 37, 38]. It was also shown that the vacuum entanglement can, to a certain extend, be swapped into a pair of UDW detectors: two initially unentangled detectors can become entangled with one another, via their respective interaction with the vacuum state of the quantum field [18, 19, 21, 23, 22, 39, 40, 41], even if the detectors are spacelike separated [33]. Within the UDW detector model, the process of entanglement harvesting has been studied for detectors not only interacting with the Minkowski vacuum, but also for instance with general coherent field states [42, 43], with quantum fields in curved spacetimes [21, 44, 45, 46, 47] and with quantum fields in spacetimes with non-trivial topology [48, 49]. It was found that the process of entanglement harvesting depends very sensitively on the detector details [22, 23, 50, 51, 52, 53]. Here, we consider two coherently delocalized detectors that are both initially in their ground states and that respectively couple to a scalar quantum field. We then study how their ability to become entangled with each other is affected by their respective mass and initial delocalization. In the limit of very large detector masses and very sharply localized center of mass degrees of freedom, we recover the results of vacuum entanglement harvesting for two pointlike UDW detectors.

In chapter 5, we finally discuss the impact of coherent center of mass delocalization on the *Unruh effect* (by which we here mean the possible excitation of an accelerated detector in the vacuum, along with the emission of radiation, rather than the fact that a detector system thermalizes when being uniformly accelerated in the vacuum for an infinite amount of time). Instead of prescribing a trajectory for an accelerated UDW detector, we dynamically account for the motion of the detector, by coupling the quantized center of mass degrees of freedom of the detector to a classical electric field. We then study the vacuum excitation process of the detector, along with the emission of radiation and the quantum recoil of the detector, which we refer to as the *massive Unruh effect*. In the limit of infinite detector mass and infinite electric field strength (in which the center of mass motion can effectively be described by a classical trajectory with some given finite acceleration), we recover the results obtained for a UDW

detector with classical center of mass. For a detector of finite mass, we then study how the emission of Unruh radiation is impacted by the coherent center of mass delocalization of the detector, and in particular, by the quantum recoil of the detector. While the recoil caused by the Unruh effect has been studied before [54, 12, 13], we here, for the first time, describe the recoil fully quantum mechanically and dynamically.

Chapter 1

UDW detector model

In this chapter, we briefly review the UDW detector model. The UDW detector model can be viewed as a simplified model for light-matter interactions [5, 52, 55, 56], in which the electromagnetic field is replaced by a massless scalar quantum field, and a small matter system (such as an atom, molecule, ion or even an electron in a magnetic field) is modelled as a simple first-quantized two-level system with classical center of mass degrees of freedom. Let us here denote the ground and excited energy eigenstates of the two-level detector system by $|g\rangle$ and $|e\rangle$ respectively, and the energy gap between the two levels by Ω. The total Hilbert space of the coupled system of detector and field factorizes into a Hilbert space for the internal degree of freedom of the detector, as well as a Hilbert space for the field degrees of freedom, $\mathcal{H} = \mathcal{H}_D \otimes \mathcal{H}_F$. The free Hamiltonian, $\hat{H}_0 = \hat{H}_D + \hat{H}_F$, consists of the free Hamiltonian $\hat{H}_D$ for the UDW detector and the free Hamiltonian $\hat{H}_F$ of the scalar quantum field, which are respectively given as

$$\hat{H}_D \;:=\; \Omega\,|e\rangle\langle e| \qquad \text{and} \qquad \hat{H}_F := \int d^3k\, ck\, \hat{a}^\dagger_{\mathbf{k}} \hat{a}_{\mathbf{k}}\,, \tag{1.1}$$

with $k := |\mathbf{k}|$. While c here stands for the speed of light in the vacuum, we will later also consider media with lower wave propagation speeds. We set $\hbar = 1$ throughout this thesis[1]. Let us here briefly review some basics and notational conventions with respect to the free Hamiltonian of the scalar quantum field (see, e.g., [57, 58]). We refer to $\hat{a}^\dagger_{\mathbf{k}}$ and $\hat{a}_{\mathbf{k}}$ respectively as the creation and annihilation operators of scalar field modes of momentum $\mathbf{k}$. These operators satisfy the

[1] except in plots in which we consider numeric values, as well as in chapter 3 in which we make quantitative order of magnitude estimates

following canonical commutation relations:

$$[\hat{a}_{\mathbf{k}_1}\,,\,\hat{a}^\dagger_{\mathbf{k}_2}] \;=\; \delta^{(3)}(\mathbf{k}_1-\mathbf{k}_2)\,, \qquad [\hat{a}_{\mathbf{k}_1}\,,\,\hat{a}_{\mathbf{k}_2}] = [\hat{a}^\dagger_{\mathbf{k}_1}\,,\,\hat{a}^\dagger_{\mathbf{k}_2}] = 0 \tag{1.2}$$

The vacuum state $|0\rangle$ of the scalar field can be defined by requiring that it is annihilated by all annihilation operators:

$$\hat{a}_{\mathbf{k}}\,|0\rangle \;=\; 0 \qquad \forall\;\mathbf{k} \tag{1.3}$$

It is easily verified that the vacuum state is the lowest energy eigenstate of the free scalar field Hamiltonian, $\hat{H}_F\,|0\rangle = 0\,|0\rangle$. By acting with the creation operators $\hat{a}^\dagger_{\mathbf{k}}$ on the vacuum state, one obtains excited field states as follows:

$$|\mathbf{k}\rangle \;:=\; \hat{a}^\dagger_{\mathbf{k}}\,|0\rangle \tag{1.4}$$

Since the energy of these excited field states, $\hat{H}_F\,|\mathbf{k}\rangle = ck\,|\mathbf{k}\rangle$, is in accordance with the dispersion relation for a massless relativistic particle of 3-momentum $\mathbf{k}$, the states $|\mathbf{k}\rangle$ are referred to as single particle states. Acting repeatedly with the creation operators on the vacuum state, we obtain $n-$particle states,

$$|\mathbf{k}_1,\ldots,\mathbf{k}_n\rangle \;:=\; \frac{1}{\sqrt{n!}}\,\hat{a}^\dagger_{\mathbf{k}_1}\ldots\hat{a}^\dagger_{\mathbf{k}_n}\,|0\rangle \tag{1.5}$$

which form an orthonormal basis for the Hilbert space of the field degrees of freedom.

Let us now discuss how to couple a UDW detector to a scalar quantum field. There are many variations and modifications of the UDW detector model. Which model to employ very much depends on the desired level of accuracy and on the physical system one wishes to model.

1.1 Standard UDW model

In its simplest form, the UDW detector model considers a *pointlike* qubit system that interacts with the quantum field along the detector's prescribed classical worldline [5]. Throughout this entire thesis, we will assume the center of mass velocities to be non-relativistic, which allows us to identify the proper time of the detector with the coordinate time t, and we write $\mathbf{x}(t)$ for the detector's spatial trajectory. The UDW detector model usually assumes the interaction Hamiltonian in the Schrödinger picture to take the simple form

$$\hat{H}_{int} \;=\; \lambda\hat{\mu}\otimes\hat{\phi}(\mathbf{x}(t))\,. \tag{1.6}$$

Here, λ denotes the coupling strength, $\hat{\mu}$ is the monopole operator of the detector in the Schrödinger picture,

$$\hat{\mu} \;=\; |e\rangle\langle g| + |g\rangle\langle e| \;, \tag{1.7}$$

and $\hat{\phi}$ is the scalar quantum field operator in the Schrödinger picture:

$$\hat{\phi}(\mathbf{x}) \;=\; \int \frac{d^3k}{(2\pi)^{3/2}}\sqrt{\frac{c^2}{2k}}\,\left(e^{i\mathbf{kx}}\hat{a}_{\mathbf{k}} + \text{H.c.}\right) \tag{1.8}$$

In the following, we will study the time evolution of the detector and the scalar field in the interaction picture (also known as the Dirac picture). We recall that in the interaction picture, operators evolve under the time evolution operator generated by the free Hamiltonian, while states evolve under the time evolution operator generated by the interaction Hamiltonian [58]. For an operator $\hat{O}$ in the Schrödinger picture, we obtain its interaction picture representation $\hat{O}(t)$ according to

$$\hat{O}(t) \;=\; \hat{U}_0(t)\,\hat{O}\,\hat{U}_0^\dagger(t)\,, \tag{1.9}$$

with $\hat{U}_0(t) := e^{i\hat{H}_0 t}$. In the interaction picture, the interaction Hamiltonian (1.6) thus reads

$$\hat{H}_{int}(t) \;=\; \lambda\hat{\mu}(t)\otimes\hat{\phi}(\mathbf{x}(t),t)\,, \tag{1.10}$$

where the monopole operator and the scalar field operators evolve according to the free Hamiltonian in Eq.(1.1) as follows:

$$\hat{\mu}(t) \;=\; e^{i\Omega t}\,|e\rangle\langle g| + \text{H.c.}\,, \tag{1.11}$$

$$\hat{\phi}(\mathbf{x},t) \;=\; \int \frac{d^3k}{(2\pi)^{3/2}}\sqrt{\frac{c^2}{2k}}\,\left(e^{-ickt+i\mathbf{kx}}\hat{a}_{\mathbf{k}} + \text{H.c.}\right) \tag{1.12}$$

In the interaction picture, the states evolve in time according to the Dyson operator

$$\hat{U} \;:=\; T\exp\left(-i\int_{-\infty}^{\infty} dt'\,\hat{H}_{int}(t')\right)\,, \tag{1.13}$$

with $T\exp$ the time-ordered exponential. For small coupling strengths λ, we can treat the interaction as a small perturbation of the free time evolution of the detector and the field, and we can perturbatively expand the time evolution operator as

$$\hat{U} \;=\; \sum_{n=0}^{\infty}\hat{U}^{(n)}\,, \tag{1.14}$$

where the $n-$th order of the time evolution operator is explicitly given as follows:

$$\hat{U}^{(n)} \;:=\; (-i)^n \int_{-\infty}^{\infty} dt_1 \hat{H}_{int}(t_1) \int_{-\infty}^{t_1} dt_2 \hat{H}_{int}(t_2) \cdots \int_{-\infty}^{t_{n-1}} dt_n \hat{H}_{int}(t_n)\,. \tag{1.15}$$

The transition probability amplitude for the coupled system to evolve from an initial state $|\Psi_i\rangle$ to a final state $|\Psi_f\rangle$ then becomes, to first perturbative order:

$$\mathcal{A} \;:=\; -i \langle \Psi_f | \int_{-\infty}^{\infty} dt\, \hat{H}_{int}(t) \, |\Psi_i\rangle \tag{1.16}$$

The transition probability follows by taking the modulus squared of the transition probability amplitude, $P := |\mathcal{A}|^2$. Within the standard UDW detector model, we are now equipped to study the probabilities for various processes in the light-matter interaction to happen, e.g., the processes of spontaneous emission, stimulated emission or absorption. Before we discuss some of these effects, let us note that a plethora of modifications of the standard UDW model can be found in the literature [52, 55, 5]. In the following two sections, we briefly mention two such modifications, namely a UDW-type model including a switching function, and a UDW-type model including a smearing profile.

1.2 UDW model including a switching function

The interaction Hamiltonian in Eq.(1.6) is oftentimes extended to include a switching function $\chi(t)$, via which the interaction between the detector and the quantum field can then be switched on and off:

$$\hat{H}_{int} \;=\; \lambda \chi(t)\, \hat{\mu} \otimes \hat{\phi}(\mathbf{x}(t)) \tag{1.17}$$

For $\chi(t) \equiv 1$, the interaction is switched on for all times and we recover the interaction Hamiltonian of the standard UDW model in Eq.(1.10). For $\chi(t) = \delta(t - t_0)$, the interaction is switched on only at time $t = t_0$. Common choices for square integrable switching functions (see, e.g., [22]) are for instance a Gaussian switching function,

$$\chi(t) \;=\; \exp\left(-\frac{(t-t_0)^2}{2\sigma^2}\right)\,, \tag{1.18}$$

a rectangular switching function,

$$\chi(t) \;=\; \begin{cases} 1, & \text{for} \quad t_0 \leq t \leq t_f \\ 0 & \text{otherwise}\,, \end{cases} \tag{1.19}$$

or a compact sine switching function:

$$\chi(t) \;=\; \begin{cases} \sin\left(t/\sigma\right), & \text{for} \quad 0 \leq t \leq \pi\sigma \\ 0 & \text{otherwise} \end{cases} \tag{1.20}$$

Oftentimes, switching functions are introduced in order to render total transition probabilities finite, which would otherwise either diverge or vanish. We note that by introducing a switching function into the interaction, time translation invariance is broken and energy is no longer a conserved quantity. One way to think about this is to imagine an external agent, who switches the interaction on and off, and who thereby provides or extracts energy to or from the system.

1.3 UDW model including a smearing profile

Another routinely employed extension of the conventional UDW detector model is obtained by introducing a spatial smearing profile into the interaction Hamiltonian (see, e.g., [52]), in an attempt to account for the finite size of the atom. A classical spatial smearing profile $\xi(\mathbf{x})$ can be included in the interaction Hamiltonian in Eq.(1.10) as follows:

$$\hat{H}_{int}(t) \;=\; \lambda\hat{\mu}(t)\int d^3x\,\xi(\mathbf{x}-\mathbf{x}_0)\hat{\phi}(\mathbf{x},t) \tag{1.21}$$

$$\;=\; \lambda\chi(t)\hat{\mu}(t)\int \frac{d^3k}{\sqrt{2ck}}\left[\hat{a}_{\mathbf{k}}e^{-i(ckt-\mathbf{k}\mathbf{x}_0)}\widetilde{\xi}(\mathbf{k})+\hat{a}^{\dagger}_{\mathbf{k}}e^{i(ckt-\mathbf{k}\mathbf{x}_0)}\widetilde{\xi}(-\mathbf{k})\right] \tag{1.22}$$

Here, $\xi(\mathbf{x})$ denotes the spatial smearing profile, $\widetilde{\xi}(\mathbf{k})$ denotes its Fourier transformation,

$$\widetilde{\xi}(\mathbf{k}) \;:=\; \int \frac{d^3x}{(2\pi)^{3/2}}\,\xi(\mathbf{x})\,e^{i\mathbf{k}\mathbf{x}}\,, \tag{1.23}$$

and $\mathbf{x}_0$ denotes the center of mass position of the spatially smeared UDW detector. We here note that by introducing a smearing profile, the momentum of the coupled system of detector and field is no longer conserved. This is analogous to breaking energy conservation by introducing a switching function. Again, we might want to imagine an external agent, who keeps the detector in place according to the spatial smearing profile, and who thus compensates any sort of recoil that the detector would otherwise experience. We can thus view this external agent as representing a momentum reservoir, thereby allowing certain transitions in the light-matter interaction (which would otherwise be excluded according to momentum conservation) to happen.

A widely employed smearing profile is a Gaussian profile such as the following:

$$\xi(\mathbf{x}) \;=\; \left(\frac{2}{\pi L^2}\right)^{3/2} e^{-2\mathbf{x}^2/L^2}\,, \qquad \widetilde{\xi}(\mathbf{k}) = \left(\frac{1}{2\pi}\right)^{3/2} e^{-L^2\mathbf{k}^2/8} \tag{1.24}$$

We will here refer to L as the width of the smearing profile. The pointlike, standard UDW detector model in Eq.(1.10) is approached in the limit $L \to 0$, in which the Gaussian smearing profile becomes a Dirac delta distribution:

$$\lim_{L\to 0}\left(\frac{2}{\pi L^2}\right)^{3/2} e^{-2\mathbf{x}^2/L^2} \;=\; \delta^{(3)}(\mathbf{x}) \tag{1.25}$$

Since the smearing profile is normalized, $\int d^3x\, \xi(\mathbf{x}) = 1$, one might be tempted to view the smearing profile $\xi(\mathbf{x})$ as a probability distribution resulting from a wave function, $\xi(\mathbf{x}) = |\psi(\mathbf{x})|^2$, according to which the charge distribution couples to the field. However, in [23] things were shown to be more subtle than that. The authors showed how to derive a physically motivated smearing profile for a UDW detector modelling an atom, in terms of the detector's orbital wave functions. What is remarkable about these findings is that it showed how to overcome the need for introducing smearing profiles in an *ad hoc* fashion into the UDW detector model. Let us here briefly summarize some of these findings. The authors started their discussion from the dipole coupling between an electric dipole and the electromagnetic field,

$$\hat{H}_{int} \;=\; \hat{\mathbf{d}}\cdot\hat{\mathbf{E}} = e\,\hat{\mathbf{x}}\cdot\hat{\mathbf{E}}\,, \tag{1.26}$$

with $\hat{\mathbf{E}}$ the electric field operator, $\hat{\mathbf{d}}$ the dipole moment operator, $\hat{\mathbf{x}}$ the position operator and e the charge of the electric dipole. The interaction Hamiltonian can be expressed in terms of an orthonormal basis $\{|i\rangle\}$ of the electric dipole as follows:

$$\hat{H}_{int} \;=\; e\sum_{i,j} \langle i|\,\hat{\mathbf{x}}\cdot\hat{\mathbf{E}}\,|j\rangle\,|i\rangle\,\langle j| \tag{1.27}$$

With the simplifying assumption that only two atomic energy levels, denoted by $|g\rangle$ and $|e\rangle$ respectively, interact with the electric field, the interaction Hamiltonian in the interaction picture becomes:

$$\hat{H}_{int}(t) \;=\; e\,\langle e|\,\hat{\mathbf{x}}\cdot\hat{\mathbf{E}}\,|g\rangle\,e^{i\Omega t}\,|e\rangle\,\langle g| + \text{H.c.} \tag{1.28}$$

Finally, inserting resolutions of the identity in the position eigenbasis, $\mathbf{1} = \int d^3x\ |\mathbf{x}\rangle\,\langle\mathbf{x}|$, the interaction Hamiltonian can be rewritten as

$$\hat{H}_{int}(t) \;=\; e\int d^3x\,\left[(\psi_e^*(\mathbf{x})\,\mathbf{x}\,\psi_g(\mathbf{x}))\cdot\hat{\mathbf{E}}(\mathbf{x},t)e^{i\Omega t}\,|e\rangle\,\langle g| + \text{H.c.}\right], \tag{1.29}$$

where $\psi_g(\mathbf{x}) = \langle \mathbf{x}|g\rangle$ and $\psi_e(\mathbf{x}) = \langle \mathbf{x}|e\rangle$ denote respectively the ground and excited energy wave functions of the detector in the position representation. The authors thus succeeded in identifying a physically motivated spatial smearing profile,

$$\mathbf{F}(\mathbf{x}) \;\; = \;\; \psi_e^*(\mathbf{x})\,\mathbf{x}\,\psi_g(\mathbf{x})\,, \tag{1.30}$$

according to which the dipole coupling can be expressed as a coupling with spatial smearing profile,

$$\hat{H}_{int}(t) \;\; = \;\; e\int d^3x\,\mathbf{F}(\mathbf{x})\cdot\hat{\mathbf{E}}(\mathbf{x},t)\,e^{i\Omega t}\,|e\rangle\,\langle g| + \text{H.c.}\,. \tag{1.31}$$

Inspired by their findings for the dipole coupling, the authors then proposed to modify the UDW detector model as follows,

$$\hat{H}_{int}(t) \;\; = \;\; \lambda\hat{\mu}(t)\int d^3x\,F(\mathbf{x})\hat{\phi}(\mathbf{x},t)\,, \tag{1.32}$$

with the smearing profile $F(\mathbf{x}) := \psi_e^*(\mathbf{x})\psi_g(\mathbf{x})$, such as to account for the finite spatial extent acquired by a UDW detector via its orbital wavefunctions. An alternative derivation of the smearing profile $F(\mathbf{x})$ in Eq.(1.32) is the following [29]: considering the interaction between the scalar field and a quantum mechanical position operator $\hat{\mathbf{x}}$ corresponding to the internal degrees of freedom of the detector,

$$\hat{H}_{int} \;\; = \;\; \lambda\int d^3x\,\hat{\phi}(\mathbf{x})\,\delta^{(3)}(\mathbf{x}-\hat{\mathbf{x}}) \tag{1.33}$$

resolutions of the identity in the energy eigenbasis of the internal degrees of freedom can be inserted, such as to obtain

$$\hat{H}_{int} \;\; = \;\; \lambda\sum_{i,j}\int d^3x\int d^3y\,\hat{\phi}(\mathbf{x})\,\delta^{(3)}(\mathbf{x}-\mathbf{y})\,\langle i|\mathbf{y}\rangle\,\langle \mathbf{y}|j\rangle\,|i\rangle\,\langle j| \tag{1.34}$$

$$\;\; = \;\; \lambda\int d^3x\,\hat{\phi}(\mathbf{x})\,\left[\psi_e^*(\mathbf{x})\psi_g(\mathbf{x})\,|e\rangle\,\langle g| + \psi_g^*(\mathbf{x})\psi_e(\mathbf{x})\,|g\rangle\,\langle e|\right] \tag{1.35}$$

$$\;\; = \;\; \lambda\int d^3x\,\hat{\phi}(\mathbf{x})\,\sum_{i\neq j}F_{ij}(\mathbf{x})\,|i\rangle\,\langle j|\;, \tag{1.36}$$

with $F_{ij}(\mathbf{x}) := \psi_i^*(\mathbf{x})\psi_j(\mathbf{x})$. We here stress that the quantum mechanical position operator $\hat{\mathbf{x}}$, which couples to the field operators, is associated with the orbital degrees of freedom of the detector, and $\psi_g(\mathbf{x})$ and $\psi_e(\mathbf{x})$ respectively denote the position representations of the orbital energy eigenfunctions of the detector. To summarize, the authors found that the finite spatial extent of an atom due to its electronic orbitals can be reflected within the UDW detector model via spatial smearing profiles.

1.4 Simple processes in the light-matter interaction

In this section, we briefly review some simple processes in the light matter interaction, modeled within the UDW detector model. We will revisit these processes in sections 2.2-2.4 of the next chapter, when taking into account the coherent delocalization of the detector.

1.4.1 Spontaneous emission process for UDW detectors

Let us start by recalling how to calculate the spontaneous emission rate for an UDW detector. We consider an initially excited UDW detector, as well as a massless scalar field initially in its vacuum state:

$$|\Psi_i\rangle \;=\; |e\rangle \otimes |0\rangle \tag{1.37}$$

For simplicity, we will here assume that the detector is at rest, $\mathbf{x}(t) \equiv \mathbf{x}_0$. To calculate the transition amplitude to a final state in which the detector is in its ground state and a field quantum of momentum $\mathbf{k}$ has been emitted,

$$|\Psi_f\rangle \;=\; |g\rangle \otimes |\mathbf{k}\rangle \;. \tag{1.38}$$

we first calculate the following matrix elements:

$$\langle g|\,\hat{\mu}(t)\,|e\rangle \;=\; e^{-i\Omega t} \tag{1.39}$$

$$\langle \mathbf{k}|\,\hat{\phi}(\mathbf{x}_0,t)\,|0\rangle \;=\; \frac{1}{(2\pi)^{3/2}}\frac{c}{\sqrt{2k}}e^{ickt-i\mathbf{k}\mathbf{x}_0} \tag{1.40}$$

Employing a rectangular switching function as in Eq.(1.19), which turns the interaction on at the initial time $t = t_i$ and turns it off at the final time $t = t_f$, we obtain the following transition amplitude, up to a complex phase:

$$\mathcal{A} \;=\; \frac{\lambda c}{\sqrt{2k}}\frac{1}{(2\pi)^{3/2}}\int_{t_i}^{t_f} dt\, e^{it(ck-\Omega)}\,. \tag{1.41}$$

In order to eliminate switching effects, we would like to take the limits $t_i \to -\infty$ and $t_f \to \infty$, in which case the energy of the coupled system of detector and field would be conserved,

$$\mathcal{A} \;=\; \frac{\lambda c}{\sqrt{4\pi k}}\delta(ck-\Omega)\,, \tag{1.42}$$

and the detector spontaneously emits a field quantum on resonance, that is, of energy $ck = \Omega$. However, we note that eliminating the switching function results in time translation invariance, see, e.g., [5], and consequently in a divergence of the total spontaneous emission probability, $P = |\mathcal{A}|^2$. In order to avoid this divergence, we instead calculate the transition rate, that is, the transition probability per unit proper time, as outlined for instance in [5, 59]. First, we take the modulus squared of the transition amplitude in Eq.(1.41) and differentiate the result with respect to the final time t_f, such as to obtain the spontaneous emission rate as a function of the magnitude k of the momentum of the emitted field quantum:

$$\mathcal{R}_k = \frac{dP}{dt_f} = \frac{\lambda^2 c^2}{2k(2\pi)^3}\left(e^{-it_f(ck-\Omega)}\int_{t_i}^{t_f} dt\, e^{it(ck-E)} + e^{it_f(ck-\Omega)}\int_{t_i}^{t_f} dt\, e^{-it(ck-\Omega)}\right) \tag{1.43}$$

Next, we set the initial time to $t_i = -T/2$ and the final time to $t_f = T/2$, such as for the interval of the interaction to be of length T, and we obtain:

$$\mathcal{R}_k = \frac{\lambda^2 c^2}{2k(2\pi)^3}\frac{2\sin\left(T(ck-\Omega)\right)}{ck-\Omega} = \frac{\lambda^2 c^2}{2k(2\pi)^3}\int_{-T}^{T} dt\, e^{it(ck-\Omega)} \tag{1.44}$$

As a final step, we take the limit $T \to \infty$, such as to avoid switching effects, and obtain the spontaneous emission rate, as a function of the momentum k of the emitted field quantum:

$$\mathcal{R}_k = \frac{\lambda^2\Omega}{2\pi}\frac{1}{4\pi k^2}\delta\left(k - \frac{\Omega}{c}\right) \tag{1.45}$$

To obtain the total spontaneous emission rate $\mathcal{R}$, irrespective of the momentum of the emitted field quantum, we trace over the Hilbert space $\mathcal{H}_F$ of the field degrees of freedom:

$$\mathcal{R} = \int_0^\infty dk\, 4\pi k^2\, \mathcal{R}_k = \frac{\lambda^2\Omega}{2\pi} \tag{1.46}$$

Equipping the UDW detector with a spatial smearing profile $\xi(\mathbf{x})$, the spontaneous emission probability amplitude becomes, up to a phase,

$$\mathcal{A} = \frac{\lambda c}{\sqrt{2k}}\frac{1}{(2\pi)^{3/2}}\int_{t_i}^{t_f} dt\, e^{it(ck-\Omega)}\int d^3x\, \xi(\mathbf{x})e^{-i\mathbf{kx}}\,, \tag{1.47}$$

and the total spontaneous emission rate becomes

$$\mathcal{R} = \lambda^2 c\pi \int d^3k \frac{|\widetilde{\xi}(\mathbf{k})|^2}{k}\delta\left(k - \frac{\Omega}{c}\right)\,. \tag{1.48}$$

For the Gaussian smearing profile in Eq.(1.24), the spontaneous emission rate further simplifies:

$$\mathcal{R} = \frac{\lambda^2\Omega}{2\pi}\exp\left(-\frac{L^2\Omega^2}{4c^2}\right) \tag{1.49}$$

We here note that in the limit $L \to 0$, the smearing profile becomes sharper and sharper and approaches a Dirac delta distribution, and as expected, the spontaneous emission rate indeed approaches the spontaneous emission rate for pointlike detectors, as given in Eq.(1.46).

1.4.2 Absorption process for UDW detectors

Next, let us recall the absorption process of a photon by a UDW detector. We consider a to-be-absorbed photon of momentum $\mathbf{k}$ and a UDW detector at rest in its ground state,

$$|\Psi_i\rangle \;=\; |g\rangle \otimes |\mathbf{k}\rangle \;, \qquad |\Psi_f\rangle = |e\rangle \otimes |0\rangle \;. \tag{1.50}$$

First, we calculate the following matrix elements:

$$\langle 0|\, \hat{\phi}(\mathbf{x},t)\, |\mathbf{k}\rangle \;=\; \frac{1}{(2\pi)^{3/2}} \frac{c}{\sqrt{2k}} e^{-ickt+i\mathbf{kx}} \tag{1.51}$$

$$\langle e|\, \hat{\mu}(t)\, |g\rangle \;=\; e^{i\Omega t} \tag{1.52}$$

Let us assume that the detector is pointlike and located at the origin. Without loss of generality, we assume that the to-be-absorbed field quantum propagates in the $z-$direction, $\mathbf{k} = (0,0,k)^T$. We obtain for the absorption probability amplitude, up to a phase and to first perturbative order:

$$\mathcal{A} \;=\; \frac{\lambda c}{\sqrt{2k}} \frac{1}{(2\pi)^{3/2}} \int_{t_i}^{t_f} dt\, e^{it(\Omega - ck)t} \tag{1.53}$$

For the absorption probability rate we obtain:

$$\mathcal{R} \;=\; \frac{\lambda^2 \Omega}{2\pi} \frac{1}{4\pi k^2}\, \delta\left(\frac{\Omega}{c} - k\right) \tag{1.54}$$

As expected, photons can only be absorbed if they are on resonance with the energy gap of the detector, $ck = \Omega$. The same holds true for spatially smeared UDW detectors, for which we obtain the absorption probability rate

$$\mathcal{R} \;=\; \frac{\lambda^2 c}{2k} \left|\widetilde{\xi}(\mathbf{k})\right|^2 2\pi\, \delta\left(\frac{\Omega}{c} - k\right) \;. \tag{1.55}$$

As we might have expected intuitively, the absorption process now indeed depends on the spatial smearing profile of the detector absorbing the photon.

1.4.3 Vacuum excitation process for UDW detectors

Lastly, let us recall the excitation process of a UDW detector in the vacuum. We consider the initial state

$$|\Psi_i\rangle \;=\; |g\rangle \otimes |0\rangle \;, \tag{1.56}$$

and study the transition to a final state in which the detector is in its excited state and a field quantum of momentum $\mathbf{k}$ has been emitted,

$$|\Psi\rangle_f \;=\; |e\rangle \otimes |\mathbf{k}\rangle \;. \tag{1.57}$$

Since the probability amplitude for this transition vanishes for a detector at rest that is switched on at all times,

$$\mathcal{A} \;=\; \frac{\lambda c}{\sqrt{4\pi k}}\delta(ck+\Omega) = 0\,, \tag{1.58}$$

we find that the vacuum excitation probability vanishes. The same holds true also for spatially smeared detectors,

$$\mathcal{A} \;=\; \frac{\lambda c}{\sqrt{2k}}\widetilde{\xi}(\mathbf{k})\,2\pi\,\delta(ck+\Omega) = 0\,. \tag{1.59}$$

The reason for this is simple: the detector is at rest, in its ground state and switched on at all times, while the stress-energy of the quantum field in the vacuum state vanishes. Therefore, there is simply no energy available for the vacuum excitation process to occur. In order to obtain a finite vacuum excitation probability, energy must be provided, which means that translation invariance needs to be broken. One possible way to achieve this is to introduce a switching function $\chi(t)$, as discussed in section 1.2. The excitation probability amplitude then becomes

$$\mathcal{A} \;=\; \frac{\lambda c}{\sqrt{2k}}\frac{1}{(2\pi)^{3/2}}\int_{-\infty}^{\infty} dt\,\chi(t)e^{it(ck+\Omega)}\,, \tag{1.60}$$

and for the total vacuum excitation probability we obtain:

$$P \;=\; \frac{\lambda^2 c^2}{(2\pi)^3}\int d^3k\,\frac{1}{2k}\left|\int_{-\infty}^{\infty} dt\,\chi(t)e^{it(ck+\Omega)}\right|^2 \tag{1.61}$$

For a spatially smeared and temporally switched detector, we obtain the following excitation probability:

$$P \;=\; \lambda^2 c^2\int d^3k\,\frac{1}{2k}\left|\int_{-\infty}^{\infty} dt\,\chi(t)e^{it(ck+\Omega)}\right|^2\left|\widetilde{\xi}(\mathbf{k})\right|^2 \tag{1.62}$$

As an example, let us consider a Gaussian switching function of width σ, as given in Eq.(1.18), and a Gaussian spatial smearing profile of width L, as given in Eq.(1.24). We obtain the following vacuum excitation probability:

$$P = \frac{\lambda^2 y^2 e^{-\sigma^2\Omega^2}}{4\pi\Omega^2\sigma^2}\left[1+\sqrt{\pi}y\, e^{-\frac{L^2y^2}{4c^2\sigma^2}+\sigma^2\Omega^2}\left[\mathrm{erf}\,(y)-1\right]\right], \quad \text{with} \quad y := \frac{2\Omega c\sigma^2}{\sqrt{L^2+4c^2\sigma^2}} \tag{1.63}$$

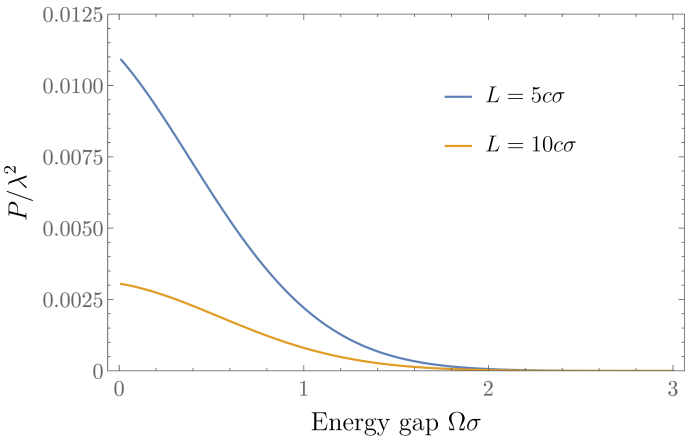

Figure 1.1: The vacuum excitation probability for a Gaussian switched and Gaussian smeared UDW detector, as a function of the energy gap Ω of the detector, for smearing widths $L = 5c\sigma$ and $L = 10c\sigma$.

In Fig.(1.1), we displayed the vacuum excitation probability given in Eq.(1.63), as a function of the energy gap Ω of the detector, for different smearing widths ($L = 5c\sigma$ and $L = 10c\sigma$). Note that, in order to render all quantities in the plot dimensionless, we expressed everything in terms of the switching width σ and the vacuum speed of light c. We find that for vanishing energy gaps, $\Omega \to 0$, the vacuum excitation probability approaches a finite value. What we here observe is radiation emitted by a simple charge, caused by switching the interaction between the charge and the quantum field on and off: Letting $\Omega \to 0$, the free Hamiltonian $\hat{H}_D$ of the internal degrees of freedom of the detector vanishes, and thus commutes with the UDW interaction Hamiltonian. The dynamics of the internal degree of freedom thus "freeze out", and we recover the Hamiltonian for a simple charge interacting with the quantum field. For the case of a simple charge without excitable internal degrees of freedom, all energy provided by the switching function can go into the excitation of the field. As the detector's energy gap increases, $\Omega \neq 0$, the excitation of the field along with the excitation of the detector becomes energetically more expensive, and the vacuum excitation probability decreases accordingly. We can further see that the vacuum excitation probability increases with decreasing smearing widths. For large energy gaps and large smearing widths, the vacuum excitation probability goes to zero: our external agent would need to provide larger and larger energy and momentum reservoirs, in order to enable the excitation of the detector and the field.

Chapter 2

Coherently delocalized detector model

We will now go beyond the conventional UDW detector model, by dropping the simplifying assumption that the center of mass of the detector follows a classical worldline. We generalize the UDW detector model, to take into account effects that arise with the quantum delocalization of the detector's center of mass. To this end, instead of prescribing a center of mass trajectory, we equip the detector with first-quantized center of mass degrees of freedom.

2.1 Setting up the interaction Hamiltonian

Equipping the detector with quantized center of mass degrees of freedom, the total Hilbert space of the coupled system of detector and quantum field factorizes into a Hilbert space for the detector's center of mass degrees of freedom, a Hilbert space for the detector's internal degree of freedom, and a Hilbert space for the field degrees of freedom:

$$\mathcal{H} \;=\; \mathcal{H}_{\rm CM} \otimes \mathcal{H}_D \otimes \mathcal{H}_F \tag{2.1}$$

Let us now write the free Hamiltonian of the UDW detector and the scalar quantum field as follows:

$$\hat{H}_0 \;=\; \hat{H}_{CM} + \hat{H}_D + \hat{H}_F \tag{2.2}$$

Let us assume that $\hat{H}_D$ and $\hat{H}_F$ are given as in Eq.(1.1), and that the time evolution of the quantum center of mass of the detector is given by

$$\hat{H}_{CM} \;=\; \frac{\hat{\mathbf{p}}^2}{2M}\,, \tag{2.3}$$

where $\hat{\mathbf{p}}$ denotes the center of mass momentum operator and M the mass of the detector. According to the free time evolution of the quantum center of mass, an initially localized center of mass wave packet dynamically delocalizes and thereby spreads in space. We now again model the interaction of the detector and the quantum field via the monopole operator coupling:

$$\hat{H}_{int} \;=\; \lambda \hat{\mu} \hat{\phi}(\hat{\mathbf{x}}) \tag{2.4}$$

As before, the coupling takes place at the center of mass position of the detector, which now however is described by the center of mass position operator $\hat{\mathbf{x}}$. How can we make sense of an operator-valued field $\hat{\phi}$ which takes a position operator $\hat{\mathbf{x}}$ as its argument? To answer this question, we apply the spectral theorem of functional calculus, as described, e.g., in [28, 29]. An operator-valued function $\hat{f}$ can take an operator $\hat{A}$ as its argument by expanding the operator in its eigenbasis and evaluating the function on the operator's eigenvalues:

$$\hat{f}(\hat{A}) \;=\; \int da\; |a\rangle \langle a| \otimes \hat{f}(a)\,, \quad \text{with} \quad \hat{A}\,|a\rangle = a\,|a\rangle \tag{2.5}$$

For the interaction Hamiltonian in Eq.(2.4), we first expand the center of mass position operator $\hat{\mathbf{x}}$ in terms of its eigenbasis,

$$\hat{\mathbf{x}} \;=\; \int d^3x\, \mathbf{x}\; |\mathbf{x}\rangle \langle \mathbf{x}|\;, \tag{2.6}$$

where $|\mathbf{x}\rangle$ are the position eigenstates and $\mathbf{x}$ are the position eigenvalues of the center of mass of the UDW detector. We then evaluate the quantum field operators on the center of mass position eigenvalues:

$$\hat{H}_{int} \;=\; \lambda \int d^3x\, \hat{\mathcal{P}}(\mathbf{x}) \otimes \hat{\mu} \otimes \hat{\phi}(\mathbf{x}) \tag{2.7}$$

We here defined the operators $\hat{\mathcal{P}}(\mathbf{x}) := |\mathbf{x}\rangle \langle \mathbf{x}|$ in terms of the position eigenstates. With the free Hamiltonian in Eq.(2.2), we find that the interaction Hamiltonian in the interaction picture becomes

$$\hat{H}_{int}(t) \;=\; \lambda \int d^3x\, \hat{\mathcal{P}}(\mathbf{x},t) \otimes \hat{\mu}(t) \otimes \hat{\phi}(\mathbf{x},t)\,, \tag{2.8}$$

where the operators $\hat{\mathcal{P}}(\mathbf{x},t)$, the monopole operators $\hat{\mu}(t)$ and the field operators $\hat{\phi}(\mathbf{x},t)$ evolve in the interaction picture as follows:

$$\hat{\mathcal{P}}(\mathbf{x},t) \;=\; \int \frac{d^3p\, d^3q}{(2\pi)^3} e^{-i(\mathbf{p}-\mathbf{q})\mathbf{x} + it\frac{p^2-q^2}{2M}}\, |\mathbf{p}\rangle \langle \mathbf{q}|\;, \tag{2.9}$$

$$\hat{\mu}(t) \;=\; e^{i\Omega t}\, |e\rangle \langle g| + \text{H.c.}\,, \tag{2.10}$$

$$\hat{\phi}(\mathbf{x},t) \;=\; \int \frac{d^3k}{(2\pi)^{3/2}} \sqrt{\frac{c^2}{2k}} \left(e^{-ickt + i\mathbf{k}\mathbf{x}} \hat{a}_{\mathbf{k}} + \text{H.c.}\right) \tag{2.11}$$

Let us here briefly comment on how to physically motivate the mathematical structure of the coupling given by Eq.(2.7): the expectation value $\langle\varphi|\,\hat{H}_{int}\,|\varphi\rangle = \lambda\hat{\mu}\int d^3x\,\varphi^*(\mathbf{x})\hat{\phi}(\mathbf{x})\varphi(\mathbf{x})$, for a center of mass state $|\varphi\rangle$, is structurally of similar form as the expectation value $\langle\psi|\,\hat{H}_{int}^{QED}\,|\psi\rangle \propto \int d^3x\,\psi^*(\mathbf{x})\hat{\not{A}}\psi(\mathbf{x})$, for the interaction Hamiltonian $\hat{H}_{int}^{QED}$ of quantum electrodynamics and a spinor state of the form $|\psi\rangle \propto \int d^3x\,\psi(\mathbf{x})\hat{a}^\dagger(\mathbf{x})\,|0\rangle$. We can thus understand the coupling given by Eq.(2.7) as a model for the one-particle sector of a quantum field theory (up to subtleties related to the localizability of particle states in quantum field theory, see, e.g., [60]).

Another comment worth making here is the following. Oftentimes, the monopole moment coupling in the UDW detector model is viewed as a simplified version of the dipole coupling. For the interaction between the electromagnetic field and a hydrogen atom whose center of mass is described classically, the dipole coupling Hamiltonian arises as the leading order term in a multipolar expansion of the full interaction Hamiltonian. However, for a coherently delocalized hydrogen atom, it was pointed out in [61] that an additional term, the so-called Röntgen term, appears at the same order as the dipole coupling term in the multipole expansion. Therefore, if one wishes to modify the standard UDW detector model in a way that mimics as closely as possible the dipole coupling of a coherently delocalized hydrogen atom, then one should include an additional term in Eq.(2.4), such as to mimic not only the dipole term, but also the Röntgen term. For our purposes here, however, we do not view the coherently delocalized detector as a model for one specific matter system. Though a delocalizing hydrogen atom is an example of a delocalizing matter system, we here merely want to qualitatively discuss effects arising with interaction Hamiltonians of the form given in Eq.(2.4), and develop methods and intuition that can then be applied towards studying specific physical situations (for instance, atoms interacting with Bose-Einstein condensates, ions trapped in a harmonic potential interacting with light, electrons in a magnetic field interacting with light, etc.). We can thus view our coherently delocalized detector model as an *exploratory tool* to uncover potential new phenomena that may arise due to the coherent spreading of the center of mass wave function of a matter system. To make qualitative and quantitative predictions about the interaction between a quantum field and a specific delocalized matter system, we should then of course not rely too much on our exploratory tool, but rather consult a realistic model tailored towards the particular system in mind. To give an example, we will discuss in chapter 3 how to apply our methods towards studying quantitatively how the coherent center of mass delocalization affects the transition rates of a hydrogen atom.

With all the above being said, we are now prepared to dive into the calculations of transition amplitudes, probabilities and rates, for detectors with coherently delocalizing center of mass

degrees of freedom that interact with a scalar quantum field.

2.2 Spontaneous emission process for coherently delocalized detectors

Let us begin by investigating the process of spontaneous emission for a detector with quantized center of mass degrees of freedom, and compare it to the results we obtained in Subsection 1.4.1 for a UDW detector with classical center of mass. To calculate the spontaneous emission rate for a coherently delocalized detector, we start by considering an initial state at time t_i of the form

$$|\psi_i\rangle \;=\; |\varphi\rangle \otimes |e\rangle \otimes |0\rangle \;, \tag{2.12}$$

that is, we consider a detector whose center of mass is initially in a state $|\varphi\rangle$ and whose internal degree of freedom is initially excited, and we consider the field to be initially in its vacuum state. We can express the initial center of mass state both in terms of the initial center of mass wave function in the position or momentum representation,

$$|\varphi\rangle \;=\; \int d^3x\, \varphi(\mathbf{x})\, |\mathbf{x}\rangle = \int d^3p\, \widetilde{\varphi}(\mathbf{p})\, |\mathbf{p}\rangle \;, \tag{2.13}$$

with $|\mathbf{x}\rangle$ and $|\mathbf{p}\rangle$ the center of mass position and momentum eigenvectors. To calculate the transition probability amplitude for the system to end up in a final state at time t_f of the form

$$|\Psi_f\rangle = |\mathbf{r}\rangle \otimes |g\rangle \otimes |\mathbf{k}\rangle \;, \tag{2.14}$$

we first calculate the matrix elements

$$\langle \mathbf{r}|\, \hat{\mathcal{P}}(\mathbf{x},t)\, |\varphi\rangle \;=\; \int \frac{d^3p}{(2\pi)^3}\, \widetilde{\varphi}(\mathbf{p}) e^{-i(\mathbf{r}-\mathbf{p})\mathbf{x} + it\frac{r^2-p^2}{2M}} \tag{2.15}$$

$$\langle g|\, \hat{\mu}(t)\, |e\rangle \;=\; e^{-i\Omega t} \tag{2.16}$$

$$\langle \mathbf{k}|\, \hat{\phi}(\mathbf{x},t)\, |0\rangle \;=\; \frac{1}{(2\pi)^{3/2}} \frac{c}{\sqrt{2k}} e^{ickt - i\mathbf{k}\mathbf{x}} \,, \tag{2.17}$$

where $\mathbf{r}$ denotes the detector's center of mass recoil momentum. To first perturbative order, the spontaneous emission transition amplitude then becomes, up to a phase:

$$\mathcal{A} \;=\; \frac{\lambda c}{\sqrt{2k}} \frac{1}{(2\pi)^{9/2}} \int d^3p\, \widetilde{\varphi}(\mathbf{p}) \int d^3x\, e^{-i(\mathbf{k}+\mathbf{r}-\mathbf{p})\mathbf{x}} \int_{t_i}^{t_f} dt\, e^{it\left(\frac{\mathbf{r}^2-\mathbf{p}^2}{2M} - \Omega + ck\right)} \tag{2.18}$$

$$\;=\; \frac{\lambda c}{\sqrt{2k}} \frac{1}{(2\pi)^{3/2}} \widetilde{\varphi}(\mathbf{r}+\mathbf{k}) \int_{t_i}^{t_f} dt\, e^{it\left(-\frac{\mathbf{r}\cdot\mathbf{k}}{M} - \frac{k^2}{2M} - \Omega + ck\right)} \tag{2.19}$$

We here note that the transition amplitude does not only depend on the momentum $\mathbf{k}$ of the emitted photon, as it was the case within the UDW detector model, but also on the recoil momentum $\mathbf{r}$ of the detector. As we can see from Eq.(2.18), momentum conservation is automatically enforced: the momentum $\mathbf{k}$ of the emitted photon and the recoil momentum $\mathbf{r}$ of the detector are equal to the initial momentum $\mathbf{p}$ of the detector. Energy is conserved as well, provided that we take the limits $t_i \to -\infty$ and $t_f \to \infty$. Finite t_i and t_f would correspond to a sudden on and off switching of the interaction by an external agent. As a consequence, time translation invariance would be broken and energy would not be conserved. As in previous sections, we again eliminate such switching effects, by taking the limits $t_i \to -\infty$ and $t_f \to \infty$ and calculating the spontaneous emission rate. To obtain the total spontaneous emission rate $\mathcal{R}$ (that is, the spontaneous emission rate irrespective of the momentum of the emitted photon or the recoil momentum of the detector), we take the modulus squared of the transition amplitude $\mathcal{A}$ and trace over the Hilbert space $\mathcal{H}_F$ of the field and the Hilbert space $\mathcal{H}_{CM}$ of the center of mass:

$$\mathcal{R} = \int d^3k \int d^3r \, |\mathcal{A}|^2 \tag{2.20}$$

$$= \lambda^2 c^2 \int d^3k \int d^3r \, \frac{1}{2k} \frac{1}{(2\pi)^3} \, |\widetilde{\varphi}(\mathbf{r}+\mathbf{k})|^2 \int_{-\infty}^{\infty} dt \, e^{it\left(-\frac{\mathbf{r}\cdot\mathbf{k}}{M} - \frac{k^2}{2M} - \Omega + ck\right)} \tag{2.21}$$

Making the substitution $\mathbf{p} = \mathbf{r} + \mathbf{k}$ and carrying out the time integration, we obtain:

$$\mathcal{R} = \lambda^2 c^2 \int d^3k \int d^3p \, \frac{1}{2k} \frac{1}{(2\pi)^2} \, |\widetilde{\varphi}(\mathbf{p})|^2 \, \delta\left(-\frac{\mathbf{p}\cdot\mathbf{k}}{M} + \frac{k^2}{2M} - \Omega + ck\right) \tag{2.22}$$

We can further simplify this expression, by writing $\mathbf{p}\cdot\mathbf{k} = pk\cos(\theta) =: pkz$, with θ the angle between the detector's initial momentum and the momentum of the emitted photon:

$$\mathcal{R} = \frac{\lambda^2 c^2 M}{4\pi} \int d^3p \, |\widetilde{\varphi}(\mathbf{p})|^2 \int_0^{\infty} dk \int_{-1}^{1} dz \, \frac{1}{p} \, \delta\left(z - \frac{M}{pk}\left(\frac{k^2}{2M} - \Omega + ck\right)\right) \tag{2.23}$$

Explicitly carrying out the integrations over k and z, and defining the function

$$\mathcal{T}(p) := 2 - \frac{1}{p}\sqrt{(p+Mc)^2 + 2\Omega M} + \frac{1}{p}\sqrt{(p-Mc)^2 + 2\Omega M}\,, \tag{2.24}$$

we finally obtain the following expression for the spontaneous emission rate for a coherently delocalized detector:

$$\mathcal{R} = \frac{\lambda^2 c^2 M}{4\pi} \int d^3p \, |\widetilde{\varphi}(\mathbf{p})|^2 \mathcal{T}(p) \tag{2.25}$$

Since $\mathcal{T}$ does not depend on the initial center of mass wave function, we call it the *template function for spontaneous emission*. We find that the transition rate does not depend on the center of mass wave function directly, but only on the probability distribution $|\widetilde{\varphi}(\mathbf{p})|^2$.

Since within our framework we describe the dynamical evolution of the center of mass via the Schrödinger equation, we need to ensure that the virtual center of mass velocities are well within the non-relativistic regime. That is, we need to consider center of mass momentum probability distributions with contributions only for momenta corresponding to virtual velocities much smaller than the speed of light, $v := p/M \ll c$. This allows us to Taylor expand the template function around $p/(Mc) = 0$, such as to obtain to second order:

$$\mathcal{R} \;=\; \frac{\lambda^2 Mc^2}{2\pi} \int d^3p\, |\widetilde{\varphi}(\mathbf{p})|^2 \left[A + B \left(\frac{p}{Mc}\right)^2 + \mathcal{O}\left(\left(\frac{p}{Mc}\right)^4\right) \right] \tag{2.26}$$

This equation is valid only in the non-relativistic regime, and we here defined the constants

$$A \;:=\; 1 - \left(1 + \frac{2\Omega}{Mc^2}\right)^{-1/2} \qquad \text{and} \qquad B := \frac{\Omega}{Mc^2} \left(1 + \frac{2\Omega}{Mc^2}\right)^{-5/2} . \tag{2.27}$$

2.2.1 Gaussian center of mass wave packet state

Let us now specify an initial center of mass state of the detector. We could, for instance, consider a Gaussian center of mass wave packet, centered around the position $\mathbf{x} = \mathbf{x}_0$, which at time $t = 0$ is of the following form:

$$\varphi(\mathbf{x}) \;=\; \left(\frac{2}{\pi L^2}\right)^{3/4} e^{-|\mathbf{x}-\mathbf{x}_0|^2/L^2} \tag{2.28}$$

Fourier transforming this wave packet, we obtain the center of mass wave function at time $t = 0$ in momentum space:

$$\widetilde{\varphi}(\mathbf{p}) \;=\; \int \frac{d^3x}{(2\pi)^{3/2}}\, \varphi(\mathbf{x})\, e^{-i\mathbf{p}\mathbf{x}} \;=\; \left(\frac{L^2}{2\pi}\right)^{3/4} e^{-p^2L^2/4 - i\mathbf{p}\mathbf{x}_0} \tag{2.29}$$

According to the Schrödinger equation, a wave packet of this form flows together in space from past infinity towards $t = 0$, reaches a finite width L at time $t = 0$, and then flows apart again towards future infinity:

$$\varphi(\mathbf{x}, t) \;=\; \left(\frac{2}{\pi L^2}\right)^{3/4} \left(1 + \frac{2it}{ML^2}\right)^{-3/2} e^{-|\mathbf{x}-\mathbf{x}_0|^2 \left(L^2 + 2it/M\right)^{-1}} \tag{2.30}$$

The center of mass wave packet thus dynamically flows together and then spreads in position space. Meanwhile, the center of mass wave function in momentum space depends on time only via a complex phase,

$$\widetilde{\varphi}(\mathbf{p},t) \;=\; \left(\frac{L^2}{2\pi}\right)^{3/4} e^{-p^2L^2/4 - i\mathbf{p}\mathbf{x}_0 - itp^2/(2M)}\,, \tag{2.31}$$

so that the center of mass momentum probability distribution is constant in time:

$$|\widetilde{\varphi}(\mathbf{p},t)|^2 \equiv |\widetilde{\varphi}(\mathbf{p})|^2 \;=\; \left(\frac{L^2}{2\pi}\right)^{3/2} e^{-p^2L^2/2} \tag{2.32}$$

Therefore, no matter at what time we choose the center of mass wave packet to be localized in space according to Eq.(2.28), the resulting momentum probability distribution will always be of the form in Eq.(2.32). For the spontaneous emission rate for a delocalized detector, as we found in Eq.(2.25), all that matters is the initial momentum probability distribution. We could therefore imagine a wave packet that is localized in space according to Eq.(2.28) at time $t = 0$, and which first flows together and then spreads in space, but we could equally well imagine that the wave packet is localized in space according to Eq.(2.28) at time $t \to -\infty$, and which coherently spreads at all times. In either case, the center of mass momentum probability distribution is given by Eq.(2.32), and we obtain the following expression for the spontaneous emission rate:

$$\mathcal{R} \;=\; \frac{\lambda^2 Mc^2}{2\pi}\left[A + \frac{3B}{L^2} + \mathcal{O}\left((LMc)^{-4}\right)\right] \tag{2.33}$$

This approximation is valid for widths $L \gg L_0$, where $L_0 := 1/(Mc)$ is the Compton wavelength of the detector. This result shows that the faster the delocalization process, (i.e., the smaller the initial width L of the wave packet), the more the spontaneous emission rate is increased.

A possible experimental setup we might imagine here is the following. Let us consider an ion that is initially localized in the quadratic potential of an ion trap[1] [62, 63, 64]. Let us for simplicity assume that the center of mass is prepared in one of the energy eigenstates of the trapping potential, which we recall to be given by Hermite functions in three spatial dimensions. After switching the ion trap off, the center of mass wave function of the ion starts to coherently spread in space and the center of mass of the ion dynamically delocalizes. In order to avoid switching effects, we push the initial time (at which we assume that the ion trap is switched off)

[1] Of course, to make reliable quantitative predictions, one should consult a more sophisticated model of a trapped ion interacting with the electromagnetic field.

to $t_i \to -\infty$, and we do not include a description of the ion trap and the initial localization process in our model here. The lowest energy eigenstate of a harmonic trapping potential is simply a Gaussian of the form we considered in Eq.(2.28). For an ion whose center of mass is initially prepared in the lowest energy eigenstate of the trapping potential, the spontaneous emission rate is therefore given by Eq.(2.33). The rate depends on how sharply localized the center of mass is initially in position space, and therefore ultimately on the width of the trapping potential via which the ion was initially localized. We can intuitively understand the increased spontaneous emission rate for sharper initial localization as follows. The sharper the center of mass distribution is in position space, the wider it is in momentum space and the detector is thus more likely to have larger initial virtual velocities and correspondingly larger kinetic energies. Since we did not include a switching function in our detector model here, the energy for the spontaneous emission of a field quantum, accompanied by the recoil of the detector, is solely provided by the energy of the initial detector excitation and the quantum uncertain kinetic energy of the center of mass of the detector. Both by increasing Ω and by decreasing L, more energy is thus available for the spontaneous emission process to happen. We display this behaviour in Fig.(2.1): we plot the spontaneous emission rate as a function of the energy gap Ω of the detector, for different detector masses M and different initial delocalization widths L. As before, we again want to render all quantities in the plot dimensionless. When we considered transition probabilities before, we introduced switching functions of compact support, and the characteristic width σ of the switching function, together with the speed of light c, sets natural time and length scales. Now that we instead consider transition rates, that is, transition probabilities per unit time, the unit time interval, which we will denote by τ, together with the speed of light c, sets natural time and length scales. Further, the Planck constant $\hbar$ sets a natural mass scale. In our plots, we render all quantities dimensionless, by expressing them in terms of τ, c and $\hbar$.

We further observe in Fig.(2.1) that the spontaneous emission rate tends to zero for the case of a simple charge, $\Omega \to 0$. The initial quantum uncertain kinetic energy of the detector alone is not enough to excite the field: one could always perform a quantum reference frame transformation into the quantum uncertain rest frame of the detector, in which the kinetic energy of the detector vanishes, and in which the spontaneous emission process is thus energetically impossible. Finally, we see from Fig.(2.1) that the spontaneous emission rate increases for larger detector mass M. The smaller the detector mass, the more energy is required for the detector to recoil. The spontaneous emission of a field quantum is always accompanied by the recoil of the detector. As the detector mass decreases, the spontaneous emission process becomes energetically more

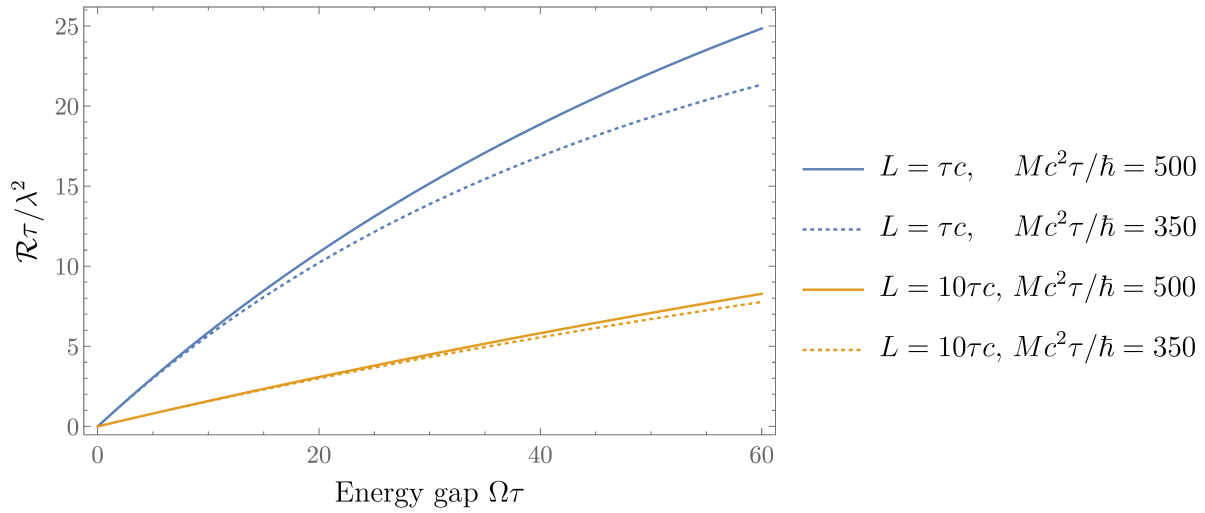

Figure 2.1: The spontaneous emission rate $\mathcal{R}$, as a function of the energy gap Ω of the detector, plotted for different detector masses M and initial delocalization widths L.

expensive and consequently, the spontaneous emission rate decreases.

2.2.2 Excited center of mass wave packet states

We might also be interested in the spontaneous emission rates for ions initially prepared in excited center of mass energy eigenstates of the harmonic trapping potential of an ion trap. For instance, we could prepare the ion in the first exited eigenstate of the trapping potential in each direction, described by the product of linear Hermite polynomials and a Gaussian:

$$|\varphi\rangle \;=\; \int d^3x \, \frac{8}{L^3} \, x_1 x_2 x_3 \left(\frac{2}{\pi L^2}\right)^{3/4} e^{-|\mathbf{x}-\mathbf{x}_0|^2/L^2} \, |\mathbf{x}\rangle \tag{2.34}$$

Compared to the spontaneous emission rate in Eq.(2.33), within our coherently delocalized detector model we find an increase in the spontaneous emission rate:

$$\mathcal{R} \;=\; \frac{\lambda^2 Mc^2}{2\pi} \left[A + \frac{9B}{L^2} + \mathcal{O}\left((LMc)^{-4}\right)\right] \tag{2.35}$$

This increase is sensible since the excited center of mass wave function in Eq.(2.34) possesses more energy and momentum than the ground state wave function of the trapping potential in Eq.(2.28). The center of mass therefore spreads faster and has more kinetic energy, leading to a larger energy budget for the process of spontaneous emission to happen.

2.2.3 Recovering the UDW detector results in the limit of large detector mass and correspondingly slow delocalization

Intuitively, the dynamical coherent delocalization of matter affects processes such as spontaneous emission, since the dynamical delocalization process introduces an effective time-dependence into the interaction. As we discussed, the center of mass of a coherently delocalized matter system dynamically spreads in space. The virtual velocities at which our detector spreads however depends on the detector mass. For a given a center of mass momentum probability distribution, in the limit of larger and larger detector mass, the center of mass wave function spreads more and more slowly. In the limit of infinite detector mass, the dynamical delocalization process of the center of mass "freezes out", and the wave function only phase rotates in time. Provided a certain initial center of mass delocalization, the center of mass therefore does not delocalize any further in space. Let us here see what happens to the spontaneous emission rate in the infinite mass limit. First, we expand the template function $\mathcal{T}$ for large detector masses M, i.e., for $Mc^2 \gg \Omega$ and $Mc \gg p$, to obtain to lowest order:

$$\mathcal{T}_0 \;=\; \frac{2\Omega}{Mc^2} \tag{2.36}$$

Since the template function to lowest order does not depend on $\mathbf{p}$, and since the center of mass momentum probability distribution is normalized, we can then carry out the integral in Eq.(2.25) and obtain, in the limit of infinite detector mass, the following spontaneous emission rate:

$$\mathcal{R}_0 \;=\; \frac{\lambda^2 c^2 M}{4\pi} \int d^3p \, |\widetilde{\varphi}(\mathbf{p})|^2 \, \mathcal{T}_0 \;=\; \frac{\lambda^2 \Omega}{2\pi} \tag{2.37}$$

We notice that the rate $\mathcal{R}_0$ coincides with the spontaneous emission rate which we obtained in Eq.(1.46) for a standard UDW detector with classical center of mass degrees of freedom. This means that for a coherently delocalized detector, as far as the spontaneous emission rate is concerned, we indeed recover the result for a standard UDW detector in the infinite mass limit. Consequently, it is not the *amount of initial delocalization* of the center of mass, but rather the *dynamics of its delocalization process* that affects the spontaneous emission rate.

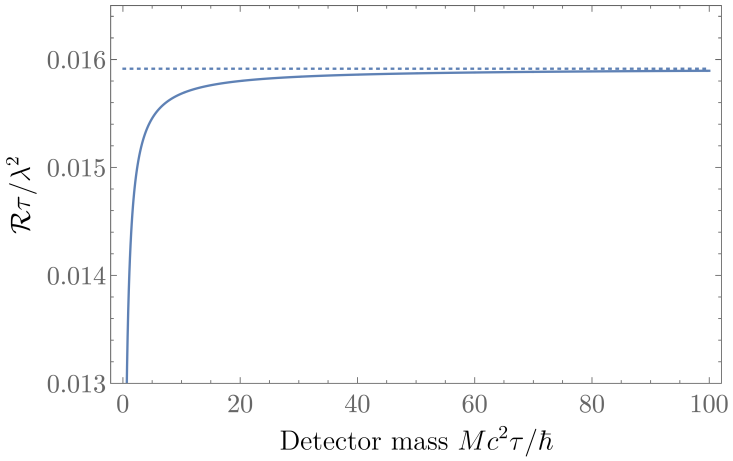

Figure 2.2: The spontaneous emission rate as a function of the detector mass, plotted for a massive detector with delocalization width $L = 100\tau c$ and energy gap $\Omega\tau = 0.1$. The dotted line represents the spontaneous emission rate for a pointlike UDW detector with energy gap $\Omega\tau = 0.1$.

For finite but large detector masses, taking into account the lowest order correction,

$$\mathcal{T} \;=\; \mathcal{T}_0 - \frac{3\Omega^2}{c^4 M^2} + \mathcal{O}\left(\left(\frac{\Omega}{Mc^2}\right)^2, \left(\frac{p}{Mc}\right)^2\right), \tag{2.38}$$

shows that the spontaneous emission rate decreases, compared to the spontaneous emission rate for a standard UDW detector. The spontaneous emission rate given in Eq.(2.33) is displayed in Fig.(2.2) as a function of the detector mass M, for a Gaussian delocalized massive detector with $L = 100\tau c$ and $\Omega\tau = 0.1$. The plot confirms that the spontaneous emission rate for a standard UDW detector is approached in the limit of $M \to \infty$. It also confirms that the spontaneous emission rate decreases for finite detector masses $M \to 0$, for which the detector spreads at non-zero virtual velocities. We note that for our choice of $L = 100\tau c$ here, the non-relativistic expansion breaks down for masses smaller than $Mc^2\tau/\hbar \approx 3.5$ and we should therefore only trust the plot for masses $Mc^2\tau/\hbar \gtrsim 3.5$.

2.2.4 Incoherent versus coherent delocalization

The delocalization process of the center of mass can be coherent or in part also incoherent, depending on the purity of the initial center of mass state. So far we assumed the center of mass of the detector to be initially in a pure wave packet state $|\varphi\rangle$. However, for instance with the help of a double-slit experiment, one could imagine preparing the center of mass of the detector in a (coherent or incoherent) superposition of several wave packet states.

For instance, the center of mass could initially be in a coherent superposition, $|\varphi\rangle \sim |\xi\rangle + \alpha\,|\chi\rangle$, with a phase $\alpha \in \mathbb{C}$ and with $|\xi\rangle$ and $|\chi\rangle$ Gaussian wave packet states, respectively centered

around $\mathbf{x} = \mathbf{x}_0$ and $\mathbf{x} = -\mathbf{x}_0$. We intuitively expect that the spontaneous emission rate could be affected by the interference between the two wave packets, except of course in the limits $x_0 \to 0$ and $x_0 \to \infty$, with $x_0 := |\mathbf{x}_0|$, in which the overlap of the two wave packets in position space would be trivial. Indeed, we find that the spontaneous emission rate for the coherent superposition,

$$\mathcal{R} \;=\; \frac{\lambda^2 Mc^2}{2\pi}\Big[A + \frac{3B}{L^2}\left(1 - f(x_0,\alpha)\right) + \mathcal{O}\left((LMc)^{-4}\right)\Big], \tag{2.39}$$

now depends both on the separation $2x_0$ and on the phase α between the two interfering wave packets:

$$f(x_0,\alpha) \;:=\; \frac{4x_0^2}{3L^2}\frac{2\,\mathrm{Re}(\alpha)e^{-2x_0^2/L^2}}{1+|\alpha|^2+2\,\mathrm{Re}(\alpha)e^{-2x_0^2/L^2}} \tag{2.40}$$

We can easily confirm that the spontaneous emission rate reduces to the rate for a single Gaussian wave packet in the limits $x_0 \to 0$ and $x_0 \to \infty$. We further notice that the rate for a single Gaussian wave packet is also recovered for a purely imaginary phase, $\mathrm{Re}(\alpha) = 0$, and whenever the two superposed wave functions are orthogonal to one another, since the spontaneous emission rate only depends on the modulus squared of the initial center of mass wave function.

Alternatively, the center of mass could initially be in a superposition which is in part also incoherent. For instance, in a double-slit experiment, one could prepare the center of mass in the mixed state $\rho = \frac{1}{2}\left(|\xi\rangle\langle\xi| + |\chi\rangle\langle\chi|\right)$, by leaving only one of the two slits open at a time. The spontaneous emission rate for the partly incoherent superposition is the same as the spontaneous emission rate for a single Gaussian wave packet, as given by Eq.(2.33).

We conclude that the light-matter interaction indeed distinguishes between coherent and incoherent delocalization.

2.3 Absorption process for coherently delocalized detectors

Let us now study the impact of a detector's coherent center of mass delocalization on the absorption process. We consider an initial state at time t_i of the form

$$|\psi_i\rangle \;=\; |\varphi\rangle \otimes |g\rangle \otimes |\mathbf{k}\rangle\ , \tag{2.41}$$

for which the quantum field is in a single particle state, and consider the transition to a final state at time t_f of the form

$$|\Psi_f\rangle \;=\; |\mathbf{r}\rangle \otimes |e\rangle \otimes |0\rangle \;. \tag{2.42}$$

We obtain the following transition amplitude, up to a phase and to first perturbative order:

$$\mathcal{A} \;=\; \frac{\lambda c}{\sqrt{2k}} \frac{1}{(2\pi)^{3/2}} \widetilde{\varphi}(\mathbf{r}-\mathbf{k}) \int_{t_i}^{t_f} dt e^{it\left(\Omega - ck + \frac{\mathbf{r}\cdot\mathbf{k}}{M} - \frac{k^2}{2M}\right)} \tag{2.43}$$

Tracing over the detector's recoil momentum $\mathbf{r}$, we obtain the absorption probability rate:

$$\mathcal{R} \;=\; \frac{\lambda^2 c^2}{2k} \frac{1}{(2\pi)^3} \int d^3p |\widetilde{\varphi}(\mathbf{p})|^2 \int_{-\infty}^{\infty} dt e^{it\left(\Omega - ck + \frac{\mathbf{p}\cdot\mathbf{k}}{M} + \frac{k^2}{2M}\right)} \tag{2.44}$$

Let us assume that the to-be-absorbed field quantum propagates along the $z-$direction, $\mathbf{k} = (0,0,k)^T$, and that the initial center of mass wave function is a Gaussian wave packet as given in Eq.(2.29). The absorption rate then simplifies to:

$$\mathcal{R} \;=\; \frac{\lambda^2 c^2}{k^2 8\pi^2} \frac{ML}{\sqrt{2\pi}} \exp\left(-\frac{L^2 M^2}{2k^2} \left(\Omega - ck + \frac{k^2}{2M} \right)^2 \right) \tag{2.45}$$

Let us confirm that in the limit of very large detector mass, we again recover the result we obtained for a standard UDW detector with classical center of mass degrees of freedom. We use the fact that we can write a delta distribution as an infinitely peaked Gaussian,

$$\delta(x) \;=\; \lim_{\epsilon \to 0^+} \frac{1}{\sqrt{2\pi\epsilon}} e^{-\frac{x^2}{2\epsilon}} \,, \tag{2.46}$$

to obtain for the absorption rate in the infinite mass limit:

$$\lim_{M\to\infty}(\mathcal{R}) \;=\; \frac{\lambda^2 \Omega}{2\pi} \frac{1}{4\pi k^2} \delta\left(\frac{\Omega}{c} - k \right) \,. \tag{2.47}$$

This is indeed the absorption rate which we obtained in Eq.(1.54) for a standard UDW detector at rest. While standard UDW detectors can only absorb photons whose momenta are on-resonance (i.e., photons whose momenta match the detector's energy gap, $ck = \Omega$), Eq.(2.45) shows that quantum delocalized detectors of finite mass M can, to a certain extent, also absorb off-resonance photons. The absorption rate for off-resonance field excitations is however Gaussian suppressed. In Fig.(2.3), we plot the absorption rate as a function of the momentum k of the to-be-absorbed photon, for different detector masses M, where we fixed $L = 10\tau c$ and $\Omega\tau = 0.2$.

The plot shows that quantum delocalized detectors can absorb off-resonance photons (i.e., for the parameters we chose here, photons with $k\tau c \neq 0.2$)[2]. We can see that the smaller the detector mass, that is, the faster the dynamical delocalization process of the detector's center of mass, the more off-resonance the absorption process becomes. Intuitively, we can understand this phenomenon by reminding ourselves that small masses correspond to large virtual velocities with correspondingly large kinetic energies. Combined with the kinetic energy uncertainty of the quantum uncertain center of mass, we expect that the spectral distribution of photons which the detector can absorb becomes wider and shifts towards higher photon momenta k. We find this intuition confirmed in Fig.(2.3).

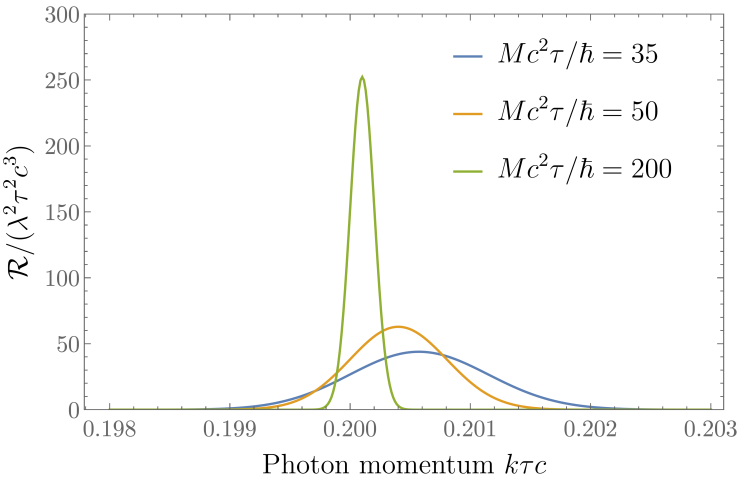

Figure 2.3: The absorption rate for a quantum delocalized detector, as a function of the momentum k of the to-be-absorbed photon, plotted for different detector masses M (with $\Omega\tau = 0.2$ and $L = 10\tau c$). The smaller the detector mass (i.e., the faster the dynamical delocalization process), the more favorable the absorption of photons with large momenta becomes.

2.4 Vacuum excitation process for coherently delocalized detectors

Lastly, let us here study the vacuum excitation process for quantum delocalized detectors. As we discussed in section 1.4.3, a UDW detector at rest, which is switched on at all times, can not become excited by the vacuum. This is simply because no energy is available for this vacuum excitation process to happen. The same holds true for an inertial UDW detector which is switched on at all times: we can always perform a reference frame transformation into the

[2]Of course, in a sense, the process is still on-resonance. However, the energy balance now includes not only the detector's energy gap and the energy of the to-be-absorbed photon, but also the quantum uncertain initial kinetic energy of the detector, as well as the recoil energy.

rest frame of the detector, in which we can easily convince ourselves that there is no energy available for the process to happen. In order to obtain a non-vanishing vacuum excitation probability for inertial UDW detectors, one needs to introduce a switching function. Taking the quantum delocalization of the detector's center of mass into account, we may now ask whether the quantum uncertainty of the kinetic energy of the detector might make the vacuum excitation process possible, without needing to introduce a switching function. The answer to this question is no: employing the formalism of quantum reference frames [65, 66, 67, 68, 69, 70], one can always transform into the quantum uncertain rest frame of the detector, for which the vacuum state of the quantum field transforms trivially and thus, again, no energy is available for the vacuum excitation process to happen.

Even without employing the formalism of quantum reference frames, we can convince ourselves [3] that the coherent dynamical delocalization process cannot trigger vacuum excitation. For this purpose, let us consider a UDW detector in its ground state, with quantized center of mass, coupled to a scalar quantum field in its ground state:

$$|\Psi_i\rangle \;=\; |\varphi\rangle \otimes |g\rangle \otimes |0\rangle \tag{2.48}$$

For the transition probability to a state in which both the detector and the field are excited,

$$|\Psi_f\rangle \;=\; |\mathbf{r}\rangle \otimes |e\rangle \otimes |\mathbf{k}\rangle \;, \tag{2.49}$$

we obtain the vacuum excitation rate

$$\mathcal{R} \;=\; \frac{\lambda^2 c^2}{4\pi} \int d^3p \, |\widetilde{\varphi}(\mathbf{p})|^2 \, \mathcal{T}(p) \,, \tag{2.50}$$

where we traced over the momentum $\mathbf{k}$ of the emitted photon and the recoil momentum $\mathbf{r}$. We here again defined a template function, $\mathcal{T}$, as follows:

$$\mathcal{T}(p) \;:=\; \int_0^\infty dk \int_{-1}^1 dz \, k \, \delta\left(-\frac{pkz}{M} + \frac{k^2}{2M} + \Omega + ck\right) \tag{2.51}$$

Remembering that $\delta(ax) = \delta(x)/|a|$, we rewrite the template function as

$$\mathcal{T}(p) \;=\; \int_0^\infty dk \int_{-1}^1 dz \, \frac{M}{p} \, \delta\left(z - \frac{M}{pk}\left(\frac{k^2}{2M} + \Omega + ck\right)\right) \tag{2.52}$$

$$=: \; \int_0^\infty dk \int_{-1}^1 dz \, \frac{M}{p} \, \delta\left(f(z,k)\right) \,. \tag{2.53}$$

[3] ... at least in the regime of non-relativistic virtual delocalization speeds. To make a general statement valid also in the relativistic regime, more sophisticated tools, such as quantum reference frames, are needed (see a soon-to-be-published paper by Flaminia Giacomini and Achim Kempf).

The here defined function f has zeros for $z = \frac{M}{pk}\left(\frac{k^2}{2M} + ck + \Omega\right)$. Since the range of the variable z is restricted to $z \in [-1, 1]$, the conditions for the delta distribution to peak are $p \geq Mc + \sqrt{2\Omega M}$ and $k_- \leq k \leq k_+$, with $k_\pm = p - cM \pm \sqrt{(p - cM)^2 - 2\Omega M}$. We can thus rewrite the template function as follows:

$$\begin{aligned} \mathcal{T}(p) &= \int_0^\infty dk\, \frac{M}{p}\, \Theta(k - k_-)\Theta(k_+ - k)\Theta(p - Mc - \sqrt{2\Omega M}) && (2.54) \\ &= \frac{2M}{p}\sqrt{(p - cM)^2 - 2\Omega M}\, \Theta(p - Mc - \sqrt{2\Omega M})\,. && (2.55) \end{aligned}$$

Since c here denotes the speed of light, and the detector's virtual center of mass velocities are strictly smaller than the speed of light, $p/M < c$, the Heaviside step function Θ in Eq.(2.55) is always zero within the physical region of interest. We conclude that the vacuum excitation process does not occur.

To obtain a non-vanishing vacuum excitation probability, an external agent needs to provide the system with energy, for instance by switching the interaction of the detector and the quantum field on and off. In section 1.4.3, we calculated in Eq.(1.63) the vacuum excitation probability for a UDW detector, whose interaction with the quantum field is switched on and off via a Gaussian switching function, and whose spatial profile is modeled via a Gaussian smearing profile. Let us here compare this result to the vacuum excitation probability for a quantum delocalized detector, whose interaction with the quantum field is switched on and off via a Gaussian switching function, and whose center of mass wave function is a Gaussian wave packet. The interaction Hamiltonian we need to use for this purpose is the following:

$$\hat{H}_{int}(t) = \lambda\chi(t) \int d^3x\, \mathcal{P}(\mathbf{x}, t) \otimes \hat{\mu}(t) \otimes \hat{\phi}(\mathbf{x}, t) \qquad (2.56)$$

We obtain the following expression for the vacuum excitation probability:

$$P = \frac{\lambda^2 c^2}{(2\pi)^3} \int d^3p \int \frac{d^3k}{2k}\, |\widetilde{\varphi}(p)|^2 \left| \int_{-\infty}^{\infty} dt\, \chi(t)\, e^{i\left(\Omega + ck + \frac{k^2 - 2\mathbf{pk}}{2M}\right)t} \right|^2 \qquad (2.57)$$

Inserting the Gaussian switching function given in Eq.(1.18), we obtain:

$$\begin{aligned} P = \frac{\lambda^2 c^2 \sqrt{\pi}\sigma M}{2} \int_0^\infty dp\, p\, |\widetilde{\varphi}(p)|^2 \int_0^\infty dk \Big[&\mathrm{Erf}\left(\sigma\left(\Omega + ck + \tfrac{k^2 + 2pk}{2M}\right)\right) \\ &- \mathrm{Erf}\left(\sigma\left(\Omega + ck + \tfrac{k^2 - 2pk}{2M}\right)\right) \Big] \end{aligned} \qquad (2.58)$$

We again Taylor expand the function over which the momentum wave function is integrated, around non-relativistic center of mass velocities, $v := p/M \ll c$, such as to obtain:

$$\begin{aligned} P &= 2\sigma^2\lambda^2c^2\int_0^\infty dp\int_0^\infty dk\, kp^2\,|\widetilde{\varphi}(p)|^2\, e^{-\sigma^2\left(\Omega+ck+\frac{k^2}{2M}\right)^2} \\ &\quad\times\left[1+p^2\,\frac{2k^2\sigma^4}{3M^2}\left(\left(\Omega+ck+\tfrac{k^2}{2M}\right)^2-\frac{1}{2\sigma^2}\right)+\mathcal{O}\left(\left(\frac{p}{Mc}\right)^4\right)\right] \end{aligned} \tag{2.59}$$

Inserting the Gaussian center of mass wave packet given in Eq.(2.29), the vacuum excitation probability finally becomes:

$$\begin{aligned} P &= \frac{\sigma^2\lambda^2c^2}{16\sqrt{2}\pi L^2M^4}\int_0^\infty dk\, e^{-\sigma^2\left(\Omega+ck+\frac{k^2}{2M}\right)^2}\Big[4kL^2M^4+2k^3M^2\sigma^2(2\sigma^2\Omega^2-1) \\ &\quad+8k^4M^2\sigma^4\Omega+4k^5M\sigma^4(M+\Omega)+4k^6M\sigma^4+k^7\sigma^4\Big]+\mathcal{O}\left((LMc)^{-4}\right) \end{aligned} \tag{2.60}$$

We can evaluate the remaining integration over the photon momenta k numerically. In Fig.(2.4), we plot the excitation probability for a quantum delocalized detector as well as for a comparable classically smeared UDW detector with Gaussian smearing profile. We can clearly see that the result for a quantum delocalized detector differs from the result we obtain by introducing a classical spatial smearing profile. For the massive detectors, we chose parameters M and L such as to keep their product fixed, $MLc/\hbar = 500$, which ensures that we compare detectors that dynamically delocalize according to the same virtual velocity distribution. We find that the vacuum excitation probability for coherently delocalized detectors of delocalization width L is larger than the vacuum excitation probability for Gaussian smeared UDW detectors of the same width L.

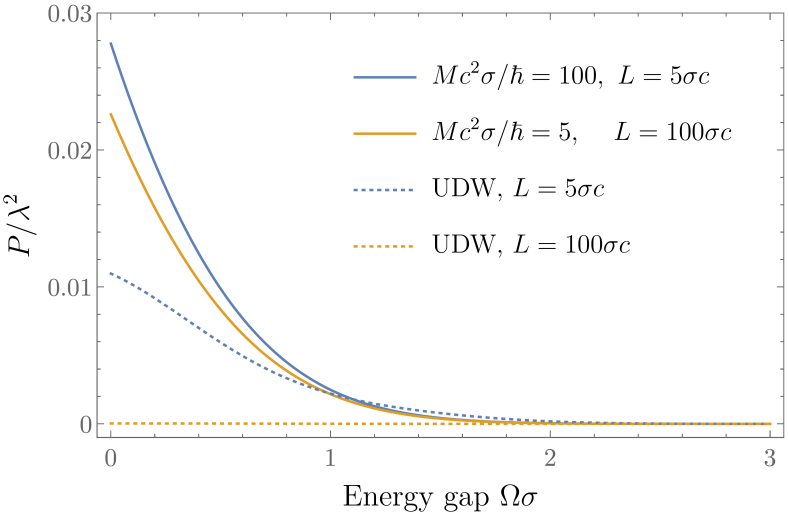

Figure 2.4: The vacuum excitation probability as a function of the energy gap $\Omega\sigma$, for Gaussian switching of width σ, both for massive detectors with Gaussian delocalized quantum centers of mass and for Gaussian smeared UDW detectors.

Let us here again take a moment to comment on the limit of large detector masses. Going back to Eq.(2.57), we find that the vacuum excitation probability becomes independent of the center of mass wave function in the limit of infinite detector masses:

$$\lim_{M\to\infty}(P) \;=\; \frac{\lambda^2 c^2}{(2\pi)^3}\int \frac{d^3k}{2k}\left|\int_{-\infty}^{\infty} dt\,\chi(t)\,e^{i(\Omega+ck)t}\right|^2 \tag{2.61}$$

We recover the vacuum excitation probability for a pointlike UDW detector with switching profile $\chi(t)$. In section 2.2 we had already observed that in the infinite detector mass limit, in which the dynamical delocalization process "freezes out", and the center of mass delocalization becomes static, we recover the results for pointlike UDW detectors, rather than the results for spatially smeared UDW detectors. In the following section, let us briefly comment on the difference between quantum center of mass delocalization on one hand, and detector delocalization modeled via classical spatial smearing profiles, as discussed in section 1.3, on the other hand.

2.5 Smearing profiles and coherent center of mass delocalization

When quantizing the center of mass degrees of freedom instead of introducing a spatial smearing profile, we found that in the infinite mass limit, processes such as spontaneous emission or vacuum excitation do *not* depend on the center of mass wave function. We concluded that these processes do not depend on the static center of mass delocalization, but rather on the dynamical delocalization process. However, if we wanted to use the center of mass probability distribution as a classical smearing function for the UDW detector model, as we saw in sections 1.4.1 and 1.4.3, we would find that the spontaneous emission or vacuum excitation rates depend explicitly on the classical smearing profile employed—even in the infinite mass limit, in which the delocalization is static. We can thus conclude that center of mass delocalization *cannot* be appropriately described by interpreting the center of mass probability distribution as a spatial smearing profile.

As we saw in section 1.3, for the delocalization arising from the orbitals of the detector, one can derive smearing functions from the orbital wave functions of an atom. The such obtained, physically motivated, spatially smeared UDW detector model then accounts for the spatial extent of the detector due to its orbital wave functions. Let us now see whether we can perform a similar calculation for the delocalization arising from the center of mass wave function of the

detector. To this end, we assume the quantum mechanical position operator $\hat{\mathbf{x}}$ in Eq.(1.33) to be no longer associated with the position operator corresponding to the detector's internal degrees of freedom, but rather with the position operator corresponding to the detector's quantized center of mass degrees of freedom. Instead of inserting resolutions of the identity in terms of the discrete orbital energy eigenfunctions, we now insert resolutions of the identity in terms of the continuous center of mass momentum eigenfunctions:

$$\begin{aligned}
\hat{H}_{int} &= \lambda\hat{\mu}\int d^3x\,\hat{\phi}(\mathbf{x})\,\delta^{(3)}(\mathbf{x}-\hat{\mathbf{x}}) && (2.62)\\
&= \lambda\hat{\mu}\int d^3p\int d^3q\int d^3x\int d^3y\,\hat{\phi}(\mathbf{x})\,\delta^{(3)}(\mathbf{x}-\mathbf{y})\,\langle\mathbf{p}|\mathbf{y}\rangle\,\langle\mathbf{y}|\mathbf{q}\rangle\,|\mathbf{p}\rangle\,\langle\mathbf{q}| && (2.63)\\
&= \lambda\hat{\mu}\int d^3x\,\hat{\phi}(\mathbf{x})\int d^3p\int d^3q\,\psi^*_{\mathbf{p}}(\mathbf{x})\,\psi_{\mathbf{q}}(\mathbf{x})\,|\mathbf{p}\rangle\,\langle\mathbf{q}| && (2.64)
\end{aligned}$$

Here, $\psi_{\mathbf{p}}(\mathbf{x}) := \langle\mathbf{x}|\mathbf{p}\rangle = (2\pi)^{-3/2}e^{i\mathbf{p}\cdot\mathbf{x}}$ denote the momentum eigenfunctions in the position representation[4]. We thus find that, in some sense, we can interpret the interaction Hamiltonian as a spatially smeared interaction:

$$\hat{H}_{int} = \lambda\hat{\mu}\int d^3x\,\hat{\phi}(\mathbf{x})\,\hat{F}(\mathbf{x})\,, \qquad \text{with} \quad \hat{F}(\mathbf{x}) = \int d^3p\int d^3q\,\psi^*_{\mathbf{p}}(\mathbf{x})\,\psi_{\mathbf{q}}(\mathbf{x})\,|\mathbf{p}\rangle\,\langle\mathbf{q}| \qquad (2.65)$$

However, now the "smearing profile" $\hat{F}(\mathbf{x})$ is operator valued. In the center of mass momentum eigenbasis, it can be expressed in terms of the center of mass energy wave functions that correspond to the continuous center of mass energy spectrum. We can thus think of the interaction Hamiltonian as a spatially smeared coupling, where the center of mass momentum eigenfunctions give rise to an operator valued smearing profile. We now also see why, throughout this chapter, we obtained different results for the coherently delocalized detector model with an operator valued smearing profile on one hand, and the UDW detector model with a classical smearing profile on the other hand.

2.6 Virtual Cherenkov-like effect

In this section, we consider a quantum delocalized detector that couples to a medium. We investigate whether the dynamical delocalization process of the detector's center of mass wave function can trigger the excitation of the detector and the medium.

[4]Note that the center of mass momentum eigenstates of the detector are also energy eigenstates.

First, let us recall that a charged classical particle traveling at a constant velocity through the Minkowski vacuum will not spontaneously emit field quanta, simply because there is no energy available to create these field quanta in the particle's rest frame. However, in a medium, a charged particle traveling at a constant velocity can emit *Cherenkov radiation*, namely if its velocity is faster than the wave propagation speed c_s in the medium [71, 72, 73]. This is because in media, boosts are nontrivial, and the ground state of the medium is perceived as an excited state in the rest frame of a particle travelling at velocities $v > c_s$.

Here, we ask whether merely *virtual* motion of a quantum delocalized detector in a medium, due to the coherent spreading of the detector, can trigger the emission of radiation along with the excitation of the detector. The idea is that this *Virtual Cherenkov-like effect* could arise due to those parts of the center of mass momentum wave function that correspond to virtual center of mass velocities exceeding the wave propagation speed c_s of the medium. To investigate this idea, we here consider a delocalized detector, coupled to a field whose wave propagation speed is smaller than the speed of light (e.g., a dispersive medium, or a field of quasiparticles or collective excitations, such as spin waves or phonons in Bose Einstein condensates). We model these fields in a very simplified manner, namely as scalar quantum fields with wave propagation speed c_s:

$$\hat{\phi}(\mathbf{x},t) \;=\; \int \frac{d^3k}{(2\pi)^{3/2}}\sqrt{\frac{c_s^2}{2k}}\left(e^{-ic_skt+i\mathbf{kx}}\hat{a}_{\mathbf{k}}+\text{H.c.}\right) \tag{2.66}$$

We now use these scalar field operators in the interaction Hamiltonian as given in Eq.(2.8), and assume that the delocalized detector and the scalar quantum field are initially both in their ground state. Following the same calculations we performed in section 2.4, we obtain the excitation probability rate

$$\mathcal{R} \;=\; \frac{\lambda^2 c_s^2}{4\pi}\int d^3p\,|\widetilde{\varphi}(\mathbf{p})|^2\,\mathcal{T}_{c_s}(p)\,, \tag{2.67}$$

where we defined the following template function:

$$\mathcal{T}_{c_s}(p) \;=\; \frac{2M}{p}\sqrt{(p-c_sM)^2-2\Omega M}\,\Theta(p-Mc_s-\sqrt{2\Omega M}) \tag{2.68}$$

The Heaviside step function Θ in the template function implies that a finite excitation probability arises, indeed, from those parts of the initial center of mass momentum distribution for which $p \geq Mc_s+\sqrt{2\Omega M}$. That is, at least parts of the center of mass wave function must spread faster than $v_{crit} := c_s + \sqrt{2\Omega/M}$. We refer to v_{crit} as the *critical velocity*, set by the wave propagation speed c_s in the medium and by the mass M and energy gap Ω of the detector.

Let us here emphasize that while the usual Cherenkov effect arises for classical charges coupled to *classical fields*, the virtual Cherenkov-like effect which we encounter here, due to virtual motion alone, arises for delocalized detectors coupled to *relativistic quantum fields*. Further, unlike usual Cherenkov radiation for *simple charges*, the Cherenkov-like emission of radiation is accompanied by the *excitation of the detector's internal degree of freedom*, as well as the *recoil of the detector's center of mass*. Concretely, for instance for an atom or ion coupling to the electromagnetic field in a medium, we expect that sufficiently superluminal virtual center of mass velocities can lead to the excitation of the atom or ion and the emission of a photon. In the same way, sufficiently supersonic center of mass virtual velocities of an atom in a Bose Einstein condensate should lead to the excitation of the atom and the emission of a phonon. We here note that since we work within the non-relativistic regime as far as the center of mass motion is concerned, we need to ensure that the supersonic virtual center of mass velocities are much smaller than the vacuum speed of light. As a potential experimental setup we could thus for instance imagine localizing an atom in a Bose Einstein condensate, for which the sound propagation speed could be as low as millimeters per second [74], so that atoms with virtual velocities above v_{crit} could still be well within the non-relativistic regime.

We can view the virtual Cherenkov-like effect as a type of friction, which, to some extent, hinders the particle's position wave function from spreading supersonically: for supersonic virtual center of mass velocities, the detector tends to become excited and emit a field quantum, which causes the detector to recoil, resulting in a slowed down spreading of the detector's center of mass wave function. To study this friction effect in more detail, let us here calculate the excitation probability rate as a function of the detector's recoil momentum:

$$\mathcal{R}(\mathbf{r}) \;=\; \frac{\lambda^2 c^2}{4\pi^2}\int d^3k\,\frac{1}{2k}\,|\widetilde{\varphi}(\mathbf{r}+\mathbf{k})|^2\,\delta\left(\Omega+ck-\frac{\mathbf{r}\cdot\mathbf{k}}{M}-\frac{k^2}{2M}\right) \tag{2.69}$$

We again consider the spherically symmetric Gaussian center of mass wave packet given in Eq.(2.29). We further rotate our coordinate system, without loss of generality, in such a way that the emitted photon propagates in the $z-$direction, $\mathbf{k}=(0,0,k)$. We finally trace over the recoil direction, to obtain the excitation rate as a function of the magnitude r of the recoil momentum:

$$\mathcal{R}(r) \;=\; \frac{\lambda^2 c\,L\,e^{-L^2(r^2+2\Omega M)/2}}{2r(2\pi)^{5/2}}\left[e^{-L^2cM\left(cM-r+\sqrt{(cM-r)^2+2\Omega M}\right)}-e^{-L^2cM\left(cM+r+\sqrt{(cM+r)^2+2\Omega M}\right)}\right] \tag{2.70}$$

In order to avoid Gaussian suppression of the excitation rate, we need the width L of the Gaussian center of mass wave packet to be sufficiently small: as we saw in Eq.(2.68), we need

the initial center of mass probability distribution $|\widetilde{\varphi}(\mathbf{p})|^2$ to have contributions for momenta $p \geq Mv_{crit}$, in order for the virtual Cherenkov-like effect to happen, and for the detector's virtual center of mass velocities to be slowed down via the recoil. The largest momenta in the Gaussian center of mass probability distribution are, within 3.5 standard deviations away from the mean, momenta with $pL \approx 3.5$. Thus, for the excitation process to happen, we need an initial wave packet width L satisfying $LMv_{crit}/\hbar \lesssim 3.5$. As an example, let us here choose parameters $c_s = 10^{-3}c$, $Mc^2\tau/\hbar = 500$ and $\Omega\tau = 10^{-2}$, which yields a critical velocity of $v_{crit} \approx 7.3 \times 10^{-3}c$. We thus need initial delocalization widths $L \lesssim \tau c$ in order for the virtual Cherenkov-like effect to occur. Assuming that velocities are non-relativistic if they are smaller than 1% of the vacuum speed of light, we find that delocalization widths $L \gtrsim 0.7\tau c$ correspond to virtual center of mass velocities within the non-relativistic regime. In Fig.(2.5) we plot the transition rate as a function of the magnitude r of the recoil momentum. For a range of different initial delocalization widths L, we find that the excitation rate reaches its maximum for recoil momentum $r = 0$, for which the initially supersonically delocalizing detector ends up at rest, as a result of the virtual Cherenkov-like effect. This confirms that virtual center of mass velocities above the critical velocity are indeed slowed down, via the emission of Cherenkov-like radiation and the excitation and recoil of the detector. The plot in Fig.(2.5) moreover confirms that the virtual Cherenkov-like effect does *not* occur for detectors whose initial center of mass wave functions have no contributions above the critical velocity (the curve with $L = 1.2\tau c$ in our plot), and their center of mass position wave functions spread unhindered.

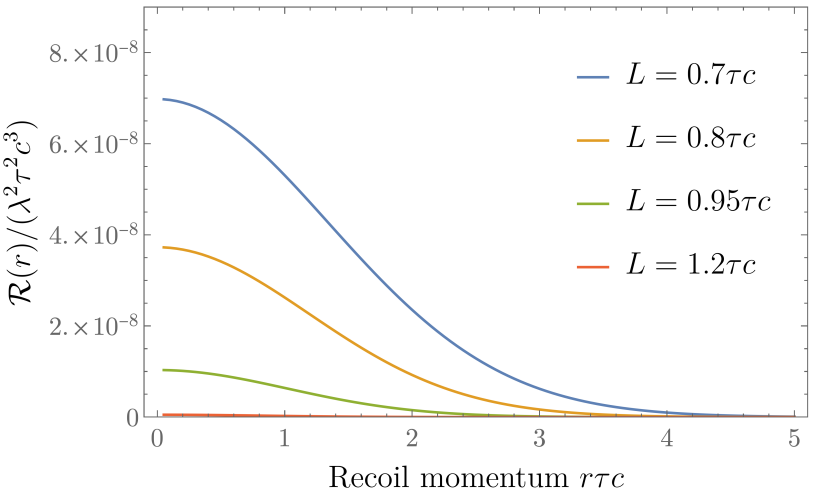

Figure 2.5: The vacuum excitation probability rate as a function of the magnitude r of the detector's recoil momentum, for different initial delocalization widths L, where we fixed $\Omega\tau = 10^{-2}$ and $Mc^2\tau/\hbar = 500$. We here considered a wave propagation speed $c_s = 10^{-3}c$.

For coherent delocalization above the critical velocity, the virtual Cherenkov-like effect represents a source of decoherence, which might become important in certain practical applications of

quantum technologies. Let us imagine, for instance, that a quantum delocalized atom in a medium absorbs a photon carrying preexisting entanglement with an ancilla. The absorption process might then localize the atom so strongly that after the absorption process, the atom's center of mass wave function contains significant components above the critical velocity. Via the virtual Cherenkov-like effect, the entanglement transfer would then be vulnerable to decoherence. However, one could try to eliminate this source of decoherence due to the virtual Cherenkov-like effect, by externally manipulating the energy gap of the detector, and thus the critical velocity, e.g. via the Zeeman or Stark effects: depending on the size of the detector gap Ω, the critical velocity v_{crit} can be significantly larger than the wave propagation speed c_s in the medium. We close by remarking that the case of a charge without an internal degree of freedom is obtained as the limiting case $\Omega \to 0$, for which the interaction Hamiltonian commutes with the then vanishing free Hamiltonian of the internal degree of freedom.

2.7 Inverse virtual Cherenkov-like effect

Lastly, let us here consider the transition from an initial state of the form $|\Psi_i\rangle = |\varphi\rangle \otimes |e\rangle \otimes |\mathbf{k}\rangle$ to a final state of the form $|\Psi_f\rangle = |\mathbf{r}\rangle \otimes |g\rangle \otimes |0\rangle$. This transition resembles the process of induced emission: both the field and the detector are initially excited, and the detector ends up in its ground state. However, while for induced emission the field ends up in a twice excited state, we here ask whether the field may end up in the vacuum state. In a sense, we could view this process as an exotic "absorption" process, in which the initial field excitation gets "absorbed" by an initially excited detector. We will refer to this transition here as the *inverse virtual Cherenkov-like effect*, for the following reason: The initial and final field and internal detector states for the virtual Cherenkov-like effect are respectively the final and initial states for the inverse virtual Cherenkov-like effect. If it were not for the initial and final center of mass states, the inverse Cherenkov effect would thus simply be the time-reversed process of the Cherenkov effect.

Applying similar reasoning as we did for the virtual Cherenkov-like effect, we can again convince ourselves that without introducing a switching function, this process can happen neither for UDW detectors, nor for quantum delocalized detectors. However, again just like the virtual Cherenkov-like effect, the inverse virtual Cherenkov-like effect becomes possible if the detector couples to a medium and undergoes (real or virtual) supersonic motion. Taking the center of mass delocalization of the detector into account, we obtain for the transition

probability amplitude, up to a phase and to first perturbative order:

$$\mathcal{A} \;=\; \frac{\lambda c_s}{\sqrt{2k}}\frac{1}{(2\pi)^{3/2}}\widetilde{\varphi}(\mathbf{r}-\mathbf{k})\int_{t_i}^{t_f} dt\, e^{it\left(-\frac{k^2}{2M}+\frac{\mathbf{r}\cdot\mathbf{k}}{M}-\Omega-c_s k\right)} \tag{2.71}$$

Let us assume that the to-be-absorbed photon propagates in the $z-$direction, $\mathbf{k}=(0,0,k)^T$, and that the initial center of mass wave packet is spherically symmetric, $\widetilde{\varphi}(\mathbf{p})\equiv\widetilde{\varphi}(p)$. We trace over the detector's recoil, such as to obtain the following expression for the transition probability rate:

$$\mathcal{R}(k) \;=\; \frac{\lambda^2 c_s^2}{2k}\frac{1}{(2\pi)^3}\int d^3p\,|\widetilde{\varphi}(p)|^2\int_{-\infty}^{\infty} dt\, e^{it\left(\frac{k^2}{2M}+\frac{\mathbf{p}\cdot\mathbf{k}}{M}-\Omega-c_s k\right)} \tag{2.72}$$

$$=:\; \frac{\lambda^2 c_s^2 M}{4\pi k^2}\int_{p_{crit}}^{\infty} dp\, p\,|\widetilde{\varphi}(p)|^2 \tag{2.73}$$

We here defined $p_{crit}:=M\left|\frac{\Omega}{k}+c_s-\frac{k}{2M}\right|$. We thus find that the inverse virtual Cherenkov-like effect can happen only if the center of mass wave function has probability amplitudes for momenta $p\geq p_{crit}$, that is, contributions corresponding to virtual velocities faster than the critical velocity $\widetilde{v}_{crit}:=\left|\frac{\Omega}{k}+c_s-\frac{k}{2M}\right|$. Again employing a Gaussian center of mass wave packet, as given in Eq.(2.29), we obtain for the transition probability rate as a function of the magnitude k of the momentum of the photon:

$$\mathcal{R}(k) \;=\; \frac{\lambda^2 c_s^2 ML}{2k^2(2\pi)^{5/2}}\,e^{-\frac{M^2L^2}{2k^2}\left(\Omega+c_s k-\frac{k^2}{2M}\right)^2} \tag{2.74}$$

We note that for finite delocalization widths L and finite photon momentum k, in the limit $M\to\infty$, the transition probability rate vanishes:

$$\lim_{M\to\infty}(\mathcal{R}) \;=\; \frac{\lambda^2 c_s^2}{8\pi^2 k}\,\delta\left(\Omega+c_s k\right)=0 \tag{2.75}$$

This behaviour was to be anticipated, since larger and larger detector masses correspond to smaller and smaller virtual center of mass velocities. In Fig.(2.6), we plot the transition probability rate for a Gaussian delocalized detector with mass $Mc^2\tau/\hbar=100$ and energy gap $\Omega\tau=0.2$, where we set the wave propagation speed to $c_s=10^{-2}c$. We chose different values for L, while ensuring that $MLc/\hbar\geq 350$, such as for the detector's virtual center of mass velocities to be within the non-relativistic regime. We find that the transition rate peaks for to-be-absorbed photons of momentum $k\tau c\approx 20.2$. In Fig.(2.7), we plot the transition probability rate for a Gaussian delocalized detector with energy gap $\Omega\tau=0.2$ and initial delocalization width $L=10\tau c$, for various detector masses M. We find that for larger and larger masses, in

order for the inverse virtual Cherenkov-like effect to happen, the to-be-absorbed photon needs to be of larger and larger momentum.

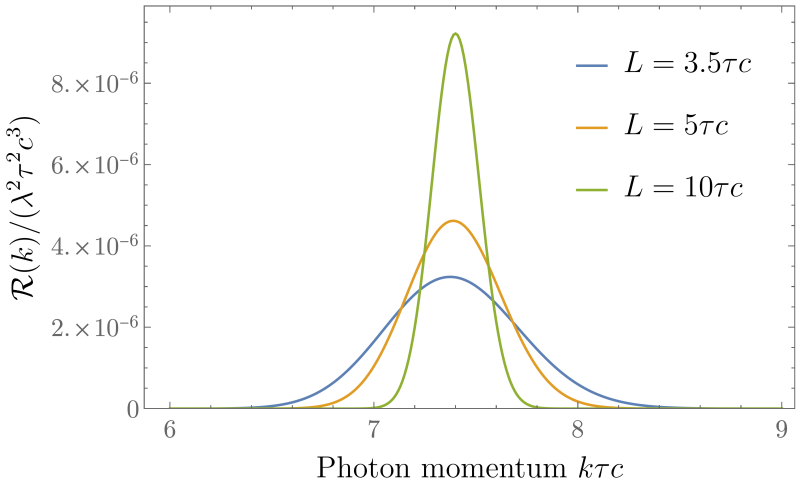

Figure 2.6: The transition probability rate as a function of the magnitude k of the momentum of the photon, for different initial delocalization widths L. We here chose the parameters $Mc^2\tau/\hbar = 100$, $\Omega\tau = 0.2$ and $c_s = 10^{-2}$.

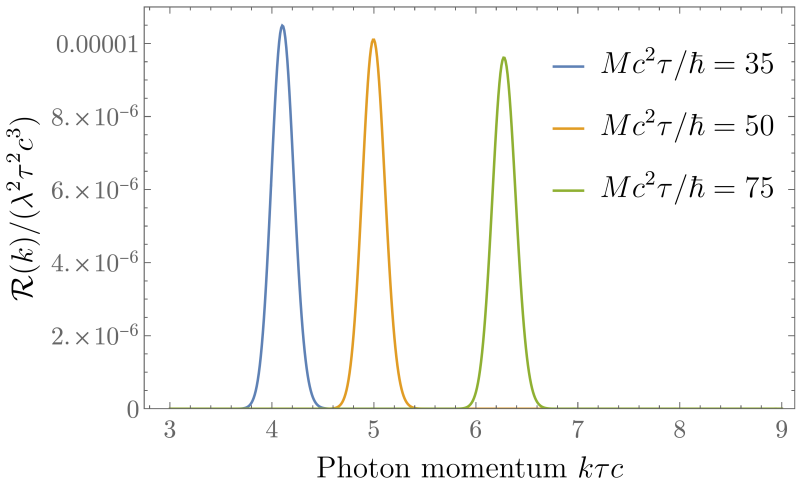

Figure 2.7: The transition probability rate as a function of the magnitude k of the momentum of the photon, for different detector masses M. We here chose the parameters $\Omega\tau = 0.2$, $L = 10\tau c$ and $c_s = 10^{-2}c$.

Coming back to Eq.(2.73), let us here finally consider the following concrete scenario: let us consider the wave propagation field to be the vacuum speed of light, $c_s = c$, and let us ask whether the inverse virtual Cherenkov-like effect might occur for a field quantum of momentum $k = \Omega/c$. This field excitation could, of course, easily trigger processes such as absorption or induced emission. However, for the inverse virtual Cherenkov-like effect, this choice of photon momentum yields $p_{crit} = 2Mc - \Omega/(2c)$. Assuming that $\Omega < 2Mc^2$, which is a reasonable assumption to make for physical detector systems such as atoms, molecules or ions, we find $p_{crit} > Mc$. A photon of momentum $k = \Omega/c$ thus *cannot* trigger the inverse virtual Cherenkov-

like effect. However, for media with wave propagation speeds significantly lower than the speed of light in vacuum, $c_s \ll c$, it would be feasible to have center of mass wave functions with significant contributions for momenta $p \gg Mc$. As we also confirmed in the Figures above, for supersonically delocalizing detector systems, we thus indeed obtain a non-zero probability for observing the inverse virtual Cherenkov-like effect.

In this chapter, we discussed how to modify the UDW detector model, such as to incorporate the detector's coherent center of mass delocalization. We discussed how a variety of simple processes are affected by the quantum center of mass delocalization. We discovered new effects, such as the virtual Cherenkov-like effect, which, as we discussed, resembles the Cherenkov effect, but is triggered in media merely via virtual supersonic delocalization. Of course, there are certainly still many more effects to be explored via the delocalized detector model. However, we now want to move on and go beyond our delocalized detector model: in the next chapter, we outline how to study the process of spontaneous emission for a realistically modeled, dynamically delocalizing hydrogen atom that interacts with the electromagnetic field. We will make quantitative order of magnitude predictions for the increase of the spontaneous emission rate due to the dynamical delocalization process of the hydrogen atom.

Chapter 3

Quantum delocalized hydrogen atom interacting with the electromagnetic field

For detector systems interacting with a scalar quantum field, in chapter 2 we discussed a variety of new effects that arise due to the detector's coherent center of mass delocalization. Our qualitative explorations, within our coherently delocalized detector model, indicate that the dynamics of the coherent center of mass delocalization of matter systems should impact their interaction with light. We here demonstrate an example for how to make order of magnitude estimates for these effects. We apply the methods we developed in the previous chapter towards calculating the spontaneous emission rate for a hydrogen atom, whose center of mass dynamically delocalizes, and which interacts with the electromagnetic field through minimal coupling.

3.1 Hydrogen atom with classical center of mass

Before taking the center of mass delocalization of the hydrogen atom into account, let us briefly review how to calculate the spontaneous emission rate for a hydrogen atom with classical center of mass. We consider an electron with quantum orbital degrees of freedom, $\hat{\mathbf{x}}$ and $\hat{\mathbf{p}}$, which is bound to a proton via a Coulomb potential and which couples to the electromagnetic field via minimal coupling. For now we assume that the proton is much heavier than the electron, and that the proton can hence be assumed to have classical orbital degrees of freedom. For

many purposes, given the mass of an electron, $m_e = 9.11 \cdot 10^{-31}$kg, and the mass of a proton, $m_p = 1.67 \cdot 10^{-27}$kg, this assumption is a reasonable one. (However, for the purpose of studying the effects of sharp center of mass localization on the light-matter interaction, we will go beyond this assumption in the subsequent section.) The Hilbert space then factors into a Hilbert space for the electronic degrees of freedom and a Hilbert space for the field degrees of freedom, $\mathcal{H} = \mathcal{H}_e \otimes \mathcal{H}_F$. Let the proton now be located at the origin of our coordinate system. In the Coulomb gauge, the full Hamiltonian of the system reads

$$\hat{H} \;=\; \int d^3k\, c\hbar k \sum_{s=1}^{2} \hat{a}_{\mathbf{k}}^{s\dagger} \hat{a}_{\mathbf{k}}^{s} + \frac{\left(\hat{\mathbf{p}} + q\hat{\mathbf{A}}(\hat{\mathbf{x}})\right)^2}{2m_e} - \frac{q^2}{4\pi\epsilon_0 |\hat{\mathbf{x}}|}\,, \tag{3.1}$$

with $q = 1.602 \times 10^{-19}$C the elementary charge, $\epsilon_0 = 8.85 \times 10^{-12}\mathrm{C}^2\mathrm{s}^2/(\mathrm{m}^3\mathrm{kg})$ the vacuum permittivity, $\hbar = 1.05 \times 10^{-34}$Js the reduced Planck constant and $c = 3 \times 10^8$m/s the vacuum speed of light. The operators $\hat{a}_{\mathbf{k}}^{s\dagger}$ and $\hat{a}_{\mathbf{k}}^{s}$ are respectively the creation and annihilation operators of electromagnetic field modes of momentum $\mathbf{k}$ and spin s. The operator $\hat{\mathbf{A}}(\mathbf{x})$ denotes the electromagnetic field operator,

$$\hat{\mathbf{A}}(\mathbf{x}) \;=\; \int \frac{d^3k}{(2\pi)^{3/2}} \sqrt{\frac{\hbar}{2\epsilon_0 ck}} \sum_{s=1}^{2} \boldsymbol{\epsilon}_s(\mathbf{k}) \left[\hat{a}_{\mathbf{k}}^{s} e^{i\mathbf{k}\mathbf{x}} + \text{h.c.}\right], \tag{3.2}$$

and the polarization vectors, $\boldsymbol{\epsilon}_s(\mathbf{k})$, satisfy the relations $\boldsymbol{\epsilon}_s(\mathbf{k}) \cdot \mathbf{k} = 0$ and $\boldsymbol{\epsilon}_r(\mathbf{k}) \cdot \boldsymbol{\epsilon}_s(\mathbf{k}) = \delta_{rs}$ in the Coulomb gauge.

Let us here mention a subtle issue, related to gauge choices, that has been discussed extensively in the literature (see, e.g., [75, 76, 77, 78, 61]). The gauge invariance of electrodynamics is broken by coupling the electromagnetic gauge field to a matter system that is described in first quantization, rather than in relativistic quantum field theory. Thus, the Hamiltonian in Eq.(3.1) is not invariant under (possibly time-dependent) gauge transformations of the electromagnetic potentials (see, e.g., [79]). The spectrum of the Hamiltonian thus generically depends on the choice of gauge—which, of course, is unphysical. Historically, a common strategy to deal with the gauge dependence of predictions has been the following. It has been shown that the multipolar Hamiltonian (related to the minimal coupling Hamiltonian via a so-called Power-Zienau-Wolley transformation [80, 81, 82, 83]), after a dipole approximation, can be expressed entirely in terms of observable and gauge-independent quantities, namely in terms of the electric and magnetic field operators. The dipolar Hamiltonian in this way allows one to make "approximately gauge invariant" predictions for the light-matter interaction, in the sense that gauge transformations only affect higher order contributions in the multipole approximation, which are controlled by

the Bohr radius and the electric charge. For the purpose of this chapter, in which we wish to demonstrate how to obtain order of magnitude estimates, we will not dive into the subtleties related to gauge invariance of predictions in the light-matter interaction. We here stick with the minimal coupling Hamiltonian in Coulomb gauge, as given in Eq.(3.1), accepting that our results will not be invariant under arbitrary gauge transformations. We rewrite the Hamiltonian as the sum of a free Hamiltonian and an interaction Hamiltonian, $\hat{H} = \hat{H}_0 + \hat{H}_{int}$, with

$$\hat{H}_0 \;:=\; \sum_{\mathbf{n}} E_n \left|\mathbf{n}\right\rangle \left\langle\mathbf{n}\right| + \int d^3k\, c\hbar k \sum_{s=1}^{2} \hat{a}^{s\dagger}_{\mathbf{k}} \hat{a}^{s}_{\mathbf{k}} \tag{3.3}$$

the free Hamiltonians of the hydrogen atom and the electromagnetic field respectively. Disregarding gauge issues, we let $\left|\mathbf{n}\right\rangle = \left|nlm\right\rangle$ denote the electronic energy eigenstates of energy $E_n = 13.6\text{eV}/n^2$, with n the principal quantum number, l the orbital quantum number and m the magnetic quantum number. For the interaction Hamiltonian, we obtain

$$\hat{H}_{int} \;=\; \frac{q}{2m_e}\left(\hat{\mathbf{p}}\hat{\mathbf{A}}(\hat{\mathbf{x}}) + \hat{\mathbf{A}}(\hat{\mathbf{x}})\hat{\mathbf{p}}\right) + \mathcal{O}(q^2) \tag{3.4}$$

$$\;=\; \frac{q}{2m_e}\int d^3x \left(\hat{\mathbf{p}}\hat{\mathbf{A}}(\mathbf{x}) + \hat{\mathbf{A}}(\mathbf{x})\hat{\mathbf{p}}\right)\left|\mathbf{x}\right\rangle \left\langle\mathbf{x}\right| + \mathcal{O}(q^2)\,, \tag{3.5}$$

where the electromagnetic field operators couple to the momentum operator $\hat{\mathbf{p}}$ of the electron, and $\left|\mathbf{x}\right\rangle$ denote the position eigenvectors of the electron. We here neglect terms of order $\mathcal{O}(q^2)$, as these terms do not contribute to the spontaneous emission process at leading order. In the interaction picture, the interaction Hamiltonian becomes:

$$\begin{aligned}\hat{H}_{int}(t) \;=\; & \frac{q}{2m_e}\int d^3x \int \frac{d^3p\, d^3q}{(2\pi\hbar)^3} \sum_{\mathbf{n},\mathbf{m}} (\mathbf{p}+\mathbf{q}) e^{\frac{it}{\hbar}(E_m - E_n) - \frac{i}{\hbar}(\mathbf{p}-\mathbf{q})\mathbf{x}}\, \widetilde{\psi}^{*}_{\mathbf{n}}(\mathbf{p}) \widetilde{\psi}_{\mathbf{m}}(\mathbf{q}) \\ & \times \left|\mathbf{n}\right\rangle \left\langle\mathbf{m}\right| \otimes \hat{\mathbf{A}}(\mathbf{x},t) + \mathcal{O}(q^2)\end{aligned} \tag{3.6}$$

We here introduced resolutions of the identity in the energy eigenbasis, $\mathbf{1} = \sum_{\mathbf{n}} \left|\mathbf{n}\right\rangle \left\langle\mathbf{n}\right|$, and we let $\psi_{\mathbf{n}}(\mathbf{x})$ and $\widetilde{\psi}_{\mathbf{n}}(\mathbf{p})$ denote the electronic energy eigenfunctions respectively in the position and momentum representation. Let us now calculate the spontaneous emission rate for an initially excited hydrogen atom, coupled to the vacuum state of the electromagnetic field,

$$\left|\Psi_i\right\rangle \;=\; \left|e\right\rangle \otimes \left|0\right\rangle\,. \tag{3.7}$$

We assume that the hydrogen atom is in one of its three first excited energy eigenstates:

$$\left|e\right\rangle \in \left\{\left|210\right\rangle, \left|211\right\rangle, \left|21-1\right\rangle\right\} \tag{3.8}$$

For the process of spontaneous emission, we consider the transition to the final state

$$|\Psi_f\rangle \;=\; |100\rangle \otimes |\mathbf{k}, s\rangle \;, \tag{3.9}$$

for which the hydrogen atom is in its energetic ground state and a photon of momentum $\mathbf{k}$ and spin s was emitted. For the energy difference between the ground state and the first excited energy eigenstates of the hydrogen atom, we write $E_1 - E_2 = 10.2\text{eV} =: \hbar\Omega$, with $\Omega = 1.55 \times 10^{16}\text{s}^{-1}$. The transition amplitude for spontaneous emission then becomes, up to a phase:

$$\mathcal{A} \;=\; \frac{1}{\sqrt{2\epsilon_0 c\hbar k}} \frac{q}{m_e} \int_{t_i}^{t_f} dt \int \frac{d^3p}{(2\pi)^{3/2}} e^{-it(\Omega - ck)} \boldsymbol{\epsilon}_s(\mathbf{k}) \cdot \mathbf{p}\, \widetilde{\psi}_e(\mathbf{p}) \widetilde{\psi}_g(\mathbf{p} - \hbar\mathbf{k}) \tag{3.10}$$

We here let $\widetilde{\psi}_g(\mathbf{p})$ and $\widetilde{\psi}_e(\mathbf{p})$ respectively denote the ground and first excited energy eigenfunctions in the momentum representation. In the position representation, the ground and excited electronic wave functions of the hydrogen atom are respectively

$$\psi_g(\mathbf{x}) \;=\; \frac{1}{\sqrt{\pi a^3}} \exp\left(-\frac{x}{a}\right) , \tag{3.11}$$

$$\psi_{210}(\mathbf{x}) \;=\; \frac{1}{\sqrt{32\pi a^5}}\, x_3\, \exp\left(-\frac{x}{2a}\right) , \tag{3.12}$$

$$\psi_{21\pm1}(\mathbf{x}) \;=\; \mp\frac{1}{\sqrt{32\pi a^5}} \frac{x_1 \pm i x_2}{\sqrt{2}} \exp\left(-\frac{x}{2a}\right) , \tag{3.13}$$

with $a = 5.29 \times 10^{-11}\text{m}$ the Bohr radius, and where we let $\mathbf{x} = (x_1, x_2, x_3)^T$ and $x := |\mathbf{x}|$. Averaging over the three initial first excited states and tracing over the momentum $\mathbf{k}$ and spin s of the emitted photon, we obtain the total spontaneous emission rate:

$$\begin{aligned} \mathcal{R} \;=\; & \frac{1}{3} \sum_e \int_{-\infty}^{\infty} dt \int d^3k\, e^{-it(\Omega - ck)} \frac{1}{2\epsilon_0 c\hbar k} \left(\delta_{ij} - \frac{k_i k_j}{k^2}\right) \frac{q^2}{m_e^2} \int \frac{d^3p\, d^3P}{(2\pi)^3}\, p_i P_j \\ & \times \widetilde{\psi}_g(\mathbf{p} - \hbar\mathbf{k}) \widetilde{\psi}_e(\mathbf{p}) \widetilde{\psi}_g^*(\mathbf{P} - \hbar\mathbf{k}) \widetilde{\psi}_e^*(\mathbf{P}) \end{aligned} \tag{3.14}$$

Since there is no preferred direction for the emitted photon, without loss of generality we can rotate the coordinate system so that the photon is emitted in the $z-$direction, $\mathbf{k} = (0, 0, k)^T$. We can then straightforwardly carry out the integrations over t and $\mathbf{k}$. Fourier transforming the electronic wave functions, as well as exploiting isotropy in the plane orthogonal to the

$z-$direction, we can then simplify the spontaneous emission rate as follows:

$$\begin{aligned}\mathcal{R} &= \frac{q^2\Omega}{3m_e^2\epsilon_0 c^3\hbar\pi}\int d^3x\int d^3y\int d^3\widetilde{x}\int d^3\widetilde{y}\left[\sum_e \psi_e(\mathbf{y})\psi_e^*(\widetilde{\mathbf{y}})\right]\psi_g(\mathbf{x})\psi_g^*(\widetilde{\mathbf{x}})e^{-i\frac{\Omega}{c}(x_3-\widetilde{x}_3)} \\ &\times\int\frac{d^3p\,d^3\widetilde{p}}{(2\pi\hbar)^6}\,e^{\frac{i}{\hbar}\mathbf{px}}e^{-\frac{i}{\hbar}\widetilde{\mathbf{p}}\widetilde{\mathbf{x}}}\left(p_1e^{\frac{i}{\hbar}\mathbf{py}}\right)\left(\widetilde{p}_1e^{-\frac{i}{\hbar}\widetilde{\mathbf{p}}\widetilde{\mathbf{y}}}\right) \qquad (3.15)\\ &= \frac{q^2\hbar\Omega}{3m_e^2\epsilon_0 c^3\pi}\int d^3y\int d^3\widetilde{y}\left[\sum_e \psi_e(\mathbf{y})\psi_e^*(\widetilde{\mathbf{y}})\right]\left[\frac{\partial}{\partial y_1}\psi_g(\mathbf{y})\right]\left[\frac{\partial}{\partial\widetilde{y}_1}\psi_g(\widetilde{\mathbf{y}})\right]e^{i\frac{\Omega}{c}(y_3-\widetilde{y}_3)} \qquad (3.16)\end{aligned}$$

The summation over the three first excited states explicitly reads

$$\sum_e \psi_e(\mathbf{y})\psi_e^*(\widetilde{\mathbf{y}}) = \frac{y_1\widetilde{y}_1+y_2\widetilde{y}_2+y_3\widetilde{y}_3}{32\pi a^5}\exp\left(-\frac{|\mathbf{y}|}{2a}-\frac{|\widetilde{\mathbf{y}}|}{2a}\right), \qquad (3.17)$$

and the derivative of the ground state wave function becomes:

$$\frac{\partial}{\partial y_1}\psi_g(\mathbf{y}) = -\frac{y_1}{|\mathbf{y}|}\frac{1}{\sqrt{\pi a^5}}\exp\left(-\frac{|\mathbf{y}|}{a}\right) \qquad (3.18)$$

Using symmetry arguments in the integrals in Eq.(3.16), we obtain for the spontaneous emission rate:

$$\begin{aligned}\mathcal{R} &= \frac{q^2\hbar\Omega}{3m_e^2\epsilon_0 c^3\pi}\frac{1}{32\pi^2a^{10}}\left(\frac{2^7c^4a^4\pi}{(4\Omega^2a^2+9c^2)^2}\right)^2 \qquad (3.19)\\ &\approx 6.27\times10^8\mathrm{s}^{-1} \qquad (3.20)\end{aligned}$$

This is indeed the spontaneous emission rate of a hydrogen atom that can be found in the literature, see, e.g., [84], and that has been measured in experiments. Note that we can repeat the above calculations using the multipolar Hamiltonian, and making the dipole approximation, and obtain the same result to the level of accuracy we are concerned with here (see, e.g., [61] for a detailed discussion of the multipolar approach). We are now prepared to study the effects of quantum center of mass delocalization on the spontaneous emission rate for a hydrogen atom.

3.2 Hydrogen atom with quantum center of mass

To take the center of mass delocalization of the hydrogen atom into account, we describe both the electron and the proton fully quantum mechanically, with position operators $\hat{\mathbf{x}}_e$ and $\hat{\mathbf{x}}_p$ and momentum operators $\hat{\mathbf{p}}_e$ and $\hat{\mathbf{p}}_p$ respectively. We let both the electron and the proton interact

with the electromagnetic field via minimal coupling. In the Coulomb gauge, the full Hamiltonian then reads:

$$\hat{H} \;=\; \int d^3k\, c\hbar k \sum_{s=1}^{2} \hat{a}_{\mathbf{k}}^{s\dagger}\hat{a}_{\mathbf{k}}^{s} + \frac{\left(\hat{\mathbf{p}}_p - q\hat{\mathbf{A}}(\hat{\mathbf{x}}_p)\right)^2}{2m_p} + \frac{\left(\hat{\mathbf{p}}_e + q\hat{\mathbf{A}}(\hat{\mathbf{x}}_e)\right)^2}{2m_e} - \frac{q^2}{4\pi\epsilon_0|\hat{\mathbf{x}}_p - \hat{\mathbf{x}}_e|} \tag{3.21}$$

Within this model for a coherently delocalized hydrogen atom interacting with the electromagnetic field, let us now calculate order of magnitude estimates for how the spontaneous emission rate of a hydrogen atom is affected by the coherent center of mass delocalization process (again, for an analogous calculation within the multipolar Hamiltonian, in which gauge issues are addressed carefully, see [61]). We again write the Hamiltonian as the sum of a free Hamiltonian and an interaction Hamiltonian, $\hat{H} = \hat{H}_0 + \hat{H}_{int}$, and define the interaction Hamiltonian as

$$\hat{H}_{int} \;:=\; q\,\frac{\hat{\mathbf{p}}_e\hat{\mathbf{A}}(\hat{\mathbf{x}}_e)}{2m_e} - q\,\frac{\hat{\mathbf{p}}_p\hat{\mathbf{A}}(\hat{\mathbf{x}}_p)}{2m_p} + \text{h.c.} + \mathcal{O}(q^2)\,, \tag{3.22}$$

where we again neglect terms of order $\mathcal{O}(q^2)$, which do not contribute to the spontaneous emission process at leading order. Let us now introduce relative and center of mass position operators, $\hat{\mathbf{x}}_{\rm rel} := \hat{\mathbf{x}}_e - \hat{\mathbf{x}}_p$ and $\hat{\mathbf{x}}_{\rm CM} := \frac{m_e}{M}\hat{\mathbf{x}}_e + \frac{m_p}{M}\hat{\mathbf{x}}_p$, as well as their conjugate momentum operators, $\hat{\mathbf{p}}_{\rm rel}$ and $\hat{\mathbf{p}}_{\rm CM}$, with M the total mass and μ the reduced mass of the atom. The total Hilbert space factorizes as $\mathcal{H} = \mathcal{H}_{\rm CM}\otimes\mathcal{H}_{\rm rel}\otimes\mathcal{H}_{\rm F}$. The free Hamiltonian of the field and the hydrogen atom then becomes

$$\hat{H}_0 \;=\; \int d^3k\, c\hbar k \sum_{s=1}^{2} \hat{a}_{\mathbf{k}}^{s\dagger}\hat{a}_{\mathbf{k}}^{s} + \frac{\hat{\mathbf{p}}_{CM}^{\,2}}{2M} + \sum_{\mathbf{n}} E_n \left|\mathbf{n}\right\rangle\left\langle\mathbf{n}\right|\,, \tag{3.23}$$

where the dynamics of the center of mass of the hydrogen atom is described via the Hamiltonian of a free quantum mechanical particle, and the relative motion gives rise to the discrete energy spectrum $\{E_n\}$ of the hydrogen atom. In terms of center of mass and relative coordinates, we further obtain for the interaction Hamiltonian:

$$\begin{aligned}\hat{H}_{int} \;=\;& \int d^3x \int d^3y\, \hat{\mathbf{p}}_{\rm CM}\left|\mathbf{x}\right\rangle\left\langle\mathbf{x}\right| \otimes \left|\mathbf{y}\right\rangle\left\langle\mathbf{y}\right| \otimes \left[\frac{q}{2M}\hat{\mathbf{A}}\left(\mathbf{x} + \tfrac{\mu}{m_e}\mathbf{y}\right) - \frac{q}{2M}\hat{\mathbf{A}}\left(\mathbf{x} - \tfrac{\mu}{m_p}\mathbf{y}\right)\right] \\ &+ \int d^3x \int d^3y \left|\mathbf{x}\right\rangle\left\langle\mathbf{x}\right| \otimes \hat{\mathbf{p}}_{\rm rel}\left|\mathbf{y}\right\rangle\left\langle\mathbf{y}\right| \otimes \left[\frac{q}{2m_e}\hat{\mathbf{A}}\left(\mathbf{x} + \tfrac{\mu}{m_e}\mathbf{y}\right) + \frac{q}{2m_p}\hat{\mathbf{A}}\left(\mathbf{x} - \tfrac{\mu}{m_p}\mathbf{y}\right)\right] \\ &+ \text{h.c.}\end{aligned} \tag{3.24}$$

Let us calculate the spontaneous emission rate for an initially excited hydrogen atom with quantized center of mass, coupled to the vacuum state of the electromagnetic field,

$$\left|\Psi_i\right\rangle \;=\; \left|\varphi\right\rangle \otimes \left|e\right\rangle \otimes \left|0\right\rangle\,. \tag{3.25}$$

We again assume that the hydrogen atom is in one of its three first excited energy eigenstates, $|e\rangle \in \{|210\rangle, |211\rangle, |21-1\rangle\}$, and we let $|\varphi\rangle$ denote the initial center of mass state of the hydrogen atom. We first calculate the transition probability amplitude for the initial state to evolve to the final state $|\Psi_f\rangle = |\mathbf{r}\rangle \otimes |g\rangle \otimes |\mathbf{k}, s\rangle$, in which the atom is in its ground state, $|g\rangle = |100\rangle$, the center of mass has momentum $\mathbf{r}$, and a photon of momentum $\mathbf{k}$ and spin s has been emitted. We obtain, up to a phase, working in the interaction picture and to first order in perturbation theory:

$$\begin{aligned}
\mathcal{A} &= \frac{1}{\hbar}\varphi(\mathbf{r}+\mathbf{k})\sqrt{\frac{\hbar}{2\epsilon_0 ck}}\boldsymbol{\epsilon}_s(\mathbf{k})\frac{1}{(2\pi)^{3/2}}\int_{t_i}^{t_f} dt\, e^{\frac{i}{\hbar}\left(\frac{-2\hbar\mathbf{r}\mathbf{k}-\hbar^2\mathbf{k}^2}{2M}-\hbar\Omega+\hbar ck\right)t} \\
&\quad\times\Bigg(\int d^3y\,\mathbf{r}\,\psi_g(\mathbf{y})\psi_e(\mathbf{y})\frac{q}{M}\left[e^{-i\frac{\mu}{m_e}\mathbf{k}\mathbf{y}}-e^{i\frac{\mu}{m_p}\mathbf{k}\mathbf{y}}\right] \\
&\quad+\int d^3p\,\mathbf{p}\,\widetilde{\psi}_g(\mathbf{p})\left[\frac{q}{m_e}\widetilde{\psi}_e(\mathbf{p}+\tfrac{\mu\hbar}{m_e}\mathbf{k})+\frac{q}{m_p}\widetilde{\psi}_e(\mathbf{p}-\tfrac{\mu\hbar}{m_p}\mathbf{k})\right]\Bigg)+\mathcal{O}(q^2)
\end{aligned} \tag{3.26}$$

Here, $\psi_g(\mathbf{y})$, $\psi_e(\mathbf{y})$, $\widetilde{\psi}_g(\mathbf{p})$ and $\widetilde{\psi}_e(\mathbf{p})$ are the ground state and first excited state wavefunctions of the hydrogen atom in the position and momentum representations respectively. We now average over the three first excited states of the hydrogen atom and trace over the recoil momentum $\mathbf{r}$ of the center of mass, as well as over the momentum $\mathbf{k}$ and spin s of the emitted photon, such as to obtain the spontaneous emission rate:

$$\begin{aligned}
\mathcal{R} &= \frac{q^2M}{3\epsilon_0 c\hbar}\int_{k_-}^{k_+}dk\int_0^\infty dp\,p\,|\varphi(p)|^2 \\
&\quad\times\Bigg[\left(\frac{p^2}{M^2}-\frac{G(k)^2}{k^2\hbar^2}\right)\left|\int d^3y\,\psi_g(\mathbf{y})\psi_{210}(\mathbf{y})\left(e^{-i\frac{\mu}{m_e}ky_3}-e^{i\frac{\mu}{m_p}ky_3}\right)\right|^2 \\
&\quad+2\hbar^2\int d^3x\int d^3y\sum_e\psi_e(\mathbf{x})\psi_e(\mathbf{y})\left[\frac{\partial}{\partial x_1}\psi_g(\mathbf{x})\right]\left[\frac{\partial}{\partial y_1}\psi_g(\mathbf{y})\right] \\
&\quad\times\left(\frac{1}{m_e}e^{i\frac{\mu}{m_e}kx_3}+\frac{1}{m_p}e^{-i\frac{\mu}{m_p}kx_3}\right)\left(\frac{1}{m_e}e^{-i\frac{\mu}{m_e}ky_3}+\frac{1}{m_p}e^{i\frac{\mu}{m_p}ky_3}\right)\Bigg]
\end{aligned} \tag{3.27}$$

We here made the following definitions:

$$k_\pm := \frac{1}{\hbar}\left(\pm p-cM+\sqrt{(\pm p-cM)^2+2\Omega\hbar M}\right), \tag{3.28}$$

$$G(k) := \frac{\hbar^2k^2}{2M}+c\hbar k-\hbar\Omega \tag{3.29}$$

We are now prepared to insert the electronic wave functions of the hydrogen atom, given in Eq.(3.11-3.13), such as to obtain for the spontaneous emission rate for a delocalized hydrogen atom:

$$\mathcal{R} = \frac{q^2 M}{12\pi\epsilon_0 c\hbar}\int_0^\infty dp\, 4\pi p^2 \left|\varphi(p)\right|^2 \int_{k_-}^{k_+} dk \Bigg[\left(\frac{p}{M^2} - \frac{G(k)^2}{pk^2\hbar^2}\right) 3^2 2^{15} a^2 k^2 \mu^2 \left(\frac{F_e(k)^3}{m_e} + \frac{F_p(k)^3}{m_p}\right)^2 + \frac{2^{10}\hbar^2}{pa^2}\left(\frac{F_e(k)^2}{m_e} + \frac{F_p(k)^2}{m_p}\right)^2 \Bigg], \tag{3.30}$$

with

$$F_e(k) := \left(4a^2k^2\frac{\mu^2}{m_e^2} + 9\right)^{-1} \qquad \text{and} \qquad F_p(k) := \left(4a^2k^2\frac{\mu^2}{m_p^2} + 9\right)^{-1}. \tag{3.31}$$

We again carry out the k integration and Taylor expand around small and non-relativistic center of mass velocities, that is, around $p/(Mc) = 0$, to obtain:

$$\mathcal{R} = C\int d^3p\, \left|\varphi(\mathbf{p})\right|^2 \left[1 + D\left(\frac{p}{Mc}\right)^2 + \mathcal{O}\left(\left(\frac{p}{Mc}\right)^4\right)\right] \tag{3.32}$$

Here, we defined the constants

$$C \approx 6.27\times 10^8 \mathrm{s}^{-1} \qquad \text{and} \qquad D \approx 1.33\,. \tag{3.33}$$

For center of mass wave packets that delocalize very slowly, we thus recover the spontaneous emission rate for a hydrogen atom for which the center of mass is assumed classical. Considering a Gaussian wave packet for the initial center of mass wave function, with probability distribution

$$\left|\varphi(\mathbf{p})\right|^2 = \left(\frac{L^2}{2\pi\hbar^2}\right)^{3/2} e^{-p^2L^2/(2\hbar)^2}, \tag{3.34}$$

the spontaneous emission rate becomes a function of the initial width L of the Gaussian wave packet:

$$\mathcal{R} = C\left[1 + 3D(LMc/\hbar)^{-2} + \mathcal{O}\left((LMc/\hbar)^{-4}\right)\right] \tag{3.35}$$

Let us now assume that the center of mass of the hydrogen atom is initially coherently localized to some moderate extent. Namely, let us assume that the initial Gaussian center of mass wave packet is of width $L = 7.37\times 10^{-14}$m, which ensures that basically all virtual center of mass velocities (namely all velocities in the Gaussian probability distribution within 3.5 standard

deviations from the mean) are smaller than 1% of the speed of light, which in turn ensures that the virtual center of mass velocities stay well within the non-relativistic regime. From Eq.(3.35), we obtain that this should lead to an increase of the spontaneous emission rate of $3.26 \times 10^{-3}\%$, compared to the spontaneous emission rate obtained for a harmonic hydrogen atom whose center of mass dynamically delocalizes infinitely slowly. It should be interesting to explore whether this increase in the spontaneous emission rate due to the coherent delocalization process of the hydrogen atom could be observed experimentally.

Along similar lines, it should also be interesting to explore whether there could be a connection between increased transition rates due to coherent center of mass delocalization on one hand, and recent experimental findings by researchers at University College London [85]: they confirmed, for the $n = 2$ fine structure transition rate of a positronium atom, a deviation from the theoretically predicted transition rate. As opposed to the hydrogen atom, the positronium atom is considered a "clean" system, in that it can be described entirely within quantum electrodynamics (QED). Thus, a persisting discrepancy between theoretical predictions and experimental observations for transition rates of positronium atoms (see also for instance [86, 87, 88]) seems to indicate that either QED and thus the Standard Model of Particle Physics requires modification, or that the theoretical treatment of the positronium atom needs to be revisited. It might be interesting to study the assumptions made about the center of mass degrees of freedom of the positronium atom. Especially since the mass of the positronium atom is so small, there is reason to believe that coherent center of mass delocalization of the positronium atom could lead to the significantly increased measured transition rates.

3.3 Implications of center of mass delocalization on selection rules

Let us now briefly discuss the impact of center of mass delocalization on selection rules in the light matter interaction. Electric dipole transitions that would otherwise be omitted by the selection rules may be allowed to a certain extent when taking the delocalization of the center of mass of a hydrogen atom into account. As an example, let us consider an atom in its ground state, which absorbs a photon propagating in the $z-$direction, $\mathbf{k} = (0, 0, k)^T$, with polarization vector $\boldsymbol{\epsilon} = (1, 0, 0)^T$. For an atom whose center of mass is treated classically, the absorption

probability amplitude becomes, up to a phase,

$$\mathcal{A} \;=\; \int_{t_i}^{t_f} dt e^{-it(ck-\Omega)} \int \frac{d^3p}{(2\pi)^{3/2}} \frac{q}{m_e} \frac{1}{\sqrt{2\epsilon_0 c\hbar k}} p_1 \widetilde{\psi}_e(\mathbf{p}) \widetilde{\psi}_g(\mathbf{p}-\hbar\mathbf{k})\,, \tag{3.36}$$

so that the absorption probability rate becomes:

$$\mathcal{R}_{g\to e} \;=\; \frac{q^2\pi}{m_e^2\epsilon_0 c^2\hbar k}\delta(k-\Omega/c)\left|\int \frac{d^3x}{(2\pi)^{3/2}}\psi_e(\mathbf{x})e^{ikx_3}\left(-i\hbar\frac{\partial}{\partial x_1}\psi_g(\mathbf{x})\right)\right|^2 \tag{3.37}$$

Because of the symmetry of the integral, we can immediately deduce that after absorbing the photon, the atom will never be left in the excited state $e = 210$,

$$\mathcal{R}_{g\to 210} \;=\; 0\,, \tag{3.38}$$

which is in accordance with the selection rules. We further find that the transition rates to either of the two excited states $e = 21 \pm 1$ are as follows:

$$\mathcal{R}_{g\to 21\pm 1} \;=\; \frac{2^5 q^2\hbar}{m_e^2\epsilon_0 c\,\Omega\,\pi^2 a^2\left(4a^2\frac{\Omega^2}{c^2}+9\right)^4}\delta(k-\Omega/c) \tag{3.39}$$

We find that the photon can only get absorbed by the atom if the photon momentum matches the energy gap, $k = \Omega/c$. We also note that the divergence in the absorption rate, for on-resonance photon momenta, results from assuming a plane wave state for the to-be-absorbed photon. To regularize this divergence, let us consider a wave packet state instead, $\int d^3k\,\psi(\mathbf{k})\,\hat{a}^\dagger_{\mathbf{k}}\,|0\rangle$, with $\psi(\mathbf{k}) = \left(\frac{L^2}{2\pi}\right)^{3/2} e^{-(\mathbf{k}-\mathbf{k}_0)^2L^2/2}$ and $\mathbf{k}_0 := (0,0,\Omega/c)^T$, and consider the limit of $L \to 0$. This yields the following absorption rates:

$$\mathcal{R}_{g\to 210} \;=\; 0\,, \tag{3.40}$$

$$\mathcal{R}_{g\to 21\pm 1} \;=\; \frac{2^7 q^2\hbar\Omega}{m_e^2\epsilon_0 c^3\,\pi a^2\left(4a^2\frac{\Omega^2}{c^2}+9\right)^4} = \frac{3}{4}\times 6.27\times 10^8 \mathrm{s}^{-1} \tag{3.41}$$

We note that the sum of the absorption rates is equal to the spontaneous emission rate for an excited hydrogen atom, $6.27\times 10^8\mathrm{s}^{-1}$, apart from a symmetry factor arising with averaging over the three initial first excited states and tracing over the spin of the emitted photon.

Now let us take the quantumness of the center of mass into account. Let us again consider the absorption of a photon propagating in the $z-$direction and with polarization $\boldsymbol{\epsilon} = (1,0,0)^T$.

Tracing over the atom's recoil momentum, we obtain the following absorption rate:

$$\begin{aligned}\mathcal{R}_{g\to e} &= \int d^3p \int_{-\infty}^{\infty} dt\, e^{it\left(-ck+\Omega+\frac{\mathbf{p}\cdot\mathbf{k}}{M}+\frac{\hbar k^2}{2M}\right)} \frac{q^2}{2\epsilon_0 c\hbar k}\frac{1}{(2\pi)^3}|\varphi(\mathbf{p})|^2 \times \\ &\times\Bigg| \int d^3y\, p_1\psi_e(\mathbf{y})\psi_g(\mathbf{y})\frac{1}{M}\left(e^{i\frac{\mu}{m_e}ky_3}-e^{-i\frac{\mu}{m_p}ky_3}\right) \\ &+\int d^3\widetilde{p}\,\widetilde{p}_1\,\widetilde{\psi}_e(\widetilde{\mathbf{p}})\left(\frac{1}{m_e}\widetilde{\psi}_g\left(\widetilde{\mathbf{p}}+\frac{\mu\hbar}{m_e}\mathbf{k}\right)+\frac{1}{m_p}\widetilde{\psi}_g\left(\widetilde{\mathbf{p}}-\frac{\mu\hbar}{m_p}\mathbf{k}\right)\right)\Bigg|^2 \end{aligned} \tag{3.42}$$

The first term in the sum vanishes for $e = 21 \pm 1$, while the second term vanishes for $e = 210$. Let us assume that the initial center of mass wave function is given by the Gaussian wave packet in Eq.(3.34). We obtain for the respective absorption rates:

$$\mathcal{R}_{g\to 210} = \frac{2^{12}3^2a^2\mu^2q^2}{\epsilon_0 c\pi^2\sqrt{2\pi}ML}\left(\frac{F_e(k)^3}{m_e}+\frac{F_p(k)^3}{m_p}\right)^2 \exp\left(-\frac{L^2M^2}{2\hbar^2k^2}\left(\Omega-ck+\frac{\hbar k^2}{2M}\right)^2\right) \tag{3.43}$$

$$\mathcal{R}_{g\to 21\pm 1} = \frac{2^5q^2}{\epsilon_0 ck^2\pi^2a^2}\frac{ML}{\sqrt{2\pi}}\left(\frac{F_e(k)^2}{m_e}+\frac{F_p(k)^2}{m_p}\right)^2 \exp\left(-\frac{L^2M^2}{2\hbar^2k^2}\left(\Omega-ck+\frac{\hbar k^2}{2M}\right)^2\right) \tag{3.44}$$

We note that the rate $\mathcal{R}_{g\to 210}$ at which the atom transitions to the excited state $e = 210$ is generically non-zero. We further note that in the limit $M \to \infty$, we recover the results which we obtained in Eq.(3.38) and Eq.(3.39) for a hydrogen atom with classical center of mass degrees of freedom. Let us now define ρ as the ratio between the absorption rates $\mathcal{R}_{g\to 210}$ and $\mathcal{R}_{g\to 21\pm 1}$. The ratio ρ then gives us a measure for the extent to which the selection rules are violated. While ρ vanishes for classical center of mass degrees of freedom, we obtain for hydrogen atoms with quantum delocalized center of mass:

$$\rho := \frac{\mathcal{R}_{g\to 210}}{\mathcal{R}_{g\to 21\pm 1}} = \left(\frac{F_e(k)^3}{m_e}+\frac{F_p(k)^3}{m_p}\right)^2\left(\frac{F_e(k)^2}{m_e}+\frac{F_p(k)^2}{m_p}\right)^{-2}\frac{2^7 3^2a^4\mu^2k^2}{M^2L^2} \tag{3.45}$$

$$\approx \frac{2^7 3^2a^4\mu^2k^2}{M^2L^2(4a^2k^2+9)^2}\,. \tag{3.46}$$

For instance, for an atom whose center of mass is initially localized as a Gaussian wave packet of width $L = 7.37 \cdot 10^{-14}$m, and for a to-be-absorbed photon of momentum $k = \Omega/c$, we obtain $\rho = 1.6 \cdot 10^{-5}$. Thus, for roughly every 10^5 photons absorbed according to the selection rules, we predict to observe one absorption violating the selection rules. Similarly, for an atom whose center of mass is initially localized at the extent of the Bohr radius, $L = 5.29 \cdot 10^{-11}$m, we predict to observe one absorption violating the selection rules per roughly every 10^{11} absorbed photons of momentum $k = \Omega/c$.

Not only are selection rules violated, but we can also have absorption of off-resonance photons. But this was already discussed in section 2.3. We conclude this section by remarking that it could also be interesting to investigate whether for instance a photon of momentum $k = \Omega/c$ could be absorbed and excite a sharply localized atom to one of its higher than first excited states. In case of such transitions happening at a significant rate, this new aspect of the light-matter interaction would also impact the quantum channel capacities of the light-matter interaction.

3.4 'Harmonic' hydrogen atom with classical center of mass

In the previous sections, we saw how to obtain quantitative estimates for the effect of delocalization on the light-matter interaction, by coupling a hydrogen atom to the electromagnetic field. Let us now briefly discuss a way to simplify these order of magnitude calculations. Namely, let us replace the Coulomb potential by a simpler harmonic potential, which is tuned such that the energy gap between ground and first excited states matches that of the Coulomb potential, $\hbar\Omega = 10.2eV$. We refer to this model as a *harmonic hydrogen atom*.

Let us again start by discussing the case of a harmonic hydrogen atom with classical center of mass. We again let the proton be fixed at the origin, and we consider an electron, with position operator $\hat{\mathbf{x}}$ and momentum operator $\hat{\mathbf{p}}$, bound to the proton via a harmonic potential. The free Hamiltonian of the harmonic hydrogen atom and the electromagnetic field becomes

$$\hat{H}_0 = \frac{\hat{\mathbf{p}}^2}{2m_e} + \frac{m_e\Omega^2}{2}\hat{\mathbf{x}}^2 + \int d^3k\, c\hbar k \sum_{s=1}^{2} \hat{a}_{\mathbf{k}}^{s\dagger}\hat{a}_{\mathbf{k}}^{s} \tag{3.47}$$

$$= \sum_{\mathbf{n}} E_n \left|\mathbf{n}\right\rangle \left\langle\mathbf{n}\right| + \int d^3k\, c\hbar k \sum_{s=1}^{2} \hat{a}_{\mathbf{k}}^{s\dagger}\hat{a}_{\mathbf{k}}^{s}\,, \tag{3.48}$$

with $\left|\mathbf{n}\right\rangle = \left|n_1\, n_2\, n_3\right\rangle$ the energy eigenstates and $E_n = \hbar\Omega\sum_i (n_i + 3/2)$ the respective energy eigenvalues of the harmonic oscillator. We again minimally couple the electron to the electromagnetic field, so that in the interaction picture, the interaction Hamiltonian is again given by Eq.(3.6). Let us again calculate the spontaneous emission rate, now for a harmonic hydrogen atom initially in either one of its three first excited states,

$$\left|e\right\rangle \in \left\{\left|100\right\rangle, \left|010\right\rangle, \left|001\right\rangle\right\}. \tag{3.49}$$

The spontaneous emission rate is again given by Eq.(3.16), where now, however, the respective wave functions are given as follows:

$$\psi_g(\mathbf{x}) = \left(\frac{\mu\Omega}{\pi\hbar}\right)^{3/4} e^{-\frac{\mu\Omega}{2\hbar}|\mathbf{x}|^2} \tag{3.50}$$

$$\psi_{100}(\mathbf{x}) = \sqrt{\frac{2\mu\Omega}{\hbar}}\, x_1 \left(\frac{\mu\Omega}{\pi\hbar}\right)^{3/4} e^{-\frac{\mu\Omega}{2\hbar}|\mathbf{x}|^2} \tag{3.51}$$

$$\psi_{010}(\mathbf{x}) = \sqrt{\frac{2\mu\Omega}{\hbar}}\, x_2 \left(\frac{\mu\Omega}{\pi\hbar}\right)^{3/4} e^{-\frac{\mu\Omega}{2\hbar}|\mathbf{x}|^2} \tag{3.52}$$

$$\psi_{001}(\mathbf{x}) = \sqrt{\frac{2\mu\Omega}{\hbar}}\, x_3 \left(\frac{\mu\Omega}{\pi\hbar}\right)^{3/4} e^{-\frac{\mu\Omega}{2\hbar}|\mathbf{x}|^2} \tag{3.53}$$

With the following identities,

$$\sum_e \psi_e(\mathbf{x})\psi_e^*(\widetilde{\mathbf{x}}) = \frac{2}{\pi^{3/2}}\left(\frac{\mu\Omega}{\hbar}\right)^{5/2} (x_1\widetilde{x}_1 + x_2\widetilde{x}_2 + x_3\widetilde{x}_3)\, e^{-\frac{\mu\Omega}{2\hbar}\left(|\mathbf{x}|^2+|\widetilde{\mathbf{x}}|^2\right)}, \tag{3.54}$$

$$\frac{\partial}{\partial x_1}\psi_g(\mathbf{x}) = -\frac{x_1}{\pi^{3/4}}\left(\frac{\mu\Omega}{\hbar}\right)^{7/4} e^{-\frac{\mu\Omega}{2\hbar}|\mathbf{x}|^2}, \tag{3.55}$$

the spontaneous emission rate then becomes:

$$\mathcal{R} = \frac{q^2(\hbar\Omega)^2}{6\pi m_e\epsilon_0 c^3\hbar^2} e^{-\hbar\Omega/(2m_ec^2)} \tag{3.56}$$

$$\approx 1.506\cdot 10^9 \mathrm{s}^{-1} \tag{3.57}$$

We find that the harmonic hydrogen atom model gives us a prediction for the spontaneous emission rate which is indeed, approximately up to a factor of two, the spontaneous emission rate of an excited hydrogen atom. This indicates that our description of the hydrogen atom as an electron bound to a proton via a harmonic potential, rather than a Coulomb potential, is a reasonably good quantitative model for our purposes here, in the sense that it yields roughly the right orders of magnitude for the spontaneous emission rate from the first excited states.

3.5 'Harmonic' hydrogen atom with quantum center of mass

Let us now again take the delocalization of the harmonic hydrogen atom into account: Let us consider an electron and a proton, with position operators $\hat{\mathbf{x}}_e$ and $\hat{\mathbf{x}}_p$ and momentum operators

$\hat{\mathbf{p}}_e$ and $\hat{\mathbf{p}}_p$, which are harmonically bound to each other and which respectively interact with the electromagnetic field via minimal coupling. In the Coulomb gauge, the Hamiltonian becomes

$$\hat{H} \;=\; \frac{\left(\hat{\mathbf{p}}_p - q\hat{\mathbf{A}}(\hat{\mathbf{x}}_p)\right)^2}{2m_p} + \frac{\left(\hat{\mathbf{p}}_e + q\hat{\mathbf{A}}(\hat{\mathbf{x}}_e)\right)^2}{2m_e} + \int d^3k\, c\hbar k \sum_{s=1}^{2} \hat{a}^{s\dagger}_{\mathbf{k}} \hat{a}^{s}_{\mathbf{k}} + \frac{\mu\Omega^2}{2}\left(\hat{\mathbf{x}}_p - \hat{\mathbf{x}}_e\right)^2 , \quad (3.58)$$

where the electromagnetic field operators couple respectively to the position operators of the electron and the proton. We define the free Hamiltonian as follows:

$$\hat{H}_0 \;=\; \frac{\hat{\mathbf{p}}^2_{\mathrm{CM}}}{2M} + \frac{\hat{\mathbf{p}}^2_{\mathrm{rel}}}{2\mu} + \frac{\mu\Omega^2}{2}\hat{\mathbf{x}}^2_{\mathrm{rel}} + \int d^3k\, c\hbar k \sum_{s=1}^{2} \hat{a}^{s\dagger}_{\mathbf{k}} \hat{a}^{s}_{\mathbf{k}} \,. \quad (3.59)$$

We can now again calculate the spontaneous emission rate for an initially excited atom with quantized center of mass, averaging over the three first excited states of the three-dimensional harmonic oscillator. We insert the electronic wave functions of the harmonic hydrogen atom, given in Eq.(3.51-3.53), into the spontaneous emission rate which we obtained in Eq.(3.27). We obtain the following spontaneous emission rate for a delocalized harmonic hydrogen atom:

$$\mathcal{R} \;=\; \frac{q^2 M\mu\Omega}{12\pi\epsilon_0 c} \int_0^\infty dp\, 4\pi p^2 \left|\varphi(p)\right|^2 \mathcal{T}(p) \quad (3.60)$$

Here, we defined the template function

$$\mathcal{T}(p) \;:=\; \frac{1}{p}\int_{k_-}^{k_+} dk \left(\frac{1}{m_e} e^{-\frac{\mu\hbar k^2}{4\Omega m_e^2}} + \frac{1}{m_p} e^{-\frac{\mu\hbar k^2}{4\Omega m_p^2}}\right)^2 \left[1 + \frac{k^2p^2}{2\Omega^2M^2} - \frac{G(k)^2}{2\Omega^2\hbar^2}\right]. \quad (3.61)$$

We carry out the k integration in the template function and Taylor expand around small and non-relativistic center of mass velocities (that is, around $p/(Mc) = 0$), to obtain:

$$\mathcal{R} \;=\; C\int d^3p\, |\varphi(\mathbf{p})|^2 \left[1 + D\left(\frac{p}{Mc}\right)^2 + \mathcal{O}\left(\left(\frac{p}{Mc}\right)^4\right)\right] \quad (3.62)$$

We here defined the constants

$$C \;\approx\; 1.506 \cdot 10^9 \mathrm{s}^{-1} \qquad \text{and} \qquad D \approx 1.33\,. \quad (3.63)$$

We again note that the expansion in Eq.(3.62) is valid in the non-relativistic regime, and that in the limit of vanishing virtual center of mass velocities, the spontaneous emission rate reduces to the rate we obtained for a harmonic hydrogen atom with classical center of mass degrees of freedom.

Chapter 4

Entanglement harvesting with coherently delocalized matter

This chapter is based on the publication "Entanglement harvesting with coherently delocalized matter" [2], which I co-authored with Laura J. Henderson, Valentina Baccetti, Nicolas C. Menicucci and Achim Kempf (see Statement of Contributions on page iv). Throughout this chapter, we set $\hbar = 1$, and in the plots we further set $c = 1$.

The aim of this chapter is to investigate how the quantum nature of the center of mass degrees of freedom of matter affects the process of entanglement harvesting. Though the term entanglement harvesting was established to refer to the extraction process of preexisting entanglement from a quantum field, in more recent literature, it has been used to refer to the entangling power of quantum fields in general, both due to extraction of preexisting vacuum entanglement from the field by the detectors, but also due to field-mediated quantum communication between the detectors. We will use the term entanglement harvesting in this broader context. In section 4.1, we review the process of entanglement harvesting for both pointlike and spatially smeared UDW detectors interacting with a scalar quantum field. In section 4.2, we employ our coherently generalized detector model to describe the interaction between quantum delocalized, first quantized matter systems and a second quantized field. We recover the results of vacuum entanglement harvesting for two pointlike UDW detectors, in the limit of very large detector masses and very sharply localized center of mass degrees of freedom. We find that there is however no limit in which one recovers the results of vacuum entanglement harvesting for two UDW detectors with classical smearing profiles, which once again is in accordance with our findings in section 2.5. Further, we find that vacuum entanglement

harvesting is Gaussian suppressed in the initial delocalization, and that very delocalized detectors can not harvest any entanglement from the vacuum. Finally, in section 4.3, we briefly discuss entanglement harvesting for delocalized detectors in media—which might be of interest not only for the purpose of experimentally observing entanglement harvesting, but also to potentially make use of entanglement harvesting in quantum technologies. For the sake of simplicity, we again model a medium as a scalar quantum field, whose wave propagation speed differs from the vacuum propagation speed of light. As the wave propagation speed decreases, we find that less entanglement can be harvested from the phononic ground state. Intuitively, this is because the phononic ground state transforms non-trivially under a quantum reference frame transformation into the rest frame of the coherently delocalized detectors, subjecting the detectors to noisy excitations that make it more difficult for the detectors to harvest entanglement. We conjecture that matter systems are less likely to become entangled with each other by interacting with a medium than they are by interacting with the electromagnetic field.

4.1 Review: Entanglement harvested by UDW detectors from the vacuum

Before taking into account the quantum delocalization of the centers of mass of the detectors, we briefly review the process of vacuum entanglement harvesting for UDW detectors, whose center of mass degrees of freedom are described classically. We consider two UDW detectors, labeled by $J = A, B$, which interact with a scalar quantum field. We assume that the two detectors have the same energy gap Ω and that their classical centers of mass are located respectively at the positions $\mathbf{x}_J$. We let $S := |\mathbf{x}_A - \mathbf{x}_B|$ denote the center of mass separation of the two detectors. In the following, we will work within the interaction picture, in which operators evolve according to the free Hamiltonian

$$\hat{H}_0 \;=\; \sum_{J=A,B} \Omega \, |e_J\rangle \langle e_J| + \int d^3k \, ck \, \hat{a}^\dagger_{\mathbf{k}} \hat{a}_{\mathbf{k}} \, . \tag{4.1}$$

We here let $|e_J\rangle$ and $|g_J\rangle$ denote the respective excited and ground energy eigenstates of the two detectors. We classically model the extended spatial profile of the detectors by introducing smearing profiles $\xi(\mathbf{x} - \mathbf{x}_J)$ for the two detectors. We let the monopole moment operators of the two detectors, $\hat{\mu}_J = |e_J\rangle \langle g_J| + |g_J\rangle \langle e_J|$, respectively couple to the field operators $\hat{\phi}(\mathbf{x})$ via the linear monopole moment operator coupling. The state of the system then evolves in time

according to the interaction Hamiltonian

$$\hat{H}_{int}(t) \;=\; \sum_{J=A,B} \hat{H}_J(t)\,, \tag{4.2}$$

where the interaction Hamiltonians $\hat{H}_J(t)$ respectively capture the interaction of the two detectors with the quantum field:

$$\hat{H}_J(t) \;:=\; \lambda\chi(t)\hat{\mu}_J(t)\int d^3x\,\xi(\mathbf{x}-\mathbf{x}_J)\hat{\phi}(\mathbf{x},t) \tag{4.3}$$

The monopole moment operators and the field operators evolve according to their free Hamiltonians as follows:

$$\hat{\mu}_J(t) \;=\; e^{i\Omega t}\,|e_J\rangle\langle g_J| + \text{h.c.}\,, \tag{4.4}$$

$$\hat{\phi}(\mathbf{x},t) \;=\; \int \frac{d^3k}{(2\pi)^{3/2}}\sqrt{\frac{c^2}{2k}}\Big[e^{-ickt+i\mathbf{kx}}\hat{a}_{\mathbf{k}} + \text{h.c.}\Big] \tag{4.5}$$

For small interaction strengths, we remember that we can perturbatively expand the time evolution operator, $\hat{U}(t) =: \sum_n \hat{U}^{(n)}(t)$, with

$$\hat{U}^{(n)}(t) \;:=\; (-i)^n\int_0^t dt_1\hat{H}_{int}(t_1)\int_0^{t_1} dt_2\hat{H}_{int}(t_2)\cdots\int_0^{t_{n-1}} dt_n\hat{H}_{int}(t_n)\,. \tag{4.6}$$

Perturbatively in the interaction strength, we can now study how much the two detectors become entangled with each other, via their respective interaction with the quantum field, see, e.g., [23, 22]. To this end, we consider the initial state $\rho(0) = |g_A\rangle\langle g_A|\otimes|g_B\rangle\langle g_B|\otimes|0\rangle\langle 0|$, for which the two detectors are unentangled and the quantum field is in its vacuum state $|0\rangle$. Next, we perturbatively time evolve this initial density matrix, such as to obtain the density matrix at a later time $t > 0$:

$$\begin{aligned}\rho(t) \;&=\; \Big(\mathbf{1}+\hat{U}^{(1)}(t)+\hat{U}^{(2)}(t)+\ldots\Big)\,\rho(0)\,\Big(\mathbf{1}+\hat{U}^{(1)}(t)+\hat{U}^{(2)}(t)+\ldots\Big)^\dagger \\ &=:\; \rho(0)+\rho^{(1,1)}(t)+\rho^{(2,0)}(t)+\rho^{(0,2)}(t)+\ldots\end{aligned} \tag{4.7}$$

We employed the notation $\rho^{(i,j)} := U^{(i)}\rho(0)U^{(j)\dagger}$ here. Note that we can disregard all terms $\rho^{(i,j)}$ with odd $i+j$, since they have vanishing vacuum expectation values. Explicitly, we have:

$$\rho^{(1,1)}(t) \;=\; \int_0^t dt_1\int_0^t dt_2\hat{H}_{int}(t_1)\rho(0)\hat{H}_{int}(t_2)\,, \tag{4.8}$$

$$\rho^{(2,0)}(t) \;=\; -\int_0^t dt_1\int_0^{t_1} dt_2\hat{H}_{int}(t_1)\hat{H}_{int}(t_2)\rho(0)\,, \tag{4.9}$$

$$\rho^{(0,2)}(t) \;=\; -\int_0^t dt_1\int_0^{t_1} dt_2\rho(0)\hat{H}_{int}(t_1)\hat{H}_{int}(t_2) \tag{4.10}$$

We now employ the basis $\{|g_A\rangle|g_B\rangle, |g_A\rangle|e_B\rangle, |e_A\rangle|g_B\rangle, |e_A\rangle|e_B\rangle\}$, and take the partial trace over the field degrees of freedom, such as to obtain the partial state $\rho_{AB}(t)$ of the two detectors after their interaction with the quantum field:

$$\begin{aligned}\rho_{AB}(t) &= \rho(0) + \mathrm{Tr}_F\left(\rho^{(1,1)}\right) + \mathrm{Tr}_F\left(\rho^{(2,0)}\right) + \mathrm{Tr}_F\left(\rho^{(0,2)}\right) + \dots \\ &=: \begin{pmatrix} 1-P_A^c-P_B^c & 0 & 0 & \mathcal{M}^{c*} \\ 0 & P_B^c & \mathcal{L}^{c*} & 0 \\ 0 & \mathcal{L}^{c*} & P_A^c & 0 \\ \mathcal{M}^c & 0 & 0 & 0 \end{pmatrix} + \mathcal{O}(\lambda^4) \end{aligned} \tag{4.11}$$

We made the following definitions,

$$P_A^c := \langle e_A|\langle g_B|\,\mathrm{Tr}_F\left(\int_0^t dt_1 \int_0^t dt_2 \hat{H}_{int}(t_1)\rho(0)\hat{H}_{int}(t_2)\right)|e_A\rangle|g_B\rangle\,, \tag{4.12}$$

$$P_B^c := \langle g_A|\langle e_B|\,\mathrm{Tr}_F\left(\int_0^t dt_1 \int_0^t dt_2 \hat{H}_{int}(t_1)\rho(0)\hat{H}_{int}(t_2)\right)|g_A\rangle|e_B\rangle\,, \tag{4.13}$$

$$\mathcal{M}^c := \langle e_A|\langle e_B|\,\mathrm{Tr}_F\left(-\int_0^t dt_1 \int_0^{t_1} dt_2 \hat{H}_{int}(t_1)\hat{H}_{int}(t_2)\rho(0)\right)|g_A\rangle|g_B\rangle\,, \tag{4.14}$$

where P_A^c and P_A^c are the excitation probabilities of the detectors A and B respectively and $\mathcal{M}^c$ has traditionally been referred to as the entangling term. We here let the superscript c remind us of the classical nature of the center of mass degrees of freedom of the two UDW detectors. When considering identical detectors (up to a spatial displacement), the excitation probabilities of the two detectors are identical and the reduced density matrix simplifies,

$$\rho_{AB}(t) =: \begin{pmatrix} 1-2P^c & 0 & 0 & \mathcal{M}^{c*} \\ 0 & P^c & \mathcal{L}^c & 0 \\ 0 & \mathcal{L}^c & P^c & 0 \\ \mathcal{M}^c & 0 & 0 & 0 \end{pmatrix} + \mathcal{O}(\lambda^4)\,, \tag{4.15}$$

to second perturbative order in the interaction strength. Here, $P_A^c = P_B^c =: P^c$ denotes the excitation probabilities of the two detectors respectively. In the scenario we are considering here, the excitation probabilities of the two detectors are equal, since we here consider the same switching function and the same smearing profile (up to a displacement in space) for the two detectors.

To measure the entanglement between the internal degrees of freedom of the two detectors, we will here employ the entanglement negativity [89], which is an entanglement monotone [90, 91]. The entanglement negativity is defined for a density matrix as the absolute value

of the sum of the negative eigenvalues of the partially transposed density matrix. To second perturbative order in the interaction strength, the negativity for the partial state of the two detectors becomes (see, e.g., [23, 22])

$$\mathcal{N} \;=\; \max\left\{0\,,\,\frac{1}{2}\left(\sqrt{(P_A^c-P_B^c)^2+4|\mathcal{M}^c|^2}\right)-P_A-P_B\right\}. \tag{4.16}$$

For detectors with equal excitation probabilities, the negativity simplifies to

$$\mathcal{N}^c \;=\; \max\left\{0\,,\,-P^c+|\mathcal{M}^c|\right\}. \tag{4.17}$$

It is worth mentioning here that a rich variety of quantitative entanglement measures have been established in the literature (see, e.g., [92]). For instance, we could just as well use concurrence [93] as our measure for entanglement. For two identical detectors and to second perturbative order, concurrence and entanglement negativity have however been shown to be equivalent entanglement measures [48]. For the purpose of this chapter, we will restrict our attention to entanglement negativity.

Let us now consider the sine switching function of compact support given in Eq.(1.20). Examples for the use of compact switching functions can be found e.g. in [94, 22]. We employ a compact switching function in order to ensure that the interaction between the detectors and the field is switched on only during a compact time interval, $t \in [0, \pi\sigma]$. The importance of employing a compact switching function will become apparent in the next section. Integrating over all times, the excitation probabilities and the entangling term become

$$P^c \;=\; \frac{\lambda^2\sigma^2}{(2\pi)^3}\int\frac{d^3k}{2ck}\,|\widetilde{\xi}(\mathbf{k})|^2\,A(k)\,, \tag{4.18}$$

$$\mathcal{M}^c \;=\; -\frac{\lambda^2\sigma^2 e^{i\pi\Omega\sigma}}{c}\int\frac{d^3k}{k}\frac{e^{2i\mathbf{k}\cdot\mathbf{x}_0}\,\widetilde{\xi}(\mathbf{k})^2 B(k)}{1-\sigma^2(\Omega+ck)^2}\,, \tag{4.19}$$

where $\widetilde{\xi}(\mathbf{k})$ denotes the Fourier transformation of the spatial smearing profile $\xi(\mathbf{x})$ and where we defined the following functions:

$$A(k) \;:=\; \frac{1+\cos(\pi\sigma(\Omega+ck))}{\left(\sigma^2(\Omega+ck)^2-1\right)^2}\,, \tag{4.20}$$

$$B(k) \;:=\; \frac{i(2\Omega+ck)\sin(\pi\Omega\sigma)}{2\Omega(1-\Omega^2\sigma^2)}+\frac{e^{-i\pi\Omega\sigma}+e^{-i\pi ck\sigma}}{1-\sigma^2(\Omega-ck)^2} \tag{4.21}$$

We can now specify a spatial smearing function according to which the detectors couple to the

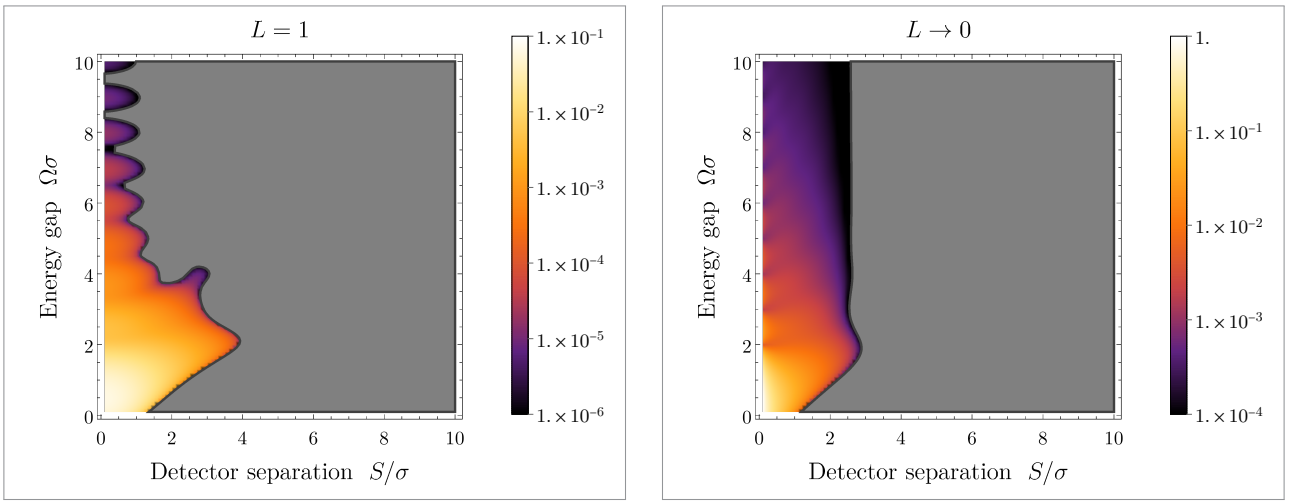

Figure 4.1: The negativity as a function of the energy gap Ω and the separation S of the detectors, plotted *(top)* for spatially smeared UDW detectors with $L = \sigma$ and *(bottom)* for pointlike UDW detectors. The regions of zero negativity are marked in grey. This Figure was taken from [2] and all credit goes to Laura J. Henderson for creating the plots.

field. We could for instance model the spatial extent of the detectors via Gaussian smearing profiles of standard deviation $L/2$:

$$\xi(\mathbf{x}) \;=\; \left(\frac{2}{\pi L^2}\right)^{3/2} e^{-2\mathbf{x}^2/L^2} \tag{4.22}$$

Since the smearing profiles are normalized, we may interpret them as classical probability distributions, according to which the detectors couple to the quantum field. The Fourier transformed smearing function then reads:

$$\widetilde{\xi}(\mathbf{k}) \;=\; \left(\frac{1}{2\pi}\right)^{3/2} \exp\left(-\frac{L^2k^2}{8}\right) \tag{4.23}$$

We find that the excitation probabilities and the entangling term depend on the width L of the smearing profiles, the energy gap Ω of the detectors and the total interaction time $\pi\sigma$, and the entangling term additionally depends on the separation S of the two detectors:

$$P_L^c \;=\; \frac{\lambda^2\sigma^2}{2\pi^2 c}\int_0^\infty dk\, k\, e^{-\frac{L^2k^2}{4}} A(k)\,, \tag{4.24}$$

$$\mathcal{M}_L^c \;=\; -\frac{\lambda^2\sigma^2 e^{i\pi\Omega\sigma}}{2\pi^2 cS}\int_0^\infty dk\, \frac{\sin(kS)e^{-\frac{L^2k^2}{4}}B(k)}{1-\sigma^2(\Omega+ck)^2} \tag{4.25}$$

We here let the subscript L indicate that we employed Gaussian smearing profiles. In the limit of very sharply peaked smearing profiles ($L \to 0$), we recover the excitation probabilities and the entangling term for pointlike UDW detectors:

$$P_0^c = \frac{\lambda^2\sigma^2}{2\pi^2 c}\int_0^\infty dk\, k\, A(k)\,, \tag{4.26}$$

$$\mathcal{M}_0^c = -\frac{\lambda^2\sigma^2 e^{i\pi\Omega\sigma}}{2\pi^2 cS}\int_0^\infty dk\, \frac{\sin(kS)B(k)}{1-\sigma^2(\Omega+ck)^2} \tag{4.27}$$

The negativity for both pointlike and Gaussian smeared UDW detectors is plotted in Fig.(4.1), as a function of the energy gap Ω of the detectors and their separation S. We can see that the negativity decreases with increasing widths L of the Gaussian smearing profiles. Intuitively, we can understand this behaviour as follows: the field amplitudes at different points in space and time are quantum correlated, which is why two spatially separated detectors can become entangled with one another in the first place. Spatially smeared UDW detectors average the quantum field fluctuations over extended spatial regions, and the larger these spatial regions are, the less entanglement the detectors can harvest from the quantum field. In the negativity plots in Fig.(4.1) we further observe a resonance-like behaviour, for energy gaps that are multiples of the switching scale σ, which manifests itself in slight ripples in the negativity for pointlike UDW detectors, and more pronounced oscillations for spatially smeared UDW detectors.

4.2 Entanglement harvested by coherently delocalized detectors from the vacuum

The results for entanglement harvesting in the previous section relied on the assumption that the center of mass degrees of freedom of the matter systems under investigation are classical. In this section, we study how the process of entanglement harvesting is affected when the centers of mass of the two detectors respectively undergo quantum uncertain motion.

A possible setup we have in mind here is the following: Let us consider two atoms, which are respectively initially localized in a certain region of space, for instance via center of mass position measurements, and which are then both left to evolve freely. Their center of mass wave functions then spread and the atoms dynamically and coherently delocalize in space. Let us now imagine that these two coherently delocalizing atoms interact with the electromagnetic vacuum. How much will the internal degrees of freedom of the atoms become entangled with each other?

How will the result depend on the mass of the detectors, their initial localization, and their dynamical delocalization process? How will the results compare to the results for entanglement harvesting with classical center of mass degrees of freedom?

To answer these questions, we once again employ our coherently delocalized detector model: We again replace the electromagnetic field by a simpler scalar field, we model the atoms as two-level detector systems, and in order to allow both detectors to coherently delocalize, we let their respective center of mass degrees of freedom be quantized. We let $\hat{\mathbf{x}}_J$ and $\hat{\mathbf{p}}_J$ denote the center of mass position and momentum operators of the two detectors respectively. We will here assume that the two detectors are of equal mass M. In the interaction picture, operators then evolve according to the free Hamiltonian

$$\hat{H}_0 \;=\; \sum_{J=A,B} \left[\frac{\hat{\mathbf{p}}_J^{\,2}}{2M} + \Omega \left|e_J\right\rangle \left\langle e_J\right| \right] + \int d^3k \, ck \, \hat{a}^\dagger_{\mathbf{k}} \hat{a}_{\mathbf{k}} \,. \tag{4.28}$$

We again couple the detectors to the quantum field via the monopole moment coupling. However, the field operators now take the center of mass position operators of the two detectors as their argument:

$$\hat{H}_{int}(t) \;=\; \lambda \chi(t) \sum_{J=A,B} \hat{\mu}_J(t) \hat{\phi}(\hat{\mathbf{x}}_J, t) \tag{4.29}$$

We again make sense of the field operators depending on position operators, $\hat{\phi}(\hat{\mathbf{x}}_J, t)$, as follows,

$$\hat{\phi}(\hat{\mathbf{x}}_J, t) \;:=\; \int d^3x_J \, \hat{\mathcal{P}}(\mathbf{x}_J, t) \hat{\phi}(\mathbf{x}_J, t) \,, \tag{4.30}$$

where we defined the operators $\hat{\mathcal{P}}(\mathbf{x}_J, t)$ as

$$\hat{\mathcal{P}}(\mathbf{x}_J, t) \;:=\; \int \frac{d^3p \, d^3q}{(2\pi)^3} e^{-i(\mathbf{p}-\mathbf{q})\cdot\mathbf{x}_J + it\frac{p^2-q^2}{2M}} \left|\mathbf{p}\right\rangle \left\langle \mathbf{q}\right| \,. \tag{4.31}$$

As in section 4.1, we again assume that initially the two detectors are in their ground states and the field is in its vacuum state. We further let $|\varphi_J\rangle$ denote the initial center of mass states of the two detectors. The initial state of the system then reads:

$$\rho(0) \;=\; \left|\varphi_A\right\rangle \left\langle \varphi_A\right| \otimes \left|g_A\right\rangle \left\langle g_A\right| \otimes \left|\varphi_B\right\rangle \left\langle \varphi_B\right| \otimes \left|g_B\right\rangle \left\langle g_B\right| \otimes \left|0\right\rangle \left\langle 0\right| \tag{4.32}$$

We can express the initial center of mass states both in terms of the initial center of mass wave functions in the position and in the momentum representation:

$$\left|\varphi_J\right\rangle \;=\; \int d^3x \, \varphi_J(\mathbf{x}) \left|\mathbf{x}\right\rangle = \int d^3p \, \widetilde{\varphi}_J(\mathbf{p}) \left|\mathbf{p}\right\rangle \tag{4.33}$$

We again want to investigate how entangled the internal degrees of freedom become with each other via the interaction of the detectors with the quantum field. To this end, we evolve the initial state in time and trace over both the field and the center of mass degrees of freedom. To second perturbative order, we again obtain the partial state of the two detectors:

$$\begin{aligned}\rho_{AB}(t) &= \rho(0) + \mathrm{Tr}_{\mathrm{F,COM}}\left(\rho^{(1,1)}\right) + \mathrm{Tr}_{\mathrm{F,COM}}\left(\rho^{(2,0)}\right) + \mathrm{Tr}_{\mathrm{F,COM}}\left(\rho^{(0,2)}\right) + \dots \\ &=: \begin{pmatrix} 1-P_A-P_B & 0 & 0 & \mathcal{M}^* \\ 0 & P_B & \mathcal{L} & 0 \\ 0 & \mathcal{L} & P_A & 0 \\ \mathcal{M} & 0 & 0 & 0 \end{pmatrix} + \mathcal{O}(\lambda^4) \end{aligned} \tag{4.34}$$

We again calculate the entanglement negativity for this density matrix, as a quantitative measure for how much entanglement the internal degrees of freedom of the two coherently delocalizing detectors can harvest from the vacuum:

$$\mathcal{N} = \max\left\{0\,,\,\frac{1}{2}\left(\sqrt{(P_A-P_B)^2+4|\mathcal{M}|^2}\,-P_A-P_B\right)\right\} \tag{4.35}$$

We find the excitation probabilities P_J of the two detectors to be

$$P_A := \langle e_A|\langle g_B|\,\mathrm{Tr}_{\mathrm{field,COM}}\left(\int_0^t dt_1\int_0^t dt_2 \hat{H}_A(t_1)\rho(0)\hat{H}_A(t_2)\right)|e_A\rangle\,|g_B\rangle \tag{4.36}$$

$$= \frac{\lambda^2}{(2\pi)^3}\int_0^t dt_1\int_0^t dt_2\chi(t_1)\chi(t_2)\int d^3p\int\frac{d^3k}{2ck}\,|\widetilde{\varphi}_A(\mathbf{p}\,)|^2\,e^{i(t_1-t_2)\left(\Omega+ck+\frac{k^2-2\mathbf{pk}}{2M}\right)}\,, \tag{4.37}$$

$$P_B := \langle g_A|\langle e_B|\,\mathrm{Tr}_{\mathrm{field,COM}}\left(\int_0^t dt_1\int_0^t dt_2 \hat{H}_B(t_1)\rho(0)\hat{H}_B(t_2)\right)|g_A\rangle\,|e_B\rangle \tag{4.38}$$

$$= \frac{\lambda^2}{(2\pi)^3}\int_0^t dt_1\int_0^t dt_2\chi(t_1)\chi(t_2)\int d^3p\int\frac{d^3k}{2ck}\,|\widetilde{\varphi}_B(\mathbf{p}\,)|^2\,e^{i(t_1-t_2)\left(\Omega+ck+\frac{k^2-2\mathbf{pk}}{2M}\right)}\,, \tag{4.39}$$

and we note that the excitation probabilities of the two detectors depend on their center of mass states only via their respective momentum probability distributions $|\widetilde{\varphi}_J(\mathbf{p})|^2$. Unlike the excitation probabilities, we find that the entangling term $\mathcal{M}$ also depends on the phases of the

initial center of mass momentum wave functions:

$$\begin{aligned}
\mathcal{M} &:= -\int_0^t dt_1 \int_0^{t_1} dt_2 \, \langle e_A| \langle e_B| \, \mathrm{Tr}_{\mathrm{F,COM}} \left(\left(\hat{H}_A(t_1)\hat{H}_B(t_2) + \hat{H}_B(t_1)\hat{H}_A(t_2) \right) \rho(0) \right) |g_A\rangle \, |g_B\rangle \\
&= -\frac{\lambda^2}{(2\pi)^3} \int_0^t dt_1 \int_0^{t_1} dt_2 \, \chi(t_1)\chi(t_2) \int d^3p_1 \int d^3p_2 \int \frac{d^3k}{2ck} \, \varphi_A(\mathbf{p_1}+\mathbf{k}) \, \varphi_B(\mathbf{p_2}-\mathbf{k}) \times \\
&\quad \times \varphi_A^*(\mathbf{p_1}) \, \varphi_B^*(\mathbf{p_2}) e^{-i(t_1+t_2)\left(\frac{k^2}{2M}-\Omega\right)} e^{-ick(t_1-t_2)} e^{i\mathbf{k}(\mathbf{p_2}t-\mathbf{p_1}t')/M} + (A \leftrightarrow B) \\
&= -\lambda^2 \int_0^t dt_1 \int_0^{t_1} dt_2 \, \chi(t_1)\chi(t_2) \int \frac{d^3p_1 d^3p_2}{(2\pi)^3} \int \frac{d^3k}{2ck} \, \widetilde{\varphi}_A(\mathbf{p_1}+\mathbf{k}) \, \widetilde{\varphi}_B(\mathbf{p_2}-\mathbf{k}) \, \widetilde{\varphi}_A^*(\mathbf{p_1}) \\
&\quad \times \widetilde{\varphi}_B^*(\mathbf{p_2}) e^{i(t_1+t_2)\left(\Omega - \frac{\mathbf{k}(\mathbf{p_1}-\mathbf{p_2})}{2M} - \frac{k^2}{2M}\right)} \left[e^{-i(t_1-t_2)\left(ck - \frac{\mathbf{k}(\mathbf{p_1}+\mathbf{p_2})}{2M}\right)} + e^{-i(t_1-t_2)\left(ck + \frac{\mathbf{k}(\mathbf{p_1}+\mathbf{p_2})}{2M}\right)} \right] \qquad (4.40)
\end{aligned}$$

The phases of the momentum wave functions carry the position information of the two wave functions, and as expected, the entangling term thus depends on the spatial locations of the two center of mass wave packets. While the excitation probabilities of the detectors respectively only depend on the properties of one detector, the entangling term thus depends on the properties of both detectors. As suggested e.g. in [23], we can thus think of the excitation of the respective detectors according to P_J as local noise, while the nonlocal entangling term $\mathcal{M}$ describes entangling excitations that are shared by the two detectors.

Let us now again consider the sine switching function in Eq.(1.20), and let us assume that the initial COM wave functions of the two detectors respectively are spherically symmetric, that is, $\varphi_J(\mathbf{p}) \equiv \varphi_J(p)$. As far as the excitation probabilities are concerned, our setup does not single out a preferred spatial direction. Thus, we can always rotate our coordinate system such that the photon is emitted along the $z-$ axis, $\mathbf{k} = (0,0,k)^T$, which simplifies our calculation as follows:

$$\begin{aligned}
P_J &= \frac{\lambda^2}{(2\pi)^3} \int d^3p \, |\varphi_J(p)|^2 \int_0^\infty dk \frac{2\pi k}{c} \left| \int_0^{\pi\sigma} dt \sin\left(\frac{t}{\sigma}\right) e^{it\left(F(k) - \frac{kp}{M}\cos(\theta_p)\right)} \right|^2 \\
&= \frac{\lambda^2\sigma^2}{(2\pi)^3} \int_0^\infty dp \int_{-1}^1 dz \, 2\pi p^2 \, |\varphi_J(p)|^2 \int_0^\infty dk \frac{2\pi k}{c} \left| \frac{e^{i\pi\sigma\left(F(k) - \frac{kpz}{M}\right)} + 1}{\sigma^2\left(F(k) - \frac{kpz}{M}\right)^2 - 1} \right|^2 \\
&= \frac{\lambda^2\sigma^2}{\pi c} \int_0^\infty dp \int_{-1}^1 dz \, p^2 \, |\varphi_J(p)|^2 \int_0^\infty dk \, k \, \frac{1 + \cos\left(\pi\sigma\left(F(k) - \frac{kpz}{M}\right)\right)}{\left[\sigma^2\left(F(k) - \frac{kpz}{M}\right)^2 - 1\right]^2} \qquad (4.41)
\end{aligned}$$

We can now specify the initial center of mass wave functions for the two detectors. Let us here consider detectors whose center of mass position wave functions are Gaussian wave packets of

initial width L, respectively centered around $\mathbf{x}_J$, at a separation $S := |\mathbf{x}_A - \mathbf{x}_B|$:

$$\varphi_J(\mathbf{x}) = \left(\frac{2}{\pi L^2}\right)^{3/4} e^{-\frac{|\mathbf{x}+\mathbf{x}_J|^2}{L^2}}, \tag{4.42}$$

$$\widetilde{\varphi}_J(\mathbf{p}) = \left(\frac{L^2}{2\pi}\right)^{3/4} e^{-\frac{p^2 L^2}{4}+i\mathbf{p}\cdot\mathbf{x}_J} \tag{4.43}$$

The momentum probability distributions resulting from these momentum wave functions are the same for both detectors, $|\widetilde{\varphi}_J(\mathbf{p})|^2 = L^3/(2\pi)^{3/2} e^{-p^2L^2/2}$. We thus find that the excitation probabilities of the two detectors are equal, $P_A = P_B =: P$, and the negativity reduces to

$$\mathcal{N} = \max\left\{0\,,\, |\mathcal{M}| - P\right\}. \tag{4.44}$$

In order for the two detectors to harvest entanglement from the vacuum, the nonlocal entangling excitations thus need to dominate over the local excitation of the respective detectors [23].

We can now see why it is important to employ a switching function of compact support. Under the free quantum mechanical time evolution, the wave packets in Eq.(4.43) start out completely delocalized in space for $t \to -\infty$, then flow together to Gaussians of width L at time $t = 0$, and then spread again into completely delocalized states for $t \to \infty$. If we employed a switching function of non-compact support, such as a Gaussian switching function, we would need to consider the completely delocalized center of mass wave packets at time $t \to -\infty$ as the initial center of mass states. However, we want to consider the localized wave packets in Eq.(4.43) as the center of mass states at the initial time $t = 0$, since our aim here is to study how entanglement harvesting is affected by the center of mass spreading of initially localized detectors. We therefore need to ensure that the interaction with the quantum field is switched on precisely at time $t = 0$, which in turn is why we need to employ a switching function of compact support. Let us here again employ the compact sine switching function in Eq.(1.20). We obtain

$$P = \frac{\lambda^2\sigma^2}{\pi c}\int_0^\infty dp\, p^2\, |\widetilde{\varphi}_J(\mathbf{p})|^2\, \mathcal{U}(p) \tag{4.45}$$

for the excitation probabilities. We here defined the template function

$$\mathcal{U}(p) := \int_{-1}^{1} dz \int_0^\infty dk\, k \left[1 + \cos\left(\pi\sigma\left(F - \frac{kpz}{M}\right)\right)\right]\left[\sigma^2\left(F - \frac{kpz}{M}\right)^2 - 1\right]^{-2}, \tag{4.46}$$

where p is the detector's recoil momentum and where we defined $F := \Omega + ck + k^2/(2M)$ for convenience of notation. We refer to $\mathcal{U}(p)$ as a "template function" due to the fact that the

function is independent of the center of mass states of the detectors. For the entangling term, we obtain

$$\mathcal{M} = \frac{\lambda^2 L^6}{(2\pi)^6}\int d^3p \int d^3P \int \frac{d^3k}{2ck} e^{-2i\mathbf{k}\cdot\mathbf{x}_0}\mathcal{I}(\mathbf{k},\mathbf{p},\mathbf{P}) e^{-\frac{L^2}{2}\left(p^2+P^2+k^2+(\mathbf{p}-\mathbf{P})\mathbf{k}\right)}, \tag{4.47}$$

with $p := |\mathbf{p}|$ and $P := |\mathbf{P}|$ and where we defined $\mathcal{I}$ as the time integrals,

$$\begin{aligned}\mathcal{I}(\mathbf{k},\mathbf{p},\mathbf{P}) := & \int_0^{\pi\sigma} dt \int_0^t dt' \sin\left(\frac{t}{\sigma}\right)\sin\left(\frac{t'}{\sigma}\right) e^{i(t+t')\left(\Omega-\frac{\mathbf{k}(\mathbf{p}-\mathbf{P})}{2M}-\frac{k^2}{2M}\right)} \times \\ & \times\left(e^{-i(t-t')\left(ck-\frac{\mathbf{k}(\mathbf{p}+\mathbf{P})}{2M}\right)} + e^{-i(t-t')\left(ck+\frac{\mathbf{k}(\mathbf{p}+\mathbf{P})}{2M}\right)}\right)\end{aligned} \tag{4.48}$$

We can again rotate the coordinate system so that the momentum of the emitted photon is aligned with the $z-$axis, that is $\mathbf{k} = (0,0,k)^T$. We write $\mathbf{p} = (p_x, p_y, p_z)^T$ as well as $\mathbf{P} = (P_x, P_y, P_z)^T$. As opposed to when we calculated the excitation probabilities, there is now a preferred direction set by $\mathbf{x}_A$ and $\mathbf{x}_B$. Thus, in order to make up for fixing $\mathbf{k}$ to be aligned with the $z-$axis (even though the photon could be emitted in any direction), we now integrate over all $\mathbf{x}_A - \mathbf{x}_B$ of fixed length (i.e. we keep the separation $S := |\mathbf{x}_A - \mathbf{x}_B|$ between the two detectors fixed). We can write $\mathbf{x}_A - \mathbf{x}_B = S(\sin(\theta)\cos(\phi),\, \sin(\theta)\sin(\phi),\, cos(\theta))^T$ and integrate over all $\theta \in [0,\pi]$ and $\phi \in [0, 2\pi]$. Instead of integrating over all $\mathbf{k}$, that is $\int d^3k$, we now only need to integrate over $\int_0^\infty dk\, k^2$ and not over the angles of the emitted photon:

$$\begin{aligned}\mathcal{M} &= \frac{\lambda^2 L^6}{(2\pi)^6}\int d^3p \int d^3P \int_0^\infty dk \frac{k}{2c}\int_0^\pi d\theta\, 2\pi\sin(\theta)\,\mathcal{I}(\mathbf{k},\mathbf{p},\mathbf{P})\, e^{-ikS\cos(\theta)} \times \\ &\quad \times e^{-\frac{L^2}{2}\left(p^2+P^2+k^2+k(p_z-P_z)\right)} \\ &= \frac{\lambda^2 L^6}{c(2\pi)^5}\int d^3p \int d^3P \int_0^\infty dk \frac{\sin(kS)}{S}\,\mathcal{I}(\mathbf{k},\mathbf{p},\mathbf{P})\, e^{-\frac{L^2}{2}\left(p^2+P^2+k^2+k(p_z-P_z)\right)}\end{aligned} \tag{4.49}$$

Finally, changing variables, $p_1 := p_z + \frac{1}{2}k$ and $p_2 := P_z - \frac{1}{2}k$, we obtain for the entangling term:

$$\mathcal{M} = \frac{\lambda^2\sigma^2 L^2}{c(2\pi)^3}\int_{-\infty}^\infty dp_1 \int_{-\infty}^\infty dp_2 \int_0^\infty dk \frac{\sin(kS)}{S} e^{-L^2(p_1^2+p_2^2)/2} e^{-L^2k^2/4}\,\mathcal{V}(k,p_1,p_2) \tag{4.50}$$

We here defined the template function

$$\mathcal{V}(k,p_1,p_2) := \sum_{j=0}^{1}\frac{e^{i\pi\alpha\sigma}}{1-\sigma^2(\alpha+\beta_j)^2}\left(\frac{i(2\alpha+\beta_j)\sin(\pi\alpha\sigma)}{2\alpha\,(1-\alpha^2\sigma^2)} + \frac{e^{-i\pi\alpha\sigma}+e^{-i\pi\beta_j\sigma}}{1-\sigma^2(\alpha-\beta_j)^2}\right), \tag{4.51}$$

with $\alpha(k,p_1,p_2) := \Omega - k(p_1-p_2)/(2M)$ and $\beta_j(k,p_1,p_2) := ck + (-1)^j k(p_1+p_2)/(2M)$.

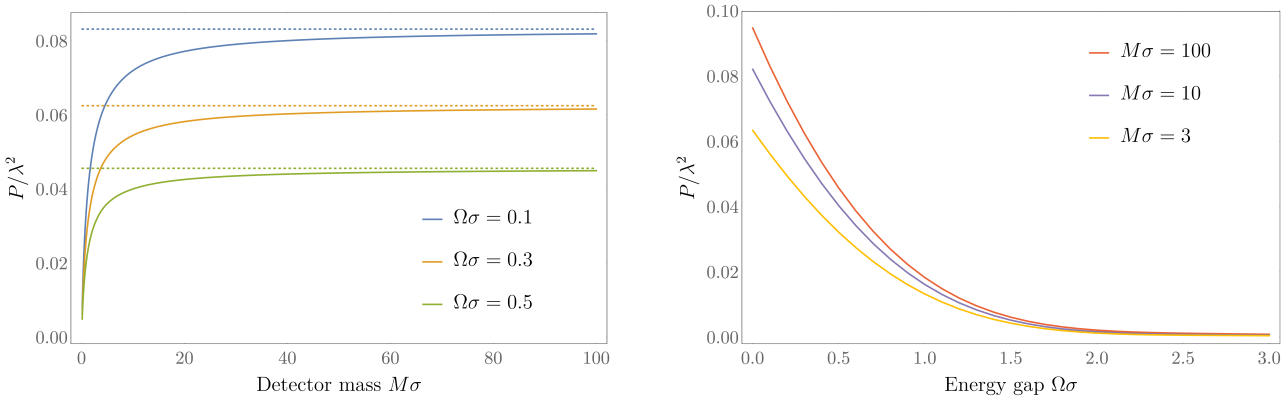

Figure 4.2: The transition probability of a massive detector (with $L = 1000\sigma$), *(left)* as a function of its mass and for different energy gaps, where the dotted lines represent the excitation probabilities of pointlike UDW detectors with the same energy gaps as the respective massive detectors and *(right)* as a function of its energy gap, for different masses.

Since we work within a framework in which the center of mass dynamics are described by the Schrödinger equation, we once again need to ensure that the virtual center of mass velocities are well within the non-relativistic regime. That is, we need to ensure that the momentum probability distributions $|\widetilde{\varphi}_J(\mathbf{p})|^2$ have contributions only for momenta corresponding to virtual velocities much smaller than the speed of light. Let us again restrict the virtual velocities to velocities no larger than one percent of the vacuum speed of light, $v := p/M \leq 0.01c$. The Gaussian momentum probability distributions of the detectors have a standard deviation of $1/L$. We can thus assume to a very good approximation (within 3.5 standard deviations away from the mean) that the center of mass momenta $\mathbf{p}$ in the probability distributions satisfy $pL \lesssim 3.5$. The non-relativistic regime therefore corresponds to parameters L and M satisfying

$$LMc \gtrsim 3.5 \times 10^2 \,. \tag{4.52}$$

The center of mass wave function of a coherently delocalized detector spreads faster for smaller L and M, that is, for initially more sharply localized detectors and for smaller detector masses. Consequently, for a given detector mass, there is a minimal initial delocalization width we can consider while staying within the non-relativistic regime for the virtual center of mass velocities.

Provided that we chose appropriate parameters M and L, we can expand the template functions $\mathcal{U}$ and $\mathcal{V}$ for non-relativistic virtual center of mass velocities. We Taylor expand $\mathcal{U}$ around $p/(Mc) = 0$, and we Taylor expand $\mathcal{V}$ around both $p_1/(Mc) = 0$ and $p_2/(Mc) = 0$. To second order, we then obtain the following simplified expressions for the excitation probabilities

and the entangling term:

$$P = \frac{\lambda^2\sigma^2}{4\pi^2 c}\left[\mathcal{U}(0) + \frac{3}{2L^2}\frac{\partial^2\mathcal{U}}{\partial p^2}(0) + \mathcal{O}\left((LMc)^{-4}\right)\right], \tag{4.53}$$

$$\mathcal{M} = \frac{\lambda^2\sigma^2}{4\pi^2 c}\int_0^\infty dk \frac{\sin(kS)}{S} e^{-L^2k^2/4}\left[\mathcal{V}(k,0,0) + \frac{1}{2L^2}\left[\frac{\partial^2\mathcal{V}}{\partial p_1^2}(k,0,0) + \frac{\partial^2\mathcal{V}}{\partial p_2^2}(k,0,0)\right] + \mathcal{O}\left((LMc)^{-4}\right)\right] \tag{4.54}$$

Note that from a physical standpoint we should always ensure that $M > \Omega$, as the energy gap of an atom contributes to the atom's rest mass.

As displayed in Fig.(4.2), we find that the excitation probabilities decrease, both for increasing energy gaps Ω and decreasing detector masses M.

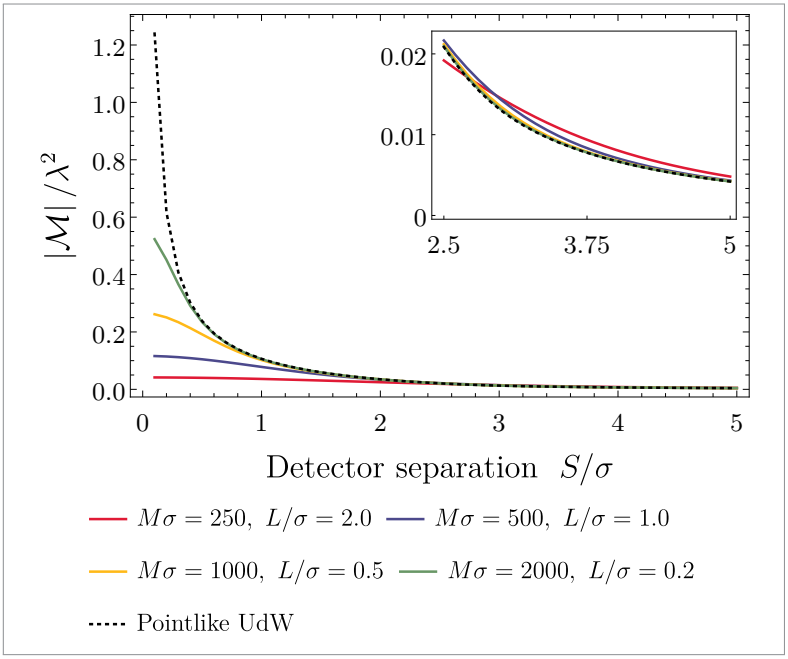

Figure 4.3: The absolute value of the entangling term, $|\mathcal{M}|$, for pointlike UDW detectors as well as for massive detectors, as a function of the detector's separation S and with $\Omega\sigma = 0.1$. For the massive detectors, we chose different values for M and L such as to keep their product constant ($ML = 500$), which fixes the virtual velocities at which the detectors dynamically delocalize.

Intuitively, this behavior can be explained as follows: switching the interaction on and off breaks time translation invariance and therefore provides energy for the excitation and the recoil of the detectors and the excitation of the field. The kinetic energy of the recoil becomes larger for smaller detector masses. Since the excitation of the detector is always accompanied by the emission of a field quantum and the recoil of the detector, the excitation process becomes energetically more expensive for larger energy gaps and smaller detector masses. In the limit

of infinitely small energy gaps, the detectors essentially turn into simple charges and all the switching energy can go into the recoil of the detectors and the excitation of the field. Similarly, in the limit of infinitely large detector masses, the kinetic recoil energy tends to zero and all the switching energy can go into the excitation of the field and the internal degrees of freedom. For the excitation probability of a very massive detector, it is therefore justifiable to neglect the recoil of the detector and to model the center of mass degrees of freedom classically. As can be seen in Fig.(4.2), the excitation probability in the limit of large detector masses indeed approaches the excitation probability of a pointlike UDW detector.

As displayed in Fig.(4.3), we further find that the entangling term is suppressed both in the separation of the two detectors and in the initial center of mass delocalization widths. Intuitively, this is because the amplitude of the quantum field fluctuations (which correlate the quantum field amplitudes at different points in space and time) decrease with the fluctuation size. The more delocalized the detectors are initially, the larger are the spatial regions in which the two detectors probe the quantum field fluctuations, and the smaller is thus the entangling term. In fact, as we can see from Eq.(4.54), the entangling term for coherently delocalized detectors is Gaussian suppressed in the initial delocalization width—contrary to the excitation probabilities, whose leading order term does not depend on the initial delocalization width at all, as we can see from Eq.(4.53). Therefore, the ability of quantum delocalized detectors to harvest entanglement from the vacuum is Gaussian suppressed in the initial center of mass delocalization.

Let us now see whether we can find a limit in which we recover the entanglement harvesting results for UDW detectors, that is, for detectors with classical center of mass degrees of freedom. We start by exploring the negativity in the limit of very large detector masses ($M \to \infty$), while keeping the initial delocalization width L fixed. One might expect to recover the classical behaviour of UDW detectors in this limit, since the dynamical quantum center of mass delocalization process becomes very slow: the virtual center of mass velocities satisfy $v \lesssim 3.5/(LM)$ and thus tend to zero in this limit. Even though the detectors each have a finite initial delocalization width, their center of mass wave packets do not coherently spread any further. We indeed find that the excitation probabilities and the entangling term respectively reduce to the excitation probabilities and the entangling term for UDW detectors. However, there is a twist: The excitation probabilities reduce to the excitation probabilities for pointlike UDW detectors, $P \to P_0^c$, while the entangling term reduces to the entangling term for Gaussian smeared UDW detectors, $\mathcal{M} \to \mathcal{M}_L^c$. Thus, in the limit of very large detector masses and for finite initial delocalization widths L, the negativity neither reduces to the negativity for a pair of pointlike UDW detectors, nor to the negativity for a pair of Gaussian smeared UDW detectors.

Intuitively, we can understand this behavior as follows. In the infinite mass limit, the kinetic energy of the recoil of the detectors tends to zero. The center of mass degrees of freedom no longer play a role in the energy balance of the excitation process of the detectors, and the recoil of the detector becomes negligible. We can thus effectively interpret the center of mass probability distributions as classical probability distributions, of finite and constant width, for the positions of two pointlike UDW detectors. Since the excitation probability of a pointlike UDW detector is independent of the position of the detector, we recover the results for pointlike UDW detectors for the excitation probabilities. On the other hand, the nonlocal entangling excitations shared by two pointlike UDW detectors depend on the detector separation, and therefore they also depend on the classical position probability distributions for the two detectors. Consequently, the entangling term for incoherently delocalized detectors does not reduce to the entangling term for pointlike UDW detectors, but rather to the entangling term for spatially smeared UDW detectors.

Let us now recall that Gaussians of width L approach delta distributions in the limit $L \to 0$. Clearly, we should be able to recover the entanglement harvesting results for a pair of pointlike UDW detectors, in the limit of very large detector masses and center of mass distributions which are very sharply peaked (and thus essentially completely localized) at all times. However, we need to approach this limit in a way that ensures that the virtual center of mass velocities stay within the non-relativistic regime identified in Eq.(4.52). To this end, we define $M =: m/\gamma$ and $L =: l\gamma$, with γ a regularization factor and with m and l constants satisfying $lmc \gtrsim 3.5 \times 10^2$. Letting $\gamma \to 0$ then lets the initial center of mass localization become very sharp ($L \to 0$) and the detector masses become very large ($M \to \infty$), while keeping the virtual center of mass velocities fixed and therefore non-relativistic. In the limit $\gamma \to 0$, the excitation probabilities and the entangling term reduce to

$$\begin{aligned} P \quad &\to P_0^c + \frac{\lambda^2\sigma^2}{4\pi^2 c(lmc)^2}\int_0^\infty dk\, \frac{\sigma^2 c^2 k^3}{((\Omega+ck)^2\sigma^2-1)^4}\Big(20(\Omega+ck)^2\sigma^2+4+\cos(\pi\sigma(\Omega+ck)) \\ &\quad \times\left[20(\Omega+ck)^2\sigma^2+4-\pi^2((\Omega+ck)^2\sigma^2-1)^2\right] \\ &\quad +8(\Omega+ck)\pi\sigma[(\Omega+ck)^2\sigma^2-1]\sin(\pi\sigma(\Omega+ck))\Big) + \mathcal{O}\left((lmc)^{-4}\right), \end{aligned} \tag{4.55}$$

$$\mathcal{M} \quad \to \mathcal{M}_0^c + \frac{\lambda^2\sigma^2}{4\pi^2 c(lmc)^2}\int_0^\infty dk \frac{\sin(kS)}{S} D(k) + \mathcal{O}\left((lmc)^{-4}\right). \tag{4.56}$$

By letting the virtual center of mass velocities go to zero, we can then describe two detectors whose center of mass degrees of freedom are localized very sharply at all times. Indeed, taking the limit $\gamma \to 0$ first and then taking the limit $1/(lmc) \to 0$, we recover the excitation probabilities

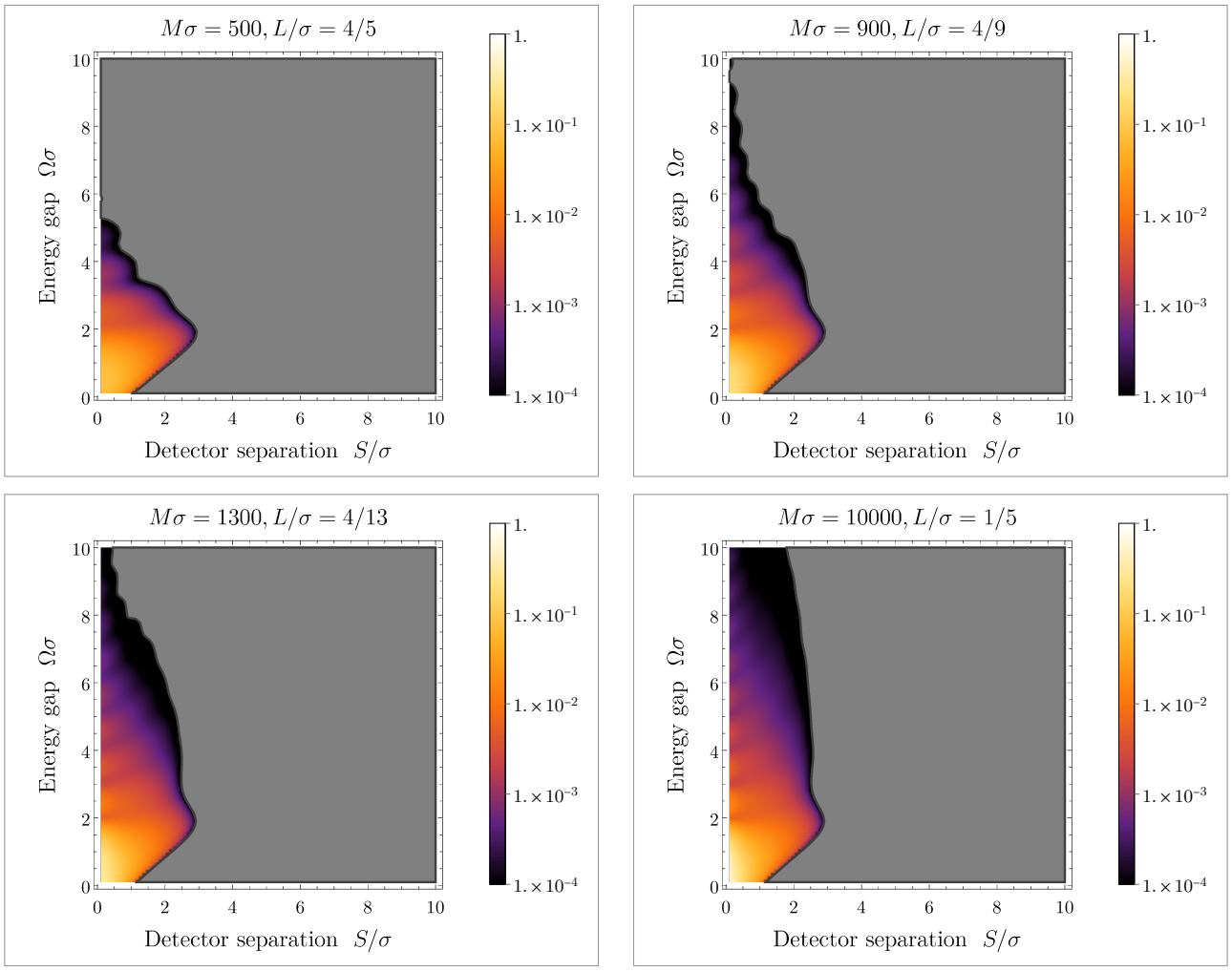

Figure 4.4: The negativity $\mathcal{N}$ for two coherently delocalizing detectors, plotted as a function of the energy gap Ω and the separation S of the two detectors. Regions of zero negativity are marked in grey. We chose the detector masses M and the initial center of mass localization widths L so that γ decreases from left to right and from top to bottom. In the first three plots we fixed $1/(lmc) = 2.5 \times 10^{-3}$, while in the fourth plot we chose parameters satisfying $1/(lmc) = 5\times10^{-4}$, such as to see what happens to the negativity as we further decrease $1/(lmc)$. As expected, as we approach the limit $\gamma \to 0$ and $1/(lmc) \to 0$, we find that the negativity resembles more and more the negativity displayed in Fig.(4.1) for two pointlike UDW detectors.

and the entangling term for two pointlike UDW detectors, $P \to P_0^c$ and $\mathcal{M} \to \mathcal{M}_0^c$. We hence identified the limit in which entanglement harvesting for a pair of coherently delocalized detectors reduces to entanglement harvesting for a pair of pointlike UDW detectors. On the other hand, we find that there is no limit in which the results reduce to entanglement harvesting for a pair of spatially smeared UDW detectors. This once again confirms what we mentioned before, namely that classical smearing profiles are appropriate to model the finite spatial extent of atoms due to their electronic orbitals [23], but not to model the coherent center of mass delocalization of an atom.

In Fig.(4.4), we plot the entanglement negativity for two coherently delocalizing detectors, as a function of the energy gap and the separation of the detectors. We can clearly see how the negativity reduces to the negativity for a pair of pointlike UDW detectors, when first letting $\gamma \to 0$ and then also letting $1/(lmc) \to 0$. We also observe that entanglement harvesting is indeed highly suppressed in the initial center of mass delocalization width.

Overall, we find that entanglement harvesting is suppressed for coherently delocalized detectors (and thus for actual physical matter systems such as atoms, ions or molecules), compared to entanglement harvesting for UDW detectors, whose center of mass degrees of freedom are assumed to be classical. An intuitive explanation for this suppression might be the following. We here focused on the entanglement harvested by the internal degrees of freedom of the two detectors. However, further entanglement could potentially build up between the respective internal and center of mass degrees of freedom of the two detectors. This entanglement, which remains to be calculated, might build up at the expense of entanglement between the internal degrees of freedom of the two coherently delocalized detectors.

Here we did not aim to distinguish between extraction of preexisting vacuum entanglement and entanglement production through interaction. However, it would certainly be interesting to investigate which one of these two harvesting effects is the dominant one in the setup we considered here. It might also be interesting to study whether there is a difference in how coherent delocalization respectively impacts these two harvesting effects. It might however require some clever tricks and gymnastics to distinguish the two effects, since one cannot straightforwardly define spacelike, null and timelike separation for the two quantum delocalizing detectors.

4.3 Entanglement harvested by coherently delocalized detectors from the ground state of a medium

Experimentally verifying entanglement harvesting from the vacuum is a difficult task [95, 96, 50, 51]. It might be more feasible to experimentally observe entanglement harvesting from the ground state of a medium, e.g., by sending atoms through a thin foil or a Bose-Einstein condensate. We here want to shed some light on whether the internal degrees of freedom of quantum delocalized atoms might become entangled with each other, via their respective interaction with the entangled ground state of a medium.

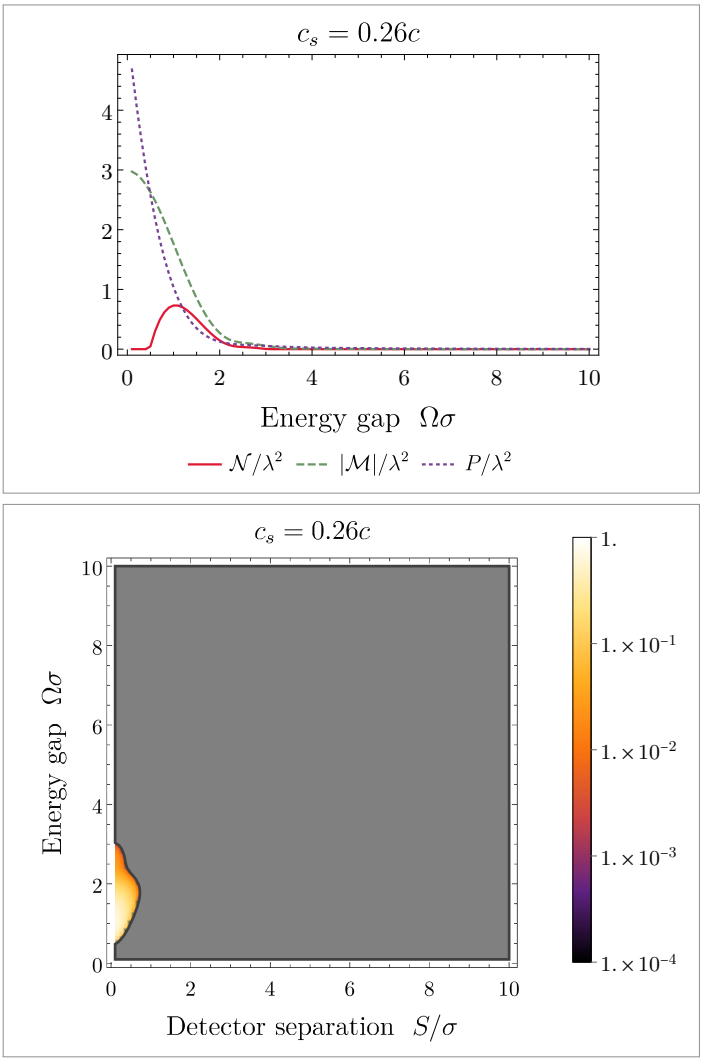

Figure 4.5: We consider two detectors (with detector masses $M\sigma = 900$ and initial localization widths $L\sigma = 4/9$) in a medium with wave propagation speed $c_s = 0.26c$. The first plot (*top*) shows the transition probability P, the entangling term $\mathcal{M}$ and the negativity $\mathcal{N}$, as function of the energy gap Ω and for a detector separation $S = \sigma/10$. The second plot (*bottom*) shows the negativity $\mathcal{N}$ as a function of the energy gap Ω and the detector separation S. The region of zero negativity is marked in grey.

In the previous sections, we modeled the electromagnetic field via a simple scalar quantum field with dispersion relation $\omega = ck$, where c stands for the vacuum propagation speed of light. We will here model a medium via a scalar quantum field with dispersion relation $\omega = c_s k$, with $c_s < c$ the wave propagation speed in the medium. The propagation of waves in the scalar field could then for instance model the propagation of light in a medium, or the propagation of sound in a phononic field, both of which are known to propagate slower than light in the vacuum. For concrete experimental setups, it will be very interesting to pursue analogous calculations with the there relevant realistic dispersion relation. Repeating the calculations we performed in the previous section, we obtain the excitation probabilities

$$P = \frac{\lambda^2\sigma^2}{4\pi^2 c_s}\left[\mathcal{U}(0) + \frac{3}{2L^2}\frac{\partial^2\mathcal{U}}{\partial p^2}(0) + \mathcal{O}\left((LMc)^{-4}\right)\right] \tag{4.57}$$

and the entangling term

$$\begin{aligned}\mathcal{M} = \frac{\lambda^2\sigma^2}{4\pi^2 c_s}\int_0^\infty dk \frac{\sin(kS)}{S} e^{-L^2k^2/4}\Bigg[\mathcal{V}(k,0,0) + \frac{1}{2L^2}\left[\frac{\partial^2\mathcal{V}}{\partial p_1^2}(k,0,0) + \frac{\partial^2\mathcal{V}}{\partial p_2^2}(k,0,0)\right] \\ + \mathcal{O}\left((LMc)^{-4}\right)\Bigg],\end{aligned} \tag{4.58}$$

where $\mathcal{U}$ and $\mathcal{V}$ are defined as in Eq.(4.46) and Eq.(4.51), with the exception that c is being replaced by c_s in the definitions of $\mathcal{U}$ and β_j.

In Fig.(4.5) we plot the excitation probability, the entangling term and the negativity for a pair of coherently delocalized detectors in a medium with wave propagation speed $c_s = 0.26c$. Compared to detectors in the vacuum, we find that both the excitation probabilities and the entangling term increase significantly. Intuitively, this behavior can be explained as follows: transforming into the quantum uncertain rest frame of the delocalizing detectors, the phononic ground state transforms non-trivially into an excited field state that might be more entangled than the phononic ground state. The entangling excitations thus potentially increase, but at the same time, also the local "noisy" excitations increase. In Fig.(4.5), we further observe that the increase in the excitation probabilities is much larger than the increase in the entangling term, leading to a significant decrease in the negativity (compared to the negativity in Fig.(4.4), in which the detectors were in the vacuum). It should be interesting to further explore this behaviour and to develop more intuition for it.

Both light and sound can be slowed down significantly in media (e.g. light in crystals or sound in Bose-Einstein condensates), to the extreme of being stopped completely [97, 74]. The detectors in such media could coherently delocalize with virtual velocities that are comparable

to, or even larger than, the propagation speed in the medium, $v \gtrsim c_s$, while remaining well within the non-relativistic regime, $v \leq 0.01c$. Gaussian center of mass wave packets with support for supersonic virtual center of mass velocities are ones for which $LMc_s \gtrsim 3.5$, while the non-relativistic regime is characterized by $LMc \gtrsim 3.5 \times 10^2$. In Fig.(4.6) we plot the excitation probabilities, the entangling term and the negativity for two detectors in a medium whose wave propagation speed is 1% of the vacuum speed of light. We chose the parameters so that the maximal virtual center of mass velocities in the Gaussian wave packet are close to the speed of sound in the medium ($LMc_s = 4$), while staying well within the non-relativistic regime ($LMc = 400$). We find that both the entangling term and the excitation probabilities for detectors in the medium are significantly enhanced, but again the excitation probabilities are much more enhanced than the entangling term, and we find that overall the negativity vanishes. We thus find that if the wave propagation speed in the medium is too small, the internal degrees of freedom of a pair of coherently delocalizing detectors cannot become entangled with each other.

We conjecture that it is generally harder for detectors to harvest entanglement from a medium than from the vacuum. Entanglement harvesting experiments in media might however still be worth considering, given that they may be more easily conducted than the harvesting of entanglement from the vacuum.

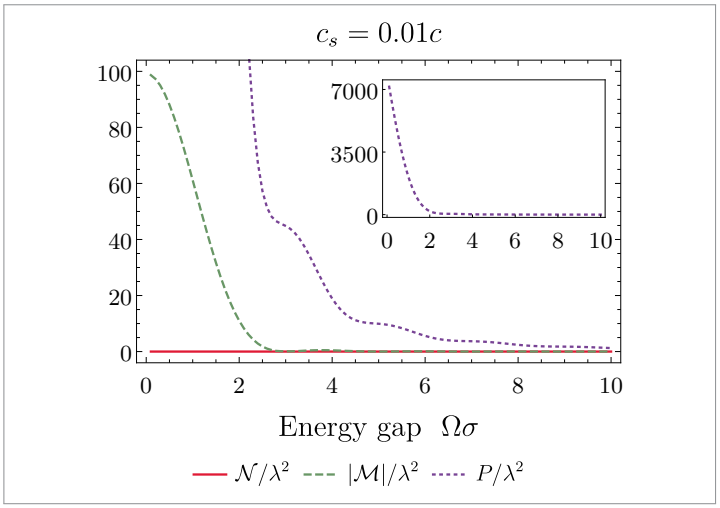

Figure 4.6: We consider two detectors (with detector masses $M\sigma = 900$, initial localization widths $L\sigma = 4/9$ and detector separation $S = \sigma/10$) in a medium with wave propagation speed $c_s = 0.01c$. We plot the transition probability P and the entangling term $\mathcal{M}$ as function of the energy gap, and we find that the negativity $\mathcal{N}$ vanishes for this choice of parameters.

Chapter 5

Unruh effect for a coherently delocalized detector in an electric field

This chapter is based on ideas and results obtained in collaboration with Vivishek Sudhir and Achim Kempf (see Statement of Contributions on page iv).

A UDW detector travelling on a prescribed trajectory with non-vanishing acceleration can experience effects according to counter-rotating wave terms in the light-matter interaction Hamiltonian. For instance, in the vacuum, the detector can become excited and at the same time emit a field quantum. When the detector is uniformly accelerated at all times, it reaches thermal equilibrium according to a temperature proportional to the acceleration [3, 4, 7, 5], and the detector is said to experience the *Unruh effect*. We here use the term Unruh effect to refer to the excitation and radiation process due to non-vanishing acceleration of a detector system in the vacuum, and we do not require the detector to be accelerated at all times.

Provided that both the detector and the field are in their energetically lowest states, one might wonder where the energy for the excitation of detector and field originates from. Here it is again helpful to imagine an "external agent", who keeps the detector on its prescribed spacetime trajectory, and who, in order to do so, needs to provide the system with energy. However, the standard UDW detector model does not include a description of such accelerating agent. By *prescribing* a spacetime trajectory, the UDW detector model consequently does not account for the recoil of the detector, which accompanies the Unruh effect experienced by a realistic physical detector system.

In this chapter, our aim is to *dynamically* account for the acceleration of the detector. We

describe the center of mass position of the detector quantum mechanically, within our coherently delocalized detector model, and we couple the quantum center of mass to a classical electric field. Within this fully quantum mechanical framework, we study the vacuum excitation process for a detector whose center of mass is coherently delocalized, and we refer to this process as the *massive Unruh effect*. We study the impact of coherent center of mass delocalization on the vacuum excitation process, and in particular, the recoil of the detector.

We start by reviewing in section 5.1 the Unruh effect for a UDW detector coupling to a massless scalar quantum field. Since we wish to stay within the non-relativistic regime as far as the center of mass motion of the detector is concerned, we assume that the detector is uniformly accelerated only during a finite time interval, while otherwise travelling inertially. In sections 5.2 - 5.4, we then discuss the massive Unruh effect for a coherently delocalized detector in an electric field that is switched on only during a finite time interval, such as to ensure that all virtual center of mass velocities stay within the non-relativistic regime. In section 5.5, we finally recover the Unruh effect as a limiting case of the massive Unruh effect.

5.1 Review: Unruh effect for a UDW detector

First, let us briefly review the Unruh effect for a UDW detector which travels, at non-relativistic velocities, along a prescribed spatial trajectory $\mathbf{x}(t)$. The restriction to non-relativistic detector velocities allows us to identify the detector's proper time with the coordinate time t, which significantly simplifies our calculations (and it also allows us to employ the Schrödinger equation when considering virtual detector velocities in the next section, which is our primary motive for working within the non-relativistic regime here). As in chapter 1, we again work in the interaction picture, in which operators evolve according to the free Hamiltonian given by Eq.(1.1). We again model the interaction between the detector and the field via the linear monopole moment operator coupling between the detector's monopole moment operator and the scalar quantum field operators. We evaluate the coupling of the monopole moment operator and the field operators along the detector's prescribed spatial trajectory, $\hat{\mu} \otimes \hat{\phi}(\mathbf{x}(t))$. The state of the detector and the field then evolves in the interaction picture according to the interaction Hamiltonian

$$\hat{H}_{int}(t) \;:=\; q\,\hat{\mu}(t) \otimes \hat{\phi}(\mathbf{x}(t), t)\,, \tag{5.1}$$

with q the detector's charge. The interaction picture representations of the monopole moment operator and the field operators are given as follows:

$$\hat{\mu}(t) = e^{i\Omega t} |e\rangle \langle g| + \text{H.c.}\,, \tag{5.2}$$

$$\hat{\phi}(\mathbf{x}(t), t) = \int \frac{d^3k}{(2\pi)^{3/2}} \sqrt{\frac{c^2}{2k}} \left(e^{-ickt + i\mathbf{k}\cdot\mathbf{x}(t)} \hat{a}_{\mathbf{k}} + \text{H.c.}\right) \tag{5.3}$$

Let us now study the vacuum excitation process of the detector and the field: we assume that the detector is initially in its ground state and the field is in its vacuum state, and we let $|\psi_i\rangle = |g\rangle \otimes |0\rangle$ denote the initial state of the coupled system. Given the structure of the monopole moment coupling, it is clear that in order for the detector to become excited, the quantum field has to become excited as well. More concretely, the field has to transition to a single photon state $|\mathbf{k}\rangle$. Contrary to resonance effects such as absorption, the Unruh effect is thus caused by counter-rotating wave terms in the light-matter interaction. In order to obtain the Unruh excitation probability, we start by calculating the probability amplitude for the system to transition to the final state $|\psi_f\rangle = |e\rangle \otimes |\mathbf{k}\rangle$,

$$\mathcal{A}_{Unruh} := \langle \psi_f | \int_{-\infty}^{\infty} dt\, \hat{H}_{int}(t) \, |\psi_i\rangle \,. \tag{5.4}$$

Via straightforward calculation of the respective matrix elements, we obtain the excitation probability amplitude,

$$\mathcal{A}_{Unruh} =: \frac{qc}{2\pi\sqrt{4\pi k}} \mathcal{I}\,, \tag{5.5}$$

where we defined $\mathcal{I}$ as the following time integral:

$$\mathcal{I} := \int_{-\infty}^{\infty} dt\, e^{it(ck+\Omega) - i\mathbf{k}\cdot\mathbf{x}(t)} \tag{5.6}$$

The modulus squared of the transition probability amplitude then yields the probability for the detector to get excited and a field quantum of momentum $\mathbf{k}$ to be emitted:

$$P_{Unruh}(\mathbf{k}) := |\mathcal{A}_{Unruh}|^2 \tag{5.7}$$

In order to obtain the total excitation probability, irrespective of the momentum of the emitted photon, we further trace over the Hilbert space of the quantum field:

$$P_{Unruh} := \int d^3k \, |\mathcal{A}_{Unruh}|^2 \,. \tag{5.8}$$

We can now easily verify that inertial detector trajectories, $\mathbf{x}(t) = \mathbf{x}_0 + \mathbf{v}t$, with $\mathbf{x}_0$ the detector's initial position and $\mathbf{v}$ the detector's constant velocity, do not lead to the excitation of the detector and the field:

$$\begin{aligned} \mathcal{A}_{Unruh} &= \frac{qc}{2\pi\sqrt{4\pi k}} \int_{-\infty}^{\infty} dt\, e^{it(ck+\Omega-\mathbf{k}\cdot\mathbf{v})-i\mathbf{k}\cdot\mathbf{x}_0} && (5.9) \\ &= \frac{qc}{\sqrt{4\pi k}}\, e^{-i\mathbf{k}\cdot\mathbf{x}_0}\delta(\Omega + ck - \mathbf{k}\cdot\mathbf{v}) && (5.10) \\ &= 0 && (5.11) \end{aligned}$$

In order to obtain a non-vanishing excitation probability, the detector needs to travel along a non-inertial trajectory, that is, it needs to be accelerated for a non-vanishing amount of time. Let us here consider a UDW detector that is uniformly accelerated in the $z-$direction during the time interval $t \in [0, T]$, and that otherwise moves inertially. We can write the detector's acceleration as

$$\mathbf{a}(t) = a\,\Theta(t)\,\Theta(T-t)\,\mathbf{e}_z\,, \tag{5.12}$$

with $\mathbf{e}_z = (0,0,1)^T$, and where Θ denotes the Heaviside step function. Assuming that the detector is initially at rest, the detector's velocity becomes:

$$\mathbf{v}(t) = \left[at\Theta(t)\,\Theta(T-t) + aT\Theta(t-T)\right]\mathbf{e}_z\,. \tag{5.13}$$

Further assuming that the detector's initial position coincides with the origin of our coordinate system, the detector's spatial trajectory becomes:

$$\mathbf{x}(t) = \left[\frac{at^2}{2}\Theta(t)\,\Theta(T-t) + \frac{aT}{2}\,(2t-T)\,\Theta(t-T)\right]\mathbf{e}_z \tag{5.14}$$

We now need to restrict the regime of the parameters a and T such as to ensure that the detector's velocities stay well within the non-relativistic regime. A detector moving along the trajectory given in Eq.(5.14) reaches its maximal velocity at time $t = T$. We will here consider velocities to be non-relativistic if they are smaller than 1% of the speed of light c. Provided that the parameters a and T satisfy the following relation,

$$|\mathbf{v}(T)| = |a|T \overset{!}{\leq} 10^{-2}c\,, \tag{5.15}$$

assuming the detector's motion to be non-relativistic is then well justified. For the spatial trajectory in Eq.(5.14), together with the restriction in Eq.(5.15) on the parameters a and T,

we obtain the following expression for the time integral given in Eq.(5.6):

$$\mathcal{I} = \int_{-\infty}^{0} dt\, e^{it(\Omega+ck)} + \int_{0}^{T} dt\, e^{it(\Omega+ck)-i\frac{ak_z}{2}t^2} + e^{iT\left(\Omega+ck-\frac{ak_z}{2}T\right)} \int_{0}^{\infty} dt\, e^{it(\Omega+ck-k_z aT)} \tag{5.16}$$

$$= \frac{1}{i\beta} + \pi\delta(\beta) + \sqrt{\frac{\pi}{2iak_z}} e^{i\frac{\beta^2}{2ak_z}} \left[\mathrm{Erf}\left(\frac{i\beta}{\sqrt{2iak_z}} \right) - \mathrm{Erf}\left(\frac{i\gamma}{\sqrt{2iak_z}} \right) \right] + e^{iT\left(\Omega+ck-\frac{ak_z}{2}T\right)} \left(\frac{i}{\gamma} + \pi\delta(\gamma) \right), \tag{5.17}$$

For notational convenience, we here defined the functions $\beta := \Omega + ck$ and $\gamma := \Omega + ck - ak_zT$. We further let k_z denote the $z-$component of the momentum of the emitted Unruh photon, $\mathbf{k} = (k_x, k_y, k_z)^T = (k\sin(\theta)\cos(\phi), k\sin(\theta)\sin(\phi), k\cos(\theta))^T$, with θ and ϕ respectively the polar and azimuthal angle. Since both the energy gap of the detector and the absolute value of the momentum of the emitted photon are strictly positive, $\Omega > 0$ and $k > 0$, we find that the delta distribution $\delta(\beta)$ in Eq.(5.17) can be omitted. Further, since the detector's velocity is strictly smaller than the speed of light, we find $\gamma > 0$, and consequently, the delta distribution $\delta(\gamma)$ in Eq.(5.17) can be omitted as well. For the excitation probability we then obtain

$$P_{Unruh} = \frac{q^2c^2}{8\pi^2} \int_{-1}^{1} dz \int_{0}^{\infty} dk\, k\, |\mathcal{I}|^2, \tag{5.18}$$

where we defined a new variable, $z := \cos(\theta) \in [-1, 1]$. Instead of tracing over the entire Hilbert space $\mathcal{H}_F$ of the quantum field, we could also consider tracing only over the direction of the emitted photon, such as to obtain the excitation probability density

$$P_{Unruh}(k) := \frac{q^2c^2k}{8\pi^2} \int_{-1}^{1} dz\, |\mathcal{I}|^2, \tag{5.19}$$

or we could trace out only the azimuthal angle ϕ, such as to obtain the excitation probability density

$$P_{Unruh}(k, z) := \frac{q^2c^2k}{8\pi^2} |\mathcal{I}|^2. \tag{5.20}$$

In Fig.(5.1), we plot the excitation probability density $P_{Unruh}(k, z)$ for a range of different photon emission angles (that is, for different values of z, where $z = 1$, $z = 0$ and $z = -1$ respectively correspond to emission along, orthogonal, and opposite the direction of acceleration). In Fig.(5.2), we plot the excitation probability density $P_{Unruh}(k)$, where we carried out the $z-$integration in Eq.(5.19) numerically.[1] We find that photons are emitted preferably along the axis of

[1] When specifying numeric values for our parameters, it is sensible to render all quantities dimensionless. In our plots, we thus expressed all quantities involved in terms of c, T and $\hbar$ (while in our calculations we fixed $\hbar = 1$), which set natural length, time and mass scales.

acceleration, and no radiation is emitted orthogonal to the $z-$direction. It is worth noting that the here observed angular distribution of the emitted Unruh radiation is characteristic to considering a scalar valued quantum field. In order to make realistic predictions about the angular distribution of emitted Unruh radiation for physical systems such as atoms or ions, the above calculations should be performed for such matter systems coupling to the vector valued electromagnetic field. The excitation probability density shows oscillations when plotted as a function of k, and for certain values of k, the excitation probability even vanishes. This characteristic behaviour results from having the detector accelerate only during the compact time interval $t \in [0, T]$. Mathematically, we can trace the oscillatory behaviour back to the complex error functions in the time integral given in Eq.(5.17). These error functions appear due to the changes of the trajectory from inertial to accelerated at time $t = 0$ and from accelerated to inertial at time $t = T$. As mentioned before, the energy for accelerating the detector can be viewed as provided by an external agent not included within the UDW detector framework, and the oscillatory behaviour could be interpreted as a sort of resonance phenomenon in accordance with this energy.

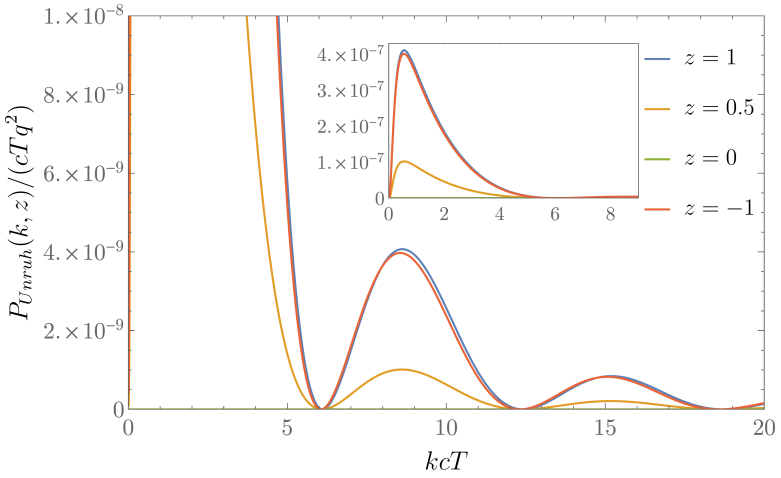

Figure 5.1: Excitation probability density $P_{Unruh}(k, z)/(cTq^2)$ for a UDW detector, for different values of z, and plotted as a function of the dimensionless variable kcT. We here chose $\Omega T = 0.2$, $aT/c = 8 \cdot 10^{-3}$.

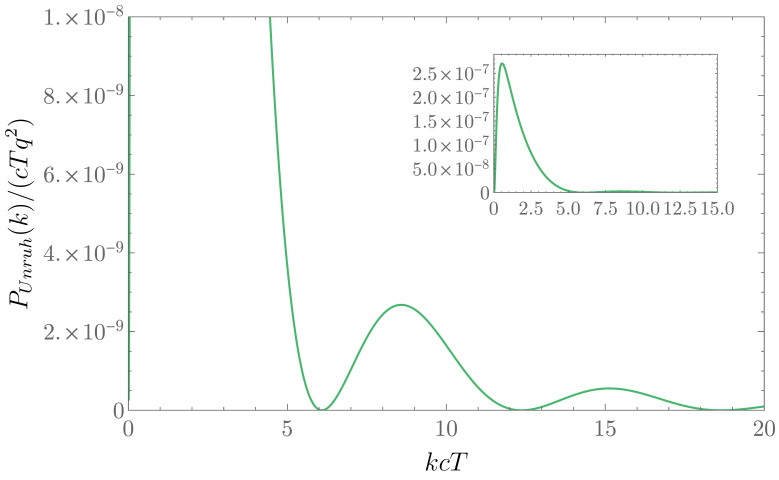

Figure 5.2: Excitation probability density $P_{Unruh}(k)/(cTq^2)$ for a UDW detector, obtained by tracing over z, plotted as a function of the dimensionless variable kcT. We again chose $\Omega T = 0.2$ and $aT/c = 8 \cdot 10^{-3}$.

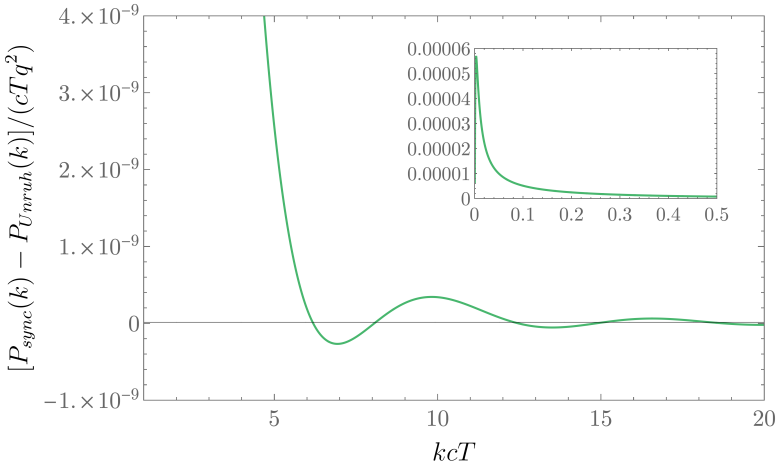

Figure 5.3: Difference between synchrotron radiation emitted by a simple charge and Unruh radiation emitted by a UDW detector with energy gap $\Omega T = 0.2$, plotted as a function of the dimensionless variable kcT. We here again chose $aT/c = 8 \cdot 10^{-3}$.

While Unruh radiation is notoriously difficult to observe experimentally [11, 98, 99, 100, 101, 102, 103], radiation emitted by a simple accelerated charge in the form of synchrotron radiation (or acceleration radiation, depending on the terminology employed, and not to be confused with William Unruh's use of the term) is a well-studied and easily observable phenomenon, see, e.g., [104]. The crucial difference is that for the Unruh effect, the accelerated and charged system needs to have excitable internal degrees of freedom. However, as we mentioned earlier, the case of a simple charge interacting with a quantum field can be recovered from the UDW detector model in the limit of $\Omega \to 0$. In order to really see the fingerprint of the Unruh effect in our plots, we might therefore find it useful to subtract the excitation probability density $P_{Unruh}(k)/q^2$ for a UDW detector from the "background contribution" caused by synchrotron radiation emitted by a simple charge, $P_{sync}(k)/q^2$, which we obtain by setting $\Omega = 0$ in Eq.(5.19). The plot of the excitation probability density, $[P_{sync}(k) - P_{Unruh}(k)]/q^2$, is displayed in Fig.(5.3). With

these baseline plots at hand, let us now turn towards the massive Unruh effect for coherently delocalized detectors.

5.2 Setting up the interaction Hamiltonian

Instead of prescribing a classical trajectory, we now want to dynamically model the acceleration of the detector. To this end, let us consider a massive detector with quantum center of mass degrees of freedom and that couples to a quantum scalar field $\hat{\phi}$, as described in chapter 2. While in previous chapters we allowed the detector's center of mass degrees of freedom to evolve freely, we here want to couple the detector's center of mass to a classical electric field $\mathbf{E}$, which allows us to dynamically model the acceleration of the detector. We consider the following total Hamiltonian for the coupled system:

$$\hat{H} \;=\; \frac{\hat{\mathbf{p}}^2}{2M} - q\,\mathbf{E}\cdot\hat{\mathbf{x}} + \Omega\,|e\rangle\langle e| + \int d^3k\, ck\, \hat{a}^\dagger_{\mathbf{k}}\hat{a}_{\mathbf{k}} + q\int d^3x\, \hat{\mathcal{P}}(\mathbf{x})\otimes\hat{\mu}\otimes\hat{\phi}(\mathbf{x})\,, \tag{5.21}$$

As we outlined in chapter 2, the interaction Hamiltonian in the interaction picture reads

$$\hat{H}_{int}(t) \;=\; q\int d^3x\, \hat{\mathcal{P}}(\mathbf{x},t)\otimes\hat{\mu}(t)\otimes\hat{\phi}(\mathbf{x},t)\,, \tag{5.22}$$

with $\hat{\mathcal{P}}(\mathbf{x},t)$, $\hat{\mu}(t)$ and $\hat{\phi}(\mathbf{x},t)$ given by Eq.(2.9), (2.10) and (2.11). In order to obtain a setup that is comparable to the situation we considered in the previous section, let us consider an electric field of the following form:

$$\mathbf{E}(t) \;=\; \mathcal{E}\,\Theta(t)\,\Theta(T-t)\mathbf{e}_z \tag{5.23}$$

The field is switched on exclusively during the time interval $t\in[0,T]$, so that the detector's center of mass degrees of freedom follow their free time evolution for $t\notin[0,T]$. During the time interval $t\in[0,T]$ however, the electric field is aligned with the $z-$axis and of constant strength $\mathcal{E}$. Before we can study the vacuum excitation process for the delocalized massive detector, we first need to calculate the time evolved operators $\hat{\mathcal{P}}(\mathbf{x},t)$. To this end, let us explicitly calculate the time evolved position eigenvectors $|\mathbf{x}(t)\rangle$ in the Heisenberg picture, for a quantum particle with position operator $\hat{\mathbf{x}}(t)$ which couples to the electric field in Eq.(5.23). The Heisenberg equations for the position and momentum operators in the Heisenberg picture read

$$\frac{d}{dt}\hat{\mathbf{x}}(t) \;=\; \frac{\hat{\mathbf{p}}(t)}{M}\,, \qquad \frac{d}{dt}\hat{\mathbf{p}}(t) = q\mathcal{E}(t)\mathbf{e}_z\,. \tag{5.24}$$

Solving these coupled equations of motion, we obtain the following time dependent position operator,

$$\hat{\mathbf{x}}(t) \;=\; \hat{\mathbf{x}}(0) + \hat{\mathbf{p}}(0)t/M + f(t)\,\mathbf{e}_z\,, \tag{5.25}$$

where we defined the following function

$$f(t) \;:=\; \frac{a}{2}\Big[t^2\Theta(t)\,\Theta(T-t) + T(2t-T)\Theta(t-T)\Big]\,, \tag{5.26}$$

with $a := q\mathcal{E}/M$. We note that $f(t)$ is of the same form as the $z-$component of the classical trajectory which we prescribed in Eq.(5.14) for the UDW detector with classical center of mass. We let the position and momentum operators in the Heisenberg picture coincide at time $t = 0$ with the position and momentum operators in the Schrödinger picture, so that $\hat{\mathbf{x}}(0)$ and $\hat{\mathbf{p}}(0)$ are represented as $\hat{\mathbf{x}}(0)\psi(\mathbf{x}) = \mathbf{x}\psi(\mathbf{x})$ and $\hat{\mathbf{p}}\,(0)\psi(\mathbf{x}) = -i\nabla\psi(\mathbf{x})$ respectively. To find the time dependent position eigenfunction $\psi_{\boldsymbol{\xi}}\,(\mathbf{x},t) = \langle\mathbf{x}|\psi_{\boldsymbol{\xi}}\,(t)\rangle$ for a given position eigenvalue $\boldsymbol{\xi}$, we need to solve the differential equation

$$\left(\mathbf{x} + f(t)\mathbf{e}_z - \frac{it}{M}\nabla\right)\psi_{\boldsymbol{\xi}}\,(\mathbf{x},t) \;=\; \boldsymbol{\xi}\,\psi_{\boldsymbol{\xi}}\,(\mathbf{x},t)\,. \tag{5.27}$$

By imposing the initial condition $|\psi_{\boldsymbol{\xi}}\,(0)\rangle = |\boldsymbol{\xi}\rangle$, and enforcing the following normalization condition for the position eigenfunctions,

$$\int d^3x\,\psi^*_{\boldsymbol{\xi}}\,(\mathbf{x},t)\psi_{\boldsymbol{\chi}}\,(\mathbf{x},t) \;\stackrel{!}{=}\; \delta^{(3)}(\boldsymbol{\xi}-\boldsymbol{\chi})\,, \tag{5.28}$$

we obtain for the time dependent position eigenvectors:

$$|\psi_{\boldsymbol{\xi}}\,(t)\rangle \;=\; \int \frac{d^3p}{(2\pi)^{3/2}}\,e^{-i\mathbf{p}\cdot\boldsymbol{\xi}+itp^2/2M+ip_zf(t)}\,|\mathbf{p}\,\rangle \tag{5.29}$$

Coming back to Eq.(5.22), for the time evolved operators $\hat{\mathcal{P}}(\mathbf{x},t)$ in the interaction picture we thus explicitly obtain:

$$\hat{\mathcal{P}}(\mathbf{x},t) \;=\; \int \frac{d^3p_1d^3p_2}{(2\pi)^3}\exp\left(i\frac{p_2^2-p_1^2}{2M}t - i(\mathbf{p}_2-\mathbf{p}_1)\mathbf{x} - i(p_{2,z}-p_{1,z})\frac{q\mathcal{E}t^2}{2M}\right)|\mathbf{p}_2\rangle\,\langle\mathbf{p}_1| \tag{5.30}$$

We are now fully equipped to study what we refer to as the *massive Unruh effect*, that is, the excitation process both of a coherently delocalized massive detector initially in its ground state and of a scalar quantum field initially in its vacuum state.

5.3 Transition amplitude, transition probability and transition probability densities

To study the massive Unruh effect, let us consider initial and final states of the form

$$|\psi_i\rangle \;=\; |\varphi\rangle \otimes |g\rangle \otimes |0\rangle \qquad \text{and} \qquad |\psi_f\rangle = |\mathbf{r}\rangle \otimes |e\rangle \otimes |\mathbf{k}\rangle \;, \tag{5.31}$$

with $|\varphi\rangle = \int d^3p\, \widetilde{\varphi}(\mathbf{p})\, |\mathbf{p}\rangle$ the initial center of mass state and $\mathbf{r}$ the detector's recoil momentum. We obtain the following transition probability amplitude, up to a complex phase:

$$\mathcal{A}_{Massive} \;=\; \frac{qc}{2\pi\sqrt{4\pi k}}\, \widetilde{\varphi}(\mathbf{r}+\mathbf{k})\, \mathcal{J}(\mathbf{r}) \tag{5.32}$$

We here defined $\mathcal{J}(\mathbf{r})$ as the following time integral:

$$\mathcal{J}(\mathbf{r}) \;:=\; \int_{-\infty}^{\infty} dt\, e^{it\left(-\frac{k^2}{2M}-\frac{\mathbf{r}\cdot\mathbf{k}}{M}+ck+\Omega\right)-ik_z f(t)} \tag{5.33}$$

The modulus squared of the transition amplitude in Eq.(5.32) then yields the probability density for the detector to get excited, to recoil with momentum $\mathbf{r}$ and to emit a field quantum of momentum $\mathbf{k}$:

$$P_{Massive}(\mathbf{k},\mathbf{r}) \;:=\; \frac{q^2c^2}{(2\pi)^2 4\pi k}\, |\widetilde{\varphi}(\mathbf{r}+\mathbf{k})|^2\, |\mathcal{J}(\mathbf{r})|^2 \tag{5.34}$$

To study the recoil of the detector, we trace over the Hilbert space of the field degrees of freedom, such as to obtain the excitation probability density, irrespective of the momentum of the emitted photon and as a function of the recoil momentum $\mathbf{r}$ of the detector:

$$P_{Massive}(\mathbf{r}) \;=\; \int d^3k\, \frac{q^2c^2}{(2\pi)^2 4\pi k}\, |\widetilde{\varphi}(\mathbf{r}+\mathbf{k})|^2\, |\mathcal{J}(\mathbf{r})|^2 \tag{5.35}$$

To obtain the total excitation probability, irrespective of the momenta of the emitted photon and the recoil of the detector, we trace over the Hilbert spaces of both the field and the center of mass degrees of freedom:

$$P_{Massive} \;:=\; \int d^3k \int d^3p\, \frac{q^2c^2}{(2\pi)^2 4\pi k}\, |\widetilde{\varphi}(\mathbf{p})|^2\, |\mathcal{J}(\mathbf{p}-\mathbf{k})|^2 \tag{5.36}$$

Since we integrate over all momenta, we here made the substitution $\mathbf{p} := \mathbf{r}+\mathbf{k}$, which simplifies working with the expression in practice. Let us again write $\mathbf{k} = (k_x, k_y, k_z)^T = (k\sin(\theta)\cos(\phi), k\sin(\theta)\sin(\phi), k\cos(\theta))^T$, with ϕ the azimuthal angle and with θ the polar angle,

that is, the angle between the momentum of the emitted photon and the direction of the electric field lines. Let us further again introduce the variable $z = \cos(\theta)$. In the following we will refer to both z and θ as the polar angle of the emitted photon. Tracing over the recoil momentum as well as over the angle of the emitted photon, we obtain the excitation probability density

$$P_{Massive}(k) \;:=\; \int_{-1}^{1} dz \int_{0}^{2\pi} d\phi \int d^3k \int d^3p \, \frac{q^2c^2k}{(2\pi)^2 4\pi} \, |\widetilde{\varphi}(\mathbf{p})|^2 \, |\mathcal{J}(\mathbf{p}-\mathbf{k})|^2 \,, \tag{5.37}$$

as a function of the magnitude k of the momentum of the emitted photon. Similarly, we obtain the excitation probability density as a function of both the magnitude k and polar angle z of the emitted photon:

$$P_{Massive}(k,z) \;:=\; \int_{0}^{2\pi} d\phi \int d^3p \, \frac{q^2c^2k}{(2\pi)^2 4\pi} \, |\widetilde{\varphi}(\mathbf{p})|^2 \, |\mathcal{J}(\mathbf{p}-\mathbf{k})|^2 \tag{5.38}$$

Let us now explicitly calculate the time integral $\mathcal{J}$. Defining the functions

$$F(k) \;:=\; \frac{k^2}{2M} + ck + \Omega \,, \qquad A(\mathbf{p},\mathbf{k}) := F(k) - \frac{\mathbf{p}\cdot\mathbf{k}}{M} \,, \qquad B(k_z) := ak_z \tag{5.39}$$

for notational convenience, we obtain the following expression:

$$\mathcal{J}(\mathbf{p}-\mathbf{k}) \;=\; \int_{-\infty}^{\infty} dt \, e^{it\left(\frac{k^2}{2M} - \frac{\mathbf{p}\cdot\mathbf{k}}{M} + ck + \Omega\right) - ik_z f(t)} \tag{5.40}$$

$$\;=\; \frac{1}{iA} + e^{iT\left(A - \frac{BT}{2}\right)} \frac{i}{A-BT} + \sqrt{\frac{\pi}{2iB}} e^{\frac{iA^2}{2B}} \left[\mathrm{Erf}\left(\tfrac{iA}{\sqrt{2iB}}\right) - \mathrm{Erf}\left(\tfrac{i(A-BT)}{\sqrt{2iB}}\right) \right] \tag{5.41}$$

We here omitted two terms, respectively involving delta distributions $\delta(A)$ and $\delta(A-BT)$, which we are justified to do for the following reason. First, let us write $\mathbf{p}\cdot\mathbf{k} = pk\cos(\kappa)$, with κ the angle between $\mathbf{p}$ and $\mathbf{k}$. The delta distribution $\delta(A)$ then peaks only for $\cos(\kappa) = \frac{MF}{pk}$. Furthermore, the delta distribution $\delta(A-BT)$ peaks only for $\cos(\kappa) = \frac{M}{pk}(F - aTk_z)$. But since $\cos(\kappa) \in [-1,1]$, a necessary condition for $\delta(A)$ to peak is $p \geq Mc$, which translates to saying that the initial virtual center of mass velocities would have to be superluminal, which is of course not possible. Similarly, a necessary condition for $\delta(A-BT)$ to peak is $p + MaT \geq Mc$, which would require the virtual center of mass velocities to be superluminal by the end of the accelerated phase. For these reasons, the delta distributions can be omitted in the physical region of interest. Physically, the delta distributions $\delta(A)$ and $\delta(A-BT)$ have their origin in the virtual inertial motion of the detector, respectively for the times $t < 0$ and $t > T$ during which the electric field is switched off. Inertial virtual motion (just like inertial real motion) should not cause excitation of the detector and the field, which is reflected in the vanishing of these delta distributions.

5.4 Gaussian center of mass wave packet

In order to be able to concretely plot the transition probability densities for the massive Unruh effect which we discussed above, we now need to specify an initial wave function, $\widetilde{\varphi}(\mathbf{p})$, for the detector's center of mass. Let us again consider a Gaussian initial center of mass wave packet of the form given in Eq.(2.28), which flows together from past infinity to time $t = 0$, and which then flows apart again from time $t = 0$ towards future infinity. In this way, we ensure that when we interrupt the free time evolution of the center of mass, by switching on the electric field at time $t = 0$, the detector's center of mass is localized in the form of a Gaussian wave packet of width L.

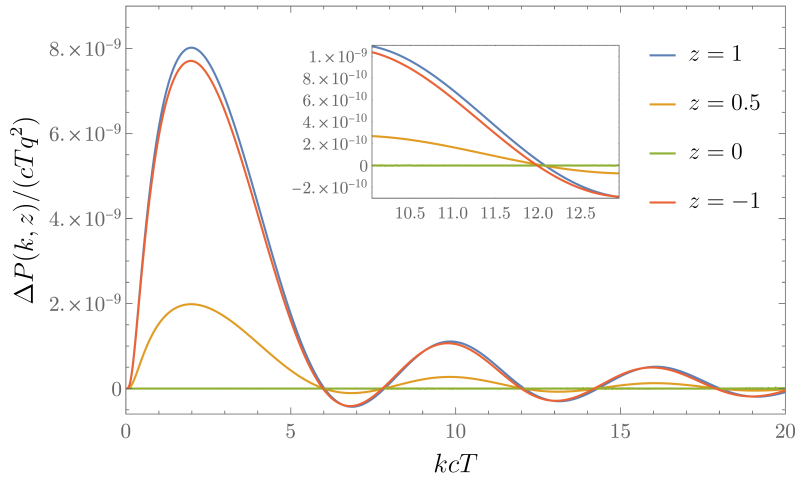

Figure 5.4: The difference $\Delta P(k, z)/(cTq^2)$, plotted as a function of the dimensionless variable kcT, for different emission angles z and with $Mc^2T/\hbar = 100$, $\Omega T = 0.2$, $aT/c = 8 \cdot 10^{-3}$ and $L/(cT) = 100$.

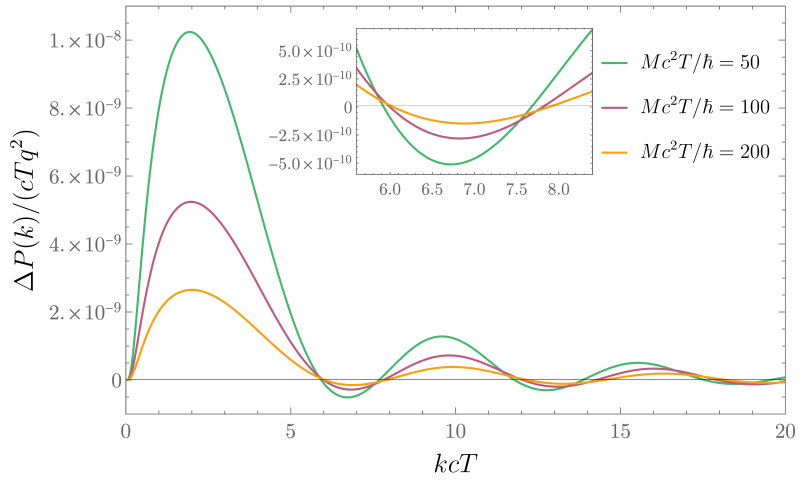

Figure 5.5: The difference $\Delta P(k)/(cTq^2)$, plotted as a function of the dimensionless variable kcT, for various choices for the detector mass (i.e., various choices for the dimensionless variable $Mc^2T/\hbar$) and with $\Omega T = 0.2$, $aT/c = 8 \cdot 10^{-3}$ and $L/(cT) = 100$.

Again, since we describe the dynamics of the detector's center of mass via the Schrödinger equation, we need to choose the parameters L, M, T and a in a way that ensures that the

detector's virtual center of mass velocities stay within the non-relativistic regime. The initial momentum of the detector in the $z-$direction, i.e., parallel to the electric field, is Gaussian distributed around $p_z = 0$, with a standard deviation of $\sqrt{2}/L$. Initial momenta that are 3.5 standard deviations away from the mean then correspond to initial virtual center of mass velocities, $v_z(0)$, of magnitude $7\sqrt{2}/(LM)$. Let us consider a fixed length T of the time interval during which the electric field is switched on. We can obtain an estimate for how small we should choose the electric field strength $\mathcal{E}$ to be, by calculating the velocity that a classical particle of initial velocity $v_z(0) = 7\sqrt{2}/(LM)$ and acceleration a would have at time T, and by then requiring this velocity to be smaller than 1% of the speed of light:

$$v_z(T) \;=\; \frac{7\sqrt{2}}{LM} + Ta \overset{!}{\leq} 10^{-2}c \tag{5.42}$$

Provided that we choose appropriate parameters $\mathcal{E}$, T, L and M, we can now Taylor expand the modulus squared of the time integral in Eq.(5.36) for non-relativistic virtual detector velocities, $v/c = p/(Mc) \ll 1$, that is, Taylor expand $|\mathcal{J}(\mathbf{p}-\mathbf{k})|^2$ around $\mathbf{p}/(Mc) = 0$. Due to the symmetry of the integral in Eq.(5.36), we only need to calculate the following Taylor coefficients:

$$C \;:=\; \left(|\mathcal{J}(\mathbf{p}-\mathbf{k})|^2\right)\Big|_{A=F} \qquad \text{and} \qquad D := \frac{1}{2}\frac{\partial^2\left(|\mathcal{J}(\mathbf{p}-\mathbf{k})|^2\right)}{\partial A^2}\Big|_{A=F} \tag{5.43}$$

Expressing C and D in terms of the variables k and z, we then obtain for the excitation probability densities we introduced above:

$$P_{Massive}(k,z) \;=\; \frac{q^2c^2k}{8\pi^2}\left[C(k,z) + D(k,z)k^2/(M^2L^2) + \mathcal{O}\left((LMc)^{-4}\right)\right], \tag{5.44}$$

$$P_{massive}(k) \;=\; \int_{-1}^{1} dz\, \frac{q^2c^2k}{8\pi^2}\left[C(k,z) + D(k,z)k^2/(M^2L^2) + \mathcal{O}\left((LMc)^{-4}\right)\right], \tag{5.45}$$

$$\begin{aligned} P_{Massive}(r,\zeta) \;=\; & \frac{L^3q^2c^2}{2(2\pi)^{5/2}}\int_0^\infty dk \int_{-1}^{1} dz\, k\, e^{-(r^2+k^2+2rk\zeta)L^2/2} \\ & \times\left[C(k,z) + D(k,z)\left(rk\zeta + k^2\right)^2/M^2\right] + \mathcal{O}\left((LMc)^{-4}\right), \end{aligned} \tag{5.46}$$

$$\begin{aligned} P_{Massive}(r) \;=\; & \frac{L^3q^2c^2}{2(2\pi)^{5/2}}\int_{-1}^{1} d\zeta\, r^2\, e^{-rk\zeta L^2}\int_0^\infty dk \int_{-1}^{1} dz\, k\, e^{-(r^2+k^2)L^2/2} \\ & \times\left[C(k,z) + D(k,z)\left(rk\zeta + k^2\right)^2/M^2\right] + \mathcal{O}\left((LMc)^{-4}\right) \end{aligned} \tag{5.47}$$

We here defined r as the magnitude of the recoil momentum and α as the angle between the recoil momentum $\mathbf{r}$ and the momentum $\mathbf{k}$ of the emitted photon, $\mathbf{r}\cdot\mathbf{k} = rk\cos(\alpha)$. We further defined the variable $\zeta := \cos(\alpha)$.

We are now prepared to plot the excitation probability densities, e.g., for different detector masses M and different energy gaps Ω, and study the dependence of the excitation process on the angle and the magnitude of the momentum of the emitted photon, as well as on the magnitude of the recoil momentum and the angle between the recoil of the detector and the emitted photon. The remaining integrations over z, k and ζ in Eq.(5.44)-(5.47) can be carried out numerically.

The plots for $P_{Massive}(k,z)$ and $P_{Massive}(k)$ look qualitatively extremely similar to the plots we obtained in section 5.1 for $P_{Unruh}(k,z)$ and $P_{Unruh}(k)$, for a UDW detector with a classical and prescribed spatial trajectory. In order to visibly resolve how the plots for coherently delocalized, massive detectors differ from the plots for UDW detectors, in Fig.(5.4) we plot the difference between the excitation probability density for UDW and massive detectors, $\Delta P(k,z) := P_{Unruh}(k,z) - P_{Massive}(k,z)$, for different emission angles z, in terms of the magnitude k of the momentum of the emitted photon. Further, in Fig.(5.5), we numerically integrate over the emission angle and plot the difference $\Delta P(k) := P_{Unruh}(k) - P_{Massive}(k)$, as a function of the magnitude k of the momentum of the emitted photon. We find that, taking the quantum delocalization of the detector's center of mass into account, there are some values of k for which the excitation process becomes less likely ($\Delta P(k) > 0$), and some for which the excitation process becomes more likely ($\Delta P(k) < 0$), compared to the Unruh effect for a UDW detector. We can intuitively understand this effect as follows: by studying the Unruh effect for a coherently delocalized detector, we expect that the different superposed virtual paths of the detector coherently interfere with each other. For $\Delta P(k) > 0$, destructive interference effects dominate overall, while for $\Delta P(k) < 0$, constructive interference effects dominate. For the purpose of measuring the effects of delocalization on the Unruh effect (provided that the Unruh effect itself becomes measurable at some point), these different regions of destructive and constructive interference might be a crucial fingerprint to look for in the Unruh radiation spectrum.

In Fig.(5.6), we depict polar plots for both the excitation probability density $P_{Unruh}(k,z)$, as well as the excitation probability densities $P_{Massive}(k,z)$ for a range of different detector masses M. We fixed the magnitude of the momentum of the emitted photon to be $kcT = 5$ in the plot on the left and $kcT = 7$ in the plot on the right. The radial axes of the plots show the excitation probability densities, while the polar angle represents the emission angle θ of the photon momentum. We find that for smaller and smaller detector masses (that is, faster and faster virtual center of mass delocalization), the difference between the Unruh and the massive Unruh effect becomes more and more significant. We further find that the probability

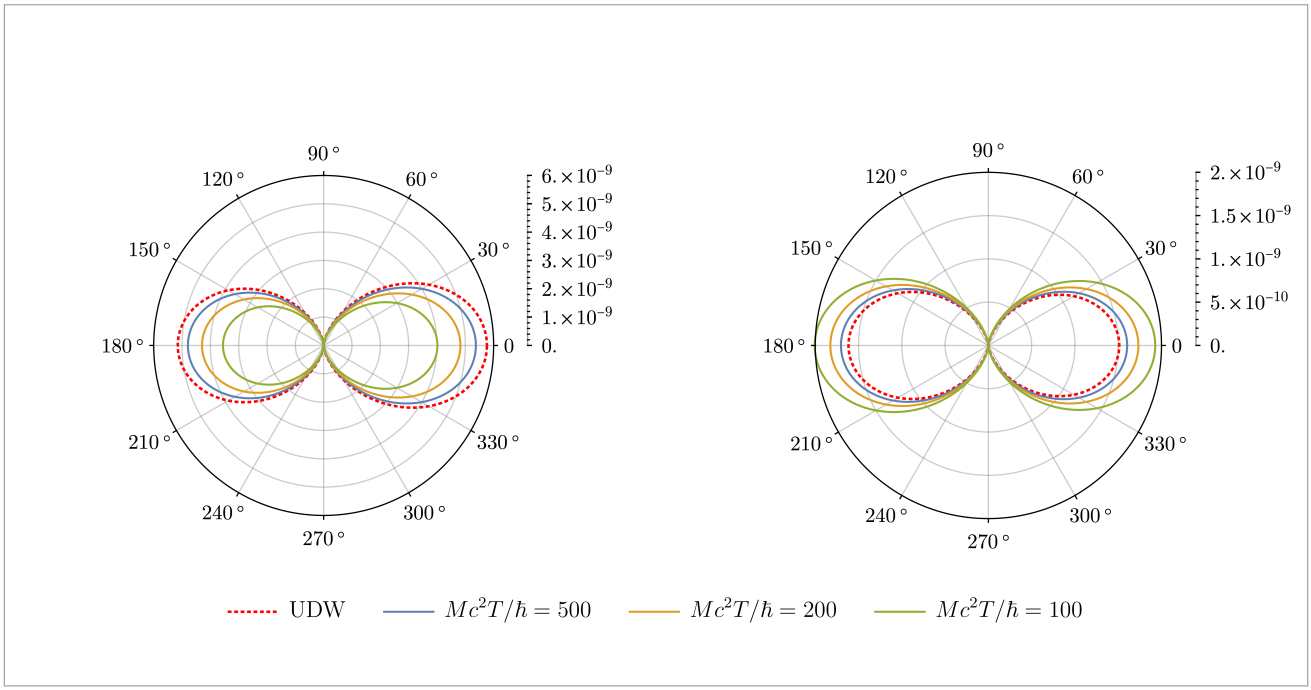

Figure 5.6: Polar plots of the excitation probability density in terms of the polar angle θ of the emitted photon, where we fixed $kcT = 5$ (*left*) and $kcT = 7$ (*right*). The radial axes of the plots show the excitation probability densities (according to the respective legends to the right of each plot), while the polar angle represents the polar emission angle θ. In both plots, we chose parameters $\Omega T = 0.2$, $aT/c = 8 \cdot 10^{-3}$ and $L/(cT) = 100$.

for the detector to emit a photon of certain momentum magnitudes, such as e.g. for $kcT = 5$, is suppressed by taking the quantum nature of the detector's center of mass into account, while for other photon momentum magnitudes, such as e.g. for $kcT = 7$, the probability becomes enhanced by it. We further find that depending on the magnitude of the photon momentum, radiation is sometimes preferably emitted in the forward direction, and sometimes preferably in the backwards direction. For all magnitudes of the photon momentum and for all detector masses, as well as for UDW detectors, we find however that no radiation is emitted orthogonal to the direction of acceleration (that is, for $\theta = 90°$ and $\theta = 270°$).

Let us now again remember that accelerated charges emit radiation in the form of synchrotron radiation. This is the case for charges following a prescribed trajectory, as well as for charges with delocalized center of mass degrees of freedom. In Fig.(5.7), we displayed polar plots of the difference both between the Unruh effect and synchrotron radiation for a simple charge, as well as between the massive Unruh effect and synchrotron radiation for a delocalized charge. Concretely, the red dotted line represents a polar plot of $[P_{sync}(k,z) - P_{Unruh}(k,z)]/q^2$, for $kcT = 5$ and where $P_{sync}(k)$ is obtained from $P_{Unruh}(k)$ by setting $\Omega = 0$. The colored solid lines represent polar plots of $[P_{Massive,\,sync}(k,z) - P_{Massive}(k,z)]/q^2$, for $kcT = 5$ and where $P_{Massive,\,sync}(k,z)$ is obtained from $P_{Massive}(k,z)$ by setting $\Omega = 0$. By subtracting the background synchrotron contribution, the plot thus shows the angular distribution of radiation emitted merely due to the (massive) Unruh effect.

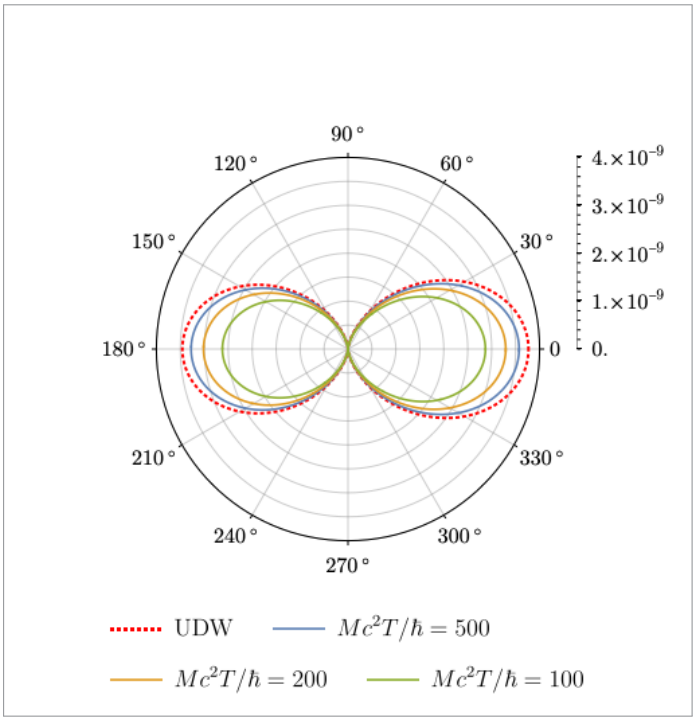

Figure 5.7: The red dotted line represents a polar plot of the difference $[P_{sync}(k,z) - P_{Unruh}(k,z)]/(cTq^2)$, for a simple charge and a UDW detector with energy gap $\Omega T = 0.2$ and a simple charge. The colored solid lines represent the difference $[P_{Massive,\,sync}(k,z) - P_{Massive}(k,z)]/(cTq^2)$, for a delocalized charge and delocalized detectors of various masses and with energy gap $\Omega T = 0.2$. We here fixed $kcT = 5$ and chose parameters $aT/c = 8 \cdot 10^{-3}$ and $L/(cT) = 100$.

In Fig.(5.8), we display a polar plot for the excitation probability density $P_{Massive}(r,\zeta)$, for a range of different fixed values of r. The radial axis again shows the excitation probability density, while the polar angle represents the angle α between the detector's recoil and the emitted photon. We find that the probability density for small recoil momenta is fairly isotropic, which is plausible since we assumed an isotropic initial center of mass momentum distribution. For larger recoil momenta however, the radiation is distorted towards the direction opposite to the direction in which the photon is emitted. This is also plausible, given that most photons are emitted preferably in the acceleration direction. We thus find that due to the massive Unruh effect and the resulting recoil of detector, the detector resists the acceleration to a certain extent, and we can interpret this result as a sort of friction, causing the detector to slow down.

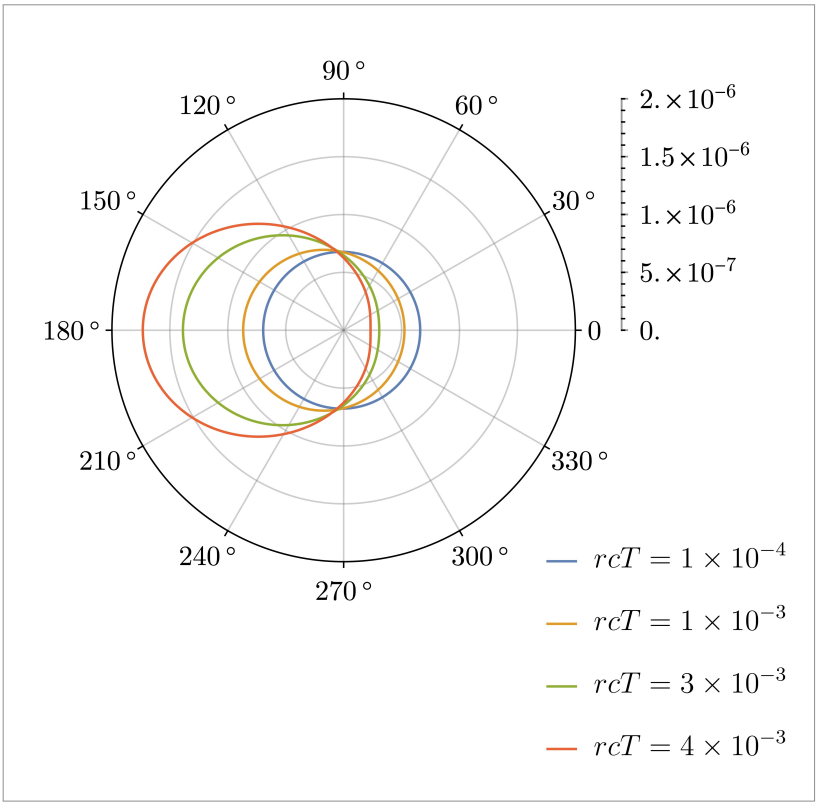

Figure 5.8: The excitation probability density $P_{Massive}(r,\zeta)/(cTq^2)$, plotted against the radial axis, as a polar plot in terms of the angle $\alpha = \arccos(\zeta)$ between the recoil momentum and the momentum of the emitted photon. We chose to show polar plots for a range of different values of the dimensionless variable rcT, and we let $Mc^2T/\hbar = 500$, $\Omega T = 0.2$, $aT/c = 8 \cdot 10^{-3}$ and $L/(cT) = 100$.

5.5 The Unruh effect as a limiting case of the massive Unruh effect

Finally, let us see how to recover the traditional Unruh effect in Eq.(5.18), for a UDW detector with a prescribed classical center of mass trajectory, from the "massive Unruh effect" in Eq.(5.36), which we obtained for a detector whose quantum center of mass is subject to an electric field.

In order to recover the traditional Unruh effect for a detector experiencing a uniform acceleration a, let us consider the limit of infinite detector mass, in which the center of mass wave function coherently delocalizes infinitely slowly and in which the center of mass degrees of freedom thus essentially behave classically. A classical particle of charge q and mass M in a constant electric field $\mathcal{E}$ experiences an acceleration $a := q\mathcal{E}/M$. Defining $M =: m\gamma$ and $\mathcal{E} =: \varepsilon\gamma$ and letting $\gamma \to \infty$ allows us to keep the acceleration a experienced by the detector constant,

while considering the infinite mass limit:

$$\lim_{\gamma\to\infty} P_{Massive} \quad = \quad P_{Unruh} \tag{5.48}$$

Starting from our quantum mechanical framework, in which we dynamically account for the acceleration of the detector via an electric field, we can thus indeed recover the "classical" Unruh effect for a UDW detector with uniform acceleration a during a finite time interval and with non-relativistic velocities. We thus, once again, find that it is not the static center of mass delocalization, but rather the dynamical coherent center of mass delocalization process, which affects the interaction of matter and light.

Conclusions

The UDW detector model can be viewed as a simplified model of the light-matter interaction, in which the electromagnetic field is modeled as a simple scalar field, and matter systems are modeled as simple first-quantized qubit systems, whose classical center of mass degrees of freedom follow a prescribed trajectory. In the past, the UDW detector model has proven to be a powerful tool to explore a wide range of phenomena in the field of relativistic quantum information. It has been used not only to study the Unruh effect, but also, for instance, to explore the vacuum entanglement of quantum fields and how to swap it into a pair of detectors, as well as simple processes such as the absorption, emission and vacuum excitation processes. We here developed a generalized detector model, which we refer to as the *coherently delocalized detector model*, such as to include the quantumness of the center of mass of the detector.

In chapter 1 of this thesis we reviewed the UDW detector model and some of its variations, as well as its application to the study of simple processes in the light-matter interaction. In chapter 2, we then introduced our coherently delocalized detector model, by dropping the simplifying assumption underlying the UDW detector model that the center of mass of the detector is classical, and by instead quantizing the center of mass degrees of freedom.

We discovered that the dynamics of the coherent center of mass delocalization of a detector influences its interaction with a quantum field. For instance, we discovered that emission and absorption rates are modified by the dynamical center of mass delocalization process, and we found that it makes a difference whether the delocalization is coherent or in part also incoherent. Looking forward, these modifications might be of interest not only for instance in view of laser cooling and the Doppler effect, but also in the context of quantum information theory. Let us here just mention some of the questions worth exploring in the future: What happens when a coherently delocalized detector system absorbs a photon that is entangled with an ancilla system? To what extent can the preexisting entanglement be preserved, that is, how much

of the preexisting entanglement can be acquired by a delocalized detector system absorbing the photon? To what extent will the detector's internal degrees of freedom become entangled with the ancilla upon the absorption of the photon, and to what extent will the center of mass degrees of freedom become entangled with the ancilla or the internal degrees of freedom? The answers to these questions will likely depend on the amount by which the photon was entangled with the ancilla via its polarization and via its orbital degrees of freedom respectively, as well as on the detector's initial center of mass state. Understanding the quantum channel capacities of the light-matter interaction, for quantum delocalized matter systems, could become particularly important with regard to modular quantum computing. It would be very interesting to study protocols such as the quantum teleportation protocol or the superdense coding protocol, within our delocalized detector model.

In section 2.5 we found that the smeared UDW detector model, which we discussed in section 1.3, is fundamentally different from our coherently delocalized detector model. While classical smearing profiles are appropriate to model the finite spatial extent of a detector system due to its orbital wave functions, operator-valued smearing profiles are needed to model coherent delocalization due to the quantum nature of the center of mass degrees of freedom.

In sections 2.6 and 2.7 we found that in a medium, the virtual motion of a detector system, due to the coherent dynamical delocalization process, can induce interesting new effects. Namely, on the one hand, a delocalized detector in its ground state, coupled to the ground state of the quantum field, can become excited, while at the same time emitting a field quantum. We referred to this effect as a *virtual Cherenkov-like effect*. Just like the Cherenkov effect can occur for charges undergoing superluminal *real motion* in a medium, we found here that the virtual Cherenkov-like effect can occur whenever the *virtual motion* of the center of mass possesses probability amplitudes for velocities faster than the critical velocity $v_{crit} = c_s + \sqrt{2\Omega/M}$, determined by maximum wave propagation speed c_s in the medium, as well as the mass M and the energy gap Ω of the detector. We found that the supersonic spreading of the detector's center of mass is slowed down, to some extent, by the energy loss due to the emission of Cherenkov-like radiation and the excitation of the detector. We concluded that the virtual Cherenkov-like effect represents a source for decoherence and can be viewed as a source of friction. On the other hand, we found that a field excitation can be 'absorbed' by a delocalized detector in its excited state, leaving both the field and the detector in their respective ground states. This *inverse virtual Cherenkov-like effect* can occur whenever the virtual motion of the center of mass possesses probability amplitudes for velocities faster than the critical velocity $\widetilde{v}_{crit} = \left|\frac{\Omega}{k} + c_s - \frac{k}{2M}\right|$.

These newly discovered effects might be experimentally observable, e.g., for an atom or molecule

left to delocalize freely in a Bose Einstein condensate. The sound propagation speed can be as low as mm/s for certain Bose Einstein condensates [74]. The (inverse) virtual Cherenkov-like effect might thus well be observable, provided that the matter system coherently delocalizes faster than the critical velocity v_{crit} (or the critical velocity $\widetilde{v}_{crit}$), determined by the phononic propagation speed c_s in the Bose Einstein condensate. However, before setting up an experiment to measure these effects, we should of course first make quantitatively accurate predictions. That is, instead of the qubit detectors we considered here, we should consider accurate quantitative models for the matter systems, and instead of the simple Klein-Gordon scalar field we considered here, we should model the medium using a more realistic field description, including a more realistic dispersion relation.

Similarly to our studies that led us to discover the virtual Cherenkov-like effect, it should also be interesting to investigate whether or not a Cherenkov-Zeno-like effect could occur in media for a detector whose center of mass wave function spreads in momentum space. For instance, we could imagine a detector exposed to an external potential that induces the coherent spreading of its momentum wave function, such as an electric field or an inverted harmonic oscillator potential, see, e.g., [62, 63, 64]. The external potential would cause the momentum wave function to spread, and the center of mass of the detector would "accelerate". Given our findings related to the virtual Cherenkov-like effect, it would be reasonable to anticipate the occurrence of a Cherenkov-Zeno-like effect: as the center of mass momentum wave function tries to spread into larger and larger momenta, we might again find a critical velocity, above which the detector might undergo a radiation and excitation effect. We predict that the medium would continually 'measure' whether or not the detector has probability amplitudes for virtual velocities above the critical velocity, and the spreading of the momentum wave function into these high momenta might be be slowed down.

In chapter 3, we proposed a model for a specific physical situation involving a delocalized matter system, namely for a hydrogen atom with quantum delocalized center of mass degrees of freedom, coupled to the vector-valued electromagnetic field via minimal coupling. Within this model, we then made qualitative predictions for the increase of the spontaneous emission rate for an excited hydrogen atom, due to the dynamical coherent delocalization process of the center of mass of the hydrogen atom. We further discussed how center of mass delocalization can lead to violations of the selection rules in the light-matter interaction. Ultimately, these violations might have profound information theoretic consequences. As a technical tool to simplify the order of magnitude estimate calculations, we finally discussed a simplified model for a delocalized

hydrogen atom, obtained by replacing the Coulomb potential by a simpler harmonic potential. It should be interesting to study further concrete physical scenarios in which delocalized matter systems interact with quantum fields, to propose realistic models, and to then make quantitative predictions for the effects of coherent delocalization in these scenarios.

In chapter 4, we studied the ability of two quantum delocalized detectors to become entangled with each other, via their respective interaction with the ground state of a scalar quantum field. We calculated the entanglement negativity for the internal degrees of freedom of the two quantum delocalized detectors, and thereby studied the impact of quantum center of mass delocalization on the process of entanglement harvesting. We found that delocalized detectors harvest less entanglement than detectors whose center of mass degrees of freedom are assumed to behave classically. We further identified the limit in which the results for entanglement harvesting for coherently delocalized detectors reduce to the results for detectors with classical external degrees of freedom: for two detectors of very large mass, whose center of mass wave functions are initially very sharply peaked and which dynamically delocalize very slowly, we recover the negativity for two pointlike UDW detectors. This limit corresponds to detectors whose centers of mass are essentially completely localized at all times. Moreover, we confirmed once again that center of mass delocalization is fundamentally different from the finite extent of a detector's charge distribution arising from the electronic orbitals. While the finite extent due to the electronic orbitals can be modeled separately through the use of smearing functions, we here restricted ourselves to modelling only the delocalization due to the detector's quantum center of mass. Finally, we discussed entanglement harvesting in media, where we found that entanglement harvesting for coherently delocalized detectors decreases with decreasing wave propagation speeds.

We focused on the entanglement harvested by the internal degrees of freedom of quantum delocalized detectors. It will be interesting to investigate to what extent the center of mass degrees of freedom of coherently delocalized detectors can harvest entanglement from the vacuum. In addition, the center of mass degrees of freedom can become entangled with the internal degrees of freedom in the harvesting process. We conjecture, for example, that for faster virtual recoil velocities, the center of mass degrees of freedom harvest larger amounts of entanglement, while, possibly due to entanglement monogamy, the internal degrees of freedom then might harvest less. It will be technically difficult, however, to calculate entanglement measures, such as the negativity, for the center of mass degrees of freedom, since they possess infinite dimensional Hilbert spaces. We anticipate that this can be addressed, for example, by either post-selecting

for specific recoil momenta, by discretizing the momentum space, e.g., by placing the detectors in a confining potential or cavity and placing an energy cutoff, or by binning momenta into a finite number of momentum regions. Such methods could then allow one, for example, to study whether preexisting entanglement between the center of mass degrees of freedom would help or hinder the harvesting of entanglement.

When studying processes within the UDW detector model, oftentimes more intuition and insights can be gained by performing a Lorentz transformation into the detector's rest frame. In our case here, however, the quantum center of mass motion possesses a range of potential velocities in coherent superposition. To transform into the quantum uncertain rest frame of the detector, one needs to perform coordinate changes to quantum uncertain reference frames via quantum uncertain Lorentz transformations. A formalism of such quantum reference frames has been developed, e.g., in [65, 66, 67, 68, 69, 70]. Adapting and applying the formalism of quantum reference frames to our studies of the light-matter interaction for coherently delocalized matter systems may be useful not only to better understand the effects which we discussed in this thesis. But also, these methods may allow us to extend our studies to relativistic virtual center of mass velocities.

Finally, in chapter 5, we studied the effects of coherent center of mass delocalization on the Unruh effect. We considered a detector whose quantum center of mass is accelerated by an external electric field, and we studied how the quantum uncertain center of mass state affects the emission of radiation along with the excitation of the massive detector. We here coined the term *massive Unruh effect* for the emission effect along with the excitation of the coherently delocalized detector. We studied, in particular, the quantum recoil of the detector. We found that the Unruh effect can be recovered from the massive Unruh effect, in the limiting case of very large detector masses and very large electric field strengths.

Here, we assumed the presence of *two* different fields, namely a classical field causing the delocalized detector to accelerate, and a quantum field which becomes excited via the massive Unruh effect. This assumption is well justified in scenarios in which the acceleration is, for instance, caused by a gravitational field, and the quantum field is the electromagnetic field. However, when considering an electric field causing the acceleration, this field of course has its origin in the quantum electromagnetic field. Looking forward, it would therefore be interesting to study the massive Unruh effect in a unified setup in which we consider a delocalized detector coupling to only *one* quantum field.

Further, we here only considered initial center of mass wave packets of Gaussian shape. It

should be interesting to tune the shape of the initial wave function in different ways, and explore whether there are certain wave function shapes which are more or less suited for the purpose of measuring the massive Unruh effect.

Looking forward, it might also be interesting to study the "inverse massive Unruh effect": similarly to the inverse virtual Cherenkov-like effect, which we discussed in section 2.7, we could consider the transition form an initial state of the form $|\Psi_i\rangle = |\varphi\rangle \otimes |e\rangle \otimes |\mathbf{k}\rangle$ to a final state of the form $|\Psi_f\rangle = |\mathbf{r}\rangle \otimes |g\rangle \otimes |0\rangle$. Apart from the initial and final center of mass states, this transition represents the time-reversed process of the massive Unruh effect. The inverse massive Unruh effect might be more easily measurable than the Unruh effect, provided that we could fine-tune both the center of mass wave function and the excited field state in a way that maximizes the transition probability. Further, the probability for the inverse Unruh effect to happen might increase by considering a coherent beam of photons with a high flux, instead of a single particle initial field state. We could then measure the detector's recoil, such as to detect the inverse massive Unruh effect. It should be interesting to investigate whether measuring the inverse massive Unruh effect could indeed be more viable than measuring the Unruh effect.

Throughout our discussion of the massive Unruh effect, we restricted ourselves to non-relativistic center of mass velocities. For an electric field of the form we considered in Eq.(5.23), the non-relativistic restriction requires the time interval during which the electric field is switched on to be appropriately short. In order to maximize the time of acceleration, while staying within the non-relativistic regime, we could alternatively consider, for instance, the oscillatory motion of a detector in an electric field, whose field lines are periodically flipped from pointing in one direction to pointing in the opposite direction. We expect that a setup like this would significantly enhance the measurability of the massive Unruh effect. A related scenario involving oscillatory acceleration, for a detector system in an electromagnetic cavity, was discussed, e.g., in [105, 106, 107], and the term *oscillatory Unruh effect* was coined for the excitation and radiation effect for such detector systems. While the Unruh effect requires extremely high accelerations in order to be observable, the accelerations required for the oscillatory Unruh effect to be observable were shown to be much more viable. The authors of [105] further showed that the oscillatory Unruh effect may be significantly enhanced, via a coherent enhancement effect similar to the superradiance effect, by considering a dense cloud of detector systems. In a similar spirit, it should be extremely interesting to study the massive Unruh effect for a periodic time dependent electric field, first for a coherently delocalized detector, and then also for a cloud of coherently delocalized detectors. Performing these calculations may well lead the way towards measurability of the massive Unruh effect.

Another possibility worth exploring, in order to possibly enhance the measurability of the massive Unruh effect, is to study the excitation and radiation effect for a coherently delocalized detector in a constant magnetic field. We could straightforwardly apply the methods developed in this thesis towards studying this "circular massive Unruh effect", that is, the radiation effect caused by circular acceleration, as well as the quantum recoil of the detector. Experimentally, we could imagine trapping an electron in a constant magnetic field. In order to trap the electron along the direction of the magnetic field lines, we could apply electric potentials. The electron's center of mass would be quantum delocalized, and we could use the quantized spin eigenstates of the electron in the constant magnetic field as the qubit states. Conceivably, the quantum recoil experienced by the electron could then be used in order to detect the circular massive Unruh effect. The advantage of considering circular acceleration, rather than uniform acceleration, is that we could leave the constant magnetic field on at all times (since detectors with virtual center of mass velocities initially within the non-relativistic regime would stay within the non-relativistic regime at all times). We could thus eliminate any switching effects interfering with the acceleration effects.

Of course, it would be extremely intriguing to study the massive Unruh effect for a coherently delocalized detector experiencing uniform acceleration at all times. However, uniform acceleration at all times causes the detector to experience relativistic virtual center of mass velocities. In order to conduct such studies, more sophisticated tools, such as quantum reference frames, will need to be employed first. It would then be exciting to investigate whether, due to the impact of the quantum recoil, quantum delocalized detectors still thermalize according to a thermal bath, and if so, how the temperature of this thermal bath would be affected by the detector's mass and initial localization.

References

[1] N. Stritzelberger and A. Kempf, "Coherent delocalization in the light-matter interaction," *Phys. Rev. D*, vol. 101, p. 036007, Feb 2020.

[2] N. Stritzelberger, L. J. Henderson, V. Baccetti, N. C. Menicucci, and A. Kempf, "Entanglement harvesting with coherently delocalized matter," 2020.

[3] W. G. Unruh, "Notes on black-hole evaporation," *Phys. Rev. D*, vol. 14, pp. 870–892, 1976.

[4] B. S. DeWitt, "Quantum gravity: The new synthesis". *General Relativity, an Einstein Centenary Survey (eds. S. W. Hawking and W. Israel)*, Cambridge University Press, 1979.

[5] N. D. Birrell and P. C. W. Davies, *Quantum Fields in Curved Space*. Cambridge Monographs on Mathematical Physics, Cambridge University Press, 1982.

[6] R. M. Wald, *Quantum field theory in curved spacetime and black hole thermodynamics.* Chicago Lectures in Physics, 1994.

[7] G. W. Gibbons and S. W. Hawking, "Cosmological event horizons, thermodynamics, and particle creation," *Phys. Rev. D*, vol. 15, pp. 2738–2751, 1977.

[8] S. A. Fulling, "Nonuniqueness of canonical field quantization in riemannian space-time," *Phys. Rev. D*, vol. 7, pp. 2850–2862, May 1973.

[9] S. A. Fulling, "Aspects of Quantum Field Theory in Curved Space-Time". Cambridge University Press, 1989.

[10] P. C. W. Davies, "Scalar production in Schwarzschild and Rindler metrics," *Journal of Physics A: Mathematical and General*, vol. 8, pp. 609–616, apr 1975.

[11] L. C. B. Crispino, A. Higuchi, and G. E. A. Matsas, "The Unruh effect and its applications," *Reviews of Modern Physics*, vol. 80, no. 3, p. 787–838, 2008.

[12] R. Casadio and G. Venturi, "The accelerated observer and quantum effects," *Physics Letters A*, vol. 199, no. 1, pp. 33 – 39, 1995.

[13] R. Casadio and G. Venturi, "The accelerated observer with back-reaction effects," *Physics Letters A*, vol. 252, no. 3, pp. 109 – 114, 1999.

[14] V. Mukhanov and S. Winitzki, *Introduction to Quantum Effects in Gravity*. Cambridge University Press, 2007.

[15] T. Jacobson, "Introduction to quantum fields in curved spacetime and the Hawking effect," in *Lectures on Quantum Gravity* (A. Gomberoff and D. Marolf, eds.), pp. 39–89, Boston, MA: Springer US, 2005.

[16] L. H. Ford, "Quantum field theory in curved spacetime," 1997.

[17] R. B. Mann and T. C. Ralph, "Relativistic quantum information," *Classical and Quantum Gravity*, vol. 29, p. 220301, oct 2012.

[18] R. D. Sorkin, "On the entropy of the vacuum outside a horizon," *Tenth International Conference on General Relativity and Gravitation, Contributed Papers*, vol. 2, pp. 734–736, 1983.

[19] M. Srednicki, "Entropy and area," *Phys. Rev. Lett.*, vol. 71, pp. 666–669, 1993.

[20] A. Valentini, "Non-local correlations in quantum electrodynamics," *Physics Letters A*, vol. 153, no. 6, pp. 321 – 325, 1991.

[21] G. V. Steeg and N. C. Menicucci, "Entangling power of an expanding universe," *Phys. Rev. D*, vol. 79, p. 044027, 2009.

[22] A. Pozas-Kerstjens and E. Martín-Martínez, "Harvesting correlations from the quantum vacuum," *Physical Review D*, vol. 92, 2015.

[23] A. Pozas-Kerstjens and E. Martín-Martínez, "Entanglement harvesting from the electromagnetic vacuum with hydrogen-like atoms," *Physical Review D*, vol. 94, 2016.

[24] E. Martín-Martínez, E. G. Brown, W. Donnelly, and A. Kempf, "Sustainable entanglement production from a quantum field," *Phys. Rev. A*, vol. 88, p. 052310, 2013.

[25] M. Cliche and A. Kempf, "Relativistic quantum channel of communication through field quanta," *Phys. Rev. A*, vol. 81, p. 012330, 2010.

[26] M. Cliche and A. Kempf, "Vacuum entanglement enhancement by a weak gravitational field," *Phys. Rev. D*, vol. 83, p. 045019, 2011.

[27] R. H. Jonsson, E. Martín-Martínez, and A. Kempf, "Information transmission without energy exchange," *Phys. Rev. Lett.*, vol. 114, p. 110505, 2015.

[28] W. G. Unruh and R. M. Wald, "What happens when an accelerating observer detects a Rindler particle," *Phys. Rev. D*, vol. 29, pp. 1047–1056, 1984.

[29] M. E. Papageorgiou, "What is a field, what is a particle?...what about algebras?," Master's thesis, University of Waterloo, 2019.

[30] S. J. Summers and R. Werner, "The vacuum violates Bell's inequalities," *Physics Letters A*, vol. 110, no. 5, pp. 257 – 259, 1985.

[31] S. J. Summers and R. Werner, "Maximal violation of Bell's inequalities is generic in quantum field theory," *Communications in Mathematical Physics*, vol. 110, no. 2, pp. 247–259, 1987.

[32] A. Valentini, "Non-local correlations in quantum electrodynamics," *Physics Letters A*, vol. 153, no. 6, pp. 321 – 325, 1991.

[33] B. Reznik, A. Retzker, and J. Silman, "Violating Bell's inequalities in vacuum," *Phys. Rev. A*, vol. 71, p. 042104, 2005.

[34] Y. Nambu, "Entanglement of Quantum Fluctuations in the Inflationary Universe," *Phys. Rev. D*, vol. 78, p. 044023, 2008.

[35] B. Reznik, A. Retzker, and J. Silman, "Violating Bell's inequalities in vacuum," *Phys. Rev. A*, vol. 71, p. 042104, 2005.

[36] S. J. Summers and R. Werner, "Maximal violation of Bell's inequalities is generic in quantum field theory," *Communications in Mathematical Physics*, vol. 110, no. 2, pp. 247–259, 1987.

[37] D. Harlow, "Jerusalem lectures on black holes and quantum information," *Rev. Mod. Phys.*, vol. 88, p. 015002, 2016.

[38] L. Susskind and J. Lindesay, *An Introduction to Black Holes, Information and the String Theory Revolution: The Holographic Universe*. World Scientific, 2005.

[39] E. Martín-Martínez, E. G. Brown, W. Donnelly, and A. Kempf, "Sustainable entanglement production from a quantum field," *Phys. Rev. A*, vol. 88, p. 052310, 2013.

[40] G. Salton, R. B. Mann, and N. C. Menicucci, "Acceleration-assisted entanglement harvesting and rangefinding," *New Journal of Physics*, vol. 17, no. 3, p. 035001, 2015.

[41] E. Martín-Martínez, E. G. Brown, W. Donnelly, and A. Kempf, "Sustainable entanglement production from a quantum field," *Physical Review A*, vol. 88, no. 5, p. 052310, 2013.

[42] P. Simidzija and E. Martín-Martínez, "All coherent field states entangle equally," *Phys. Rev. D*, vol. 96, p. 025020, 2017.

[43] P. Simidzija and E. Martín-Martínez, "Harvesting correlations from thermal and squeezed coherent states," *Physical Review D*, vol. 98, no. 8, 2018.

[44] E. Martín-Martínez and N. C. Menicucci, "Cosmological quantum entanglement," *Classical and Quantum Gravity*, vol. 29, no. 22, p. 224003, 2012.

[45] E. Martín-Martínez and N. C. Menicucci, "Entanglement in curved spacetimes and cosmology," *Classical and Quantum Gravity*, vol. 31, no. 21, p. 214001, 2014.

[46] L. Henderson, R. Hennigar, R. Mann, A. Smith, and J.-L. Zhang, "Harvesting entanglement from the black hole vacuum," *Classical and Quantum Gravity*, vol. 35, 2017.

[47] J. L. Ball, I. Fuentes-Schuller, and F. P. Schuller, "Entanglement in an expanding spacetime," *Phys. Lett. A*, vol. 359, pp. 550–554, 2006.

[48] E. Martín-Martínez, A. R. H. Smith, and D. R. Terno, "Spacetime structure and vacuum entanglement," *Phys. Rev. D*, vol. 93, p. 044001, 2016.

[49] K. K. Ng, R. B. Mann, and E. Martín-Martínez, "Over the horizon: Distinguishing the Schwarzschild spacetime and the RP3 spacetime using an Unruh-deWitt detector," *Physical Review D*, vol. 96, no. 8, 2017.

[50] C. Sabín, B. Peropadre, M. del Rey, and E. Martín-Martínez, "Extracting Past-Future Vacuum Correlations Using Circuit QED," *Phys. Rev. Lett.*, vol. 109, p. 033602, 2012.

[51] E. Martín-Martínez and B. C. Sanders, "Precise space–time positioning for entanglement harvesting," *New Journal of Physics*, vol. 18, no. 4, p. 043031, 2016.

[52] E. Martín-Martínez, M. Montero, and M. del Rey, "Wavepacket detection with the Unruh-DeWitt model," *Phys. Rev.*, vol. D87, no. 6, p. 064038, 2013.

[53] P. Simidzija, R. H. Jonsson, and E. Martín-Martínez, "General no-go theorem for entanglement extraction," *Physical Review D*, vol. 97, no. 12, 2018.

[54] R. Parentani, "The recoils of the accelerated detector and the decoherence of its fluxes," *Nuclear Physics B*, vol. 454, pp. 227–249, Nov. 1995.

[55] D. Hümmer, E. Martín-Martínez, and A. Kempf, "Renormalized Unruh-DeWitt particle detector models for boson and fermion fields," *Phys. Rev. D*, vol. 93, p. 024019, Jan 2016.

[56] E. Martín-Martínez and P. Rodriguez-Lopez, "Relativistic quantum optics: The relativistic invariance of the light-matter interaction models," *Phys. Rev. D*, vol. 97, p. 105026, May 2018.

[57] D. Tong, *Quantum Field Theory, University of Cambridge Part III Mathematical Tripos*. Lecture notes, DAMTP, Cambridge University, 2006.

[58] M. E. Peskin and D. V. Schroeder, *An Introduction To Quantum Field Theory (Frontiers in Physics)*. Westview Press, 1995.

[59] R. Blaga, "The response of a Unruh-DeWitt particle detector in a thin-shell wormhole spacetime," 2017.

[60] M. Papageorgiou and J. Pye, "Impact of relativity on particle localizability and ground state entanglement," *Journal of Physics A: Mathematical and Theoretical*, vol. 52, no. 37, p. 375304, 2019.

[61] R. Lopp and E. Martín-Martínez, "Quantum delocalization, gauge and quantum optics: The light-matter interaction in relativistic quantum information," 2020.

[62] D. Jaksch, J. García-Ripoll, J. Cirac, and P. Zoller, "Quantum computing with cold ions and atoms: Theory," *Lectures on Quantum Information*, pp. 391–422, 2007.

[63] C. Monroe and J. Kim, "Scaling the ion trap quantum processor," *Science*, vol. 339, no. 6124, pp. 1164–1169, 2013.

[64] M. Mukherjee, T. Dutta, N. V. Horne, Y. Lei, P. Liu, J. Phua, and D. Yum, "Ion Trap Quantum Computing: A New Computing Regime," *ECS Transactions*, vol. 86, no. 7, pp. 97–107, 2018.

[65] Y. Aharonov and T. Kaufherr, "Quantum frames of reference," *Phys. Rev. D*, vol. 30, pp. 368–385, 1984.

[66] Y. Aharonov and L. Susskind, "Charge superselection rule," *Phys. Rev.*, vol. 155, pp. 1428–1431, 1967.

[67] S. D. Bartlett, T. Rudolph, and R. W. Spekkens, "Reference frames, superselection rules, and quantum information," *Rev. Mod. Phys.*, vol. 79, pp. 555–609, 2007.

[68] M. C. Palmer, F. Girelli, and S. D. Bartlett, "Changing quantum reference frames," *Phys. Rev. A*, vol. 89, p. 052121, 2014.

[69] F. Giacomini, E. Castro-Ruiz, and Č. Brukner, "Quantum mechanics and the covariance of physical laws in quantum reference frames," *Nature Communications*, vol. 10, 2019.

[70] C. E. Wood and M. Zych, "Minimum uncertainty states for free particles with quantized mass-energy," arXiv:1911.06653, 2019.

[71] P. A. Cherenkov, "Visible emission of clean liquids by action of γ radiation," *Compt. Rend. Acad. Sci. URSS*, vol. 8, p. 451, 1934.

[72] I. M. Frank and I. E. Tamm, "Coherent visible radiation of fast electrons passing through matter," *Compt. Rend. Acad. Sci. URSS*, vol. 14, no. 3, p. 109, 1937.

[73] P. A. Cherenkov, "Visible radiation produced by electrons moving in a medium with velocities exceeding that of light," *Phys. Rev.*, vol. 52, p. 378, 1937.

[74] M. R. Andrews, D. M. Kurn, H.-J. Miesner, D. S. Durfee, C. G. Townsend, S. Inouye, and W. Ketterle, "Propagation of sound in a Bose-Einstein condensate," *Phys. Rev. Lett.*, vol. 79, pp. 553–556, 1997.

[75] M. Göppert-Mayer, "Über Elementarakte mit zwei Quantensprüngen," *Annalen der Physik*, vol. 401, no. 3, pp. 273–294, 1931.

[76] W. E. Lamb, R. R. Schlicher, and M. O. Scully, "Matter-field interaction in atomic physics and quantum optics," *Phys. Rev. A*, vol. 36, pp. 2763–2772, 1987.

[77] M. O. Scully and M. S. Zubairy, *Quantum Optics*. Cambridge University Press, 1997.

[78] N. Funai, J. Louko, and E. Martín-Martínez, "$\hat{p} \cdot \hat{A}$ vs $\hat{x} \cdot \hat{E}$: Gauge invariance in quantum optics and quantum field theory," *Phys. Rev. D*, vol. 99, p. 065014, 2019.

[79] S. Weinberg, *Lectures on Quantum Mechanics*. Cambridge University Press, 2 ed., 2015.

[80] R. G. Woolley, "Gauge invariant wave mechanics and the Power-Zienau-Woolley transformation," *Journal of Physics A: Mathematical and General*, vol. 13, pp. 2795–2805, aug 1980.

[81] M. Babiker and R. Loudon, "Derivation of the Power-Zienau-Woolley Hamiltonian in Quantum Electrodynamics by Gauge Transformation," *Proceedings of the Royal Society of London. Series A, Mathematical and Physical Sciences*, vol. 385, no. 1789, pp. 439–460, 1983.

[82] M. Babiker, "Crossed-beam resonance fluorescence-angular distributions of scattered atoms and photons," *Journal of Physics B: Atomic and Molecular Physics*, vol. 17, no. 24, pp. 4885–4901, 1984.

[83] C. Baxter, M. Babiker, and R. Loudon, "Canonical approach to photon pressure," *Phys. Rev. A*, vol. 47, pp. 1278–1287, Feb 1993.

[84] H. A. Bethe and E. E. Salpeter, *Quantum Mechanics of One- and Two-Electron Systems*, pp. 88–436. Springer Berlin Heidelberg, 1957.

[85] L. Gurung, T. J. Babij, S. D. Hogan, and D. B. Cassidy, "Precision microwave spectroscopy of the positronium $n = 2$ fine structure," *Phys. Rev. Lett.*, vol. 125, p. 073002, Aug 2020.

[86] A. H. Al-Ramadhan and D. W. Gidley, "New precision measurement of the decay rate of singlet positronium," *Phys. Rev. Lett.*, vol. 72, pp. 1632–1635, 1994.

[87] R. S. Vallery, P. W. Zitzewitz, and D. W. Gidley, "Resolution of the Orthopositronium-Lifetime Puzzle," *Phys. Rev. Lett.*, vol. 90, p. 203402, 2003.

[88] O. Jinnouchi, S. Asai, and T. Kobayashi, "Precision measurement of orthopositronium decay rate using SiO_2 powder," *Physics Letters B*, vol. 572, no. 3-4, p. 117–126, 2003.

[89] G. Vidal and R. F. Werner, "Computable measure of entanglement," *Phys. Rev. A*, vol. 65, p. 032314, Feb 2002.

[90] M. B. Plenio, "Logarithmic negativity: A full entanglement monotone that is not convex," *Phys. Rev. Lett.*, vol. 95, p. 090503, 2005.

[91] J. Lee, M. S. Kim, Y. J. Park, and S. Lee, "Partial teleportation of entanglement in a noisy environment," *Journal of Modern Optics*, vol. 47, no. 12, p. 2151–2164, 2000.

[92] M. Plenio and S. Virmani, "An introduction to entanglement measures," *Quantum Information and Computation*, vol. 7, 2005.

[93] W. K. Wootters, "Entanglement of formation of an arbitrary state of two qubits," *Phys. Rev. Lett.*, vol. 80, pp. 2245–2248, 1998.

[94] L. J. Henderson, A. Belenchia, E. Castro-Ruiz, C. Budroni, M. Zych, Č. Brukner, and R. B. Mann, "Quantum temporal superposition: the case of QFT," 2020.

[95] S. J. Olson and T. C. Ralph, "Entanglement between the future and the past in the quantum vacuum," *Phys. Rev. Lett.*, vol. 106, p. 110404, 2011.

[96] S. J. Olson and T. C. Ralph, "Extraction of timelike entanglement from the quantum vacuum," *Phys. Rev. A*, vol. 85, p. 012306, 2012.

[97] C. Liu, Z. Dutton, C. Behroozi, and L. Hau, "Observation of coherent optical information storage in an atomic medium using halted light pulses," *Nature*, vol. 409, pp. 490–3, 02 2001.

[98] E. T. Akhmedov and D. Singleton, "On the physical meaning of the Unruh effect," *JETP Letters*, vol. 86, p. 615–619, Jan 2008.

[99] P. Chen and T. Tajima, "Testing Unruh Radiation with Ultraintense Lasers," *Phys. Rev. Lett.*, vol. 83, pp. 256–259, Jul 1999.

[100] H. Rosu, "On the estimates to measure Hawking effect and Unruh effect in the laboratory," *Int. J. Mod. Phys. D*, vol. 3, pp. 545–548, 1994.

[101] E. Martín-Martínez, I. Fuentes, and R. B. Mann, "Using Berry's Phase to Detect the Unruh Effect at Lower Accelerations," *Physical Review Letters*, vol. 107, Sep 2011.

[102] J. Bell and J. Leinaas, "Electrons as accelerated thermometers," *Nuclear Physics B*, vol. 212, no. 1, pp. 131 – 150, 1983.

[103] J. Bell and J. Leinaas, "The Unruh effect and quantum fluctuations of electrons in storage rings," *Nuclear Physics B*, vol. 284, pp. 488 – 508, 1987.

[104] J. D. Jackson, *Classical electrodynamics*. New York: Wiley, 3rd ed., 1999.

[105] H. Wang and M. Blencowe, "Enhancing the oscillatory Unruh effect with a dense cloud of accelerating photodetectors," 2020.

[106] M. O. Scully, V. V. Kocharovsky, A. Belyanin, E. Fry, and F. Capasso, "Enhancing Acceleration Radiation from Ground-State Atoms via Cavity Quantum Electrodynamics," *Phys. Rev. Lett.*, vol. 91, p. 243004, Dec 2003.

[107] J. Doukas, S.-Y. Lin, B. L. Hu, and R. B. Mann, "Unruh effect under non-equilibrium conditions: oscillatory motion of an Unruh-DeWitt detector," *Journal of High Energy Physics*, vol. 2013, Nov 2013.